

SYNTHESIS AND CHARACTERIZATION OF NEAR-IR EMISSIVE TETRA STYRYL-  
BODIPY BASED LIGHT HARVESTING ENERGY TRANSFER CASSETTES

A THESIS

SUBMITTED TO DEPARTMENT OF CHEMISTRY  
AND THE INSTITUTE OF ENGINEERING AND SCIENCES  
OF BİLKENT UNIVERSITY  
IN PARTIAL FULFILLMENT OF THE REQUIREMENTS  
FOR THE DEGREE OF  
MASTER OF SCIENCE

By

ZİYA KÖSTERELİ

July 2011

I certify that I have read this thesis and that in my opinion it is fully adequate, in scope and in quality, as a thesis of the degree of Master of Science.

.....  
Prof. Dr. Engin U. Akkaya (Principal Advisor)

I certify that I have read this thesis and that in my opinion it is fully adequate, in scope and in quality, as a thesis of the degree of Master of Science.

.....  
Associate Prof. Dr. Dönüş Tuncel

I certify that I have read this thesis and that in my opinion it is fully adequate, in scope and in quality, as a thesis of the degree of Master of Science.

.....  
Assist. Prof. Dr. Erman Bengü

I certify that I have read this thesis and that in my opinion it is fully adequate, in scope and in quality, as a thesis of the degree of Master of Science.

.....  
Assist. Prof. Dr. Okan Esentürk

I certify that I have read this thesis and that in my opinion it is fully adequate, in scope and in quality, as a thesis of the degree of Master of Science.

.....

Assist. Prof. Dr. Ali ırpan

Approved for the Institute of Engineering and Science:

.....

Prof. Dr. Levent Onural

Director of the Institute of Engineering and Science

## ABSTRACT

### SYNTHESIS AND CHARACTERIZATION OF NEAR-IR EMISSIVE TETRA STYRYL-BODIPY BASED LIGHT HARVESTING ENERGY TRANSFER CASSETTES

Ziya Köstereli

M.S. in Department of Chemistry  
Supervisor: Prof. Dr. Engin U. Akkaya  
July, 2011

Light harvesting antenna systems are being used to harvest light through its antenna units. Using these systems, light is channeled into an acceptor chromophore and much more concentrated energy is obtained in acceptor unit with a specific wavelength. In this study, we have rationally designed and synthesized two different novel Förster-type light harvesting energy transfer cassettes which have large Stokes shifts and emit in near-IR region. The first cassette has four boradiazaindacene (BODIPY) as donor groups and one tetrasteryl-BODIPY as an acceptor group. The second cassette has four distyryl-BODIPY units as donor groups and one tetrasteryl-BODIPY as an acceptor group. Click chemistry is successfully used to combine donor and acceptor groups to each other. Efficient energy transfer from donor groups to acceptor group in both cassettes was observed and characterized using emission spectrum, quantum yields and lifetimes. Energy transfer efficiencies and rate of energy transfer were calculated and it is demonstrated that there is more efficient energy transfer in cassette that has better overlap in donor emission and acceptor absorption spectrum which is in accordance with expected behaviour for Förster-type of energy transfer cassettes.

*Keywords:* Boradiazaindacene, light harvesting, energy transfer, Förster-type energy transfer, tetra-styryl BODIPY

## ÖZET

### YAKIN KIZIL ÖTESİ EMİSYONU OLAN TETRASTİRİL-BODİPY YAPISINDAKİ IŞIK HASATI YAPAN ENERJİ TRASNFER KASETLERİNİN SENTEZİ VE KARAKTERİZASYONU

Ziya Köstereli

Yüksek Lisans, Kimya Bölümü  
Tez Yöneticisi: Prof. Dr. Engin U. Akkaya  
Temmuz, 2011

Işık hasat eden anten sistemleri anten birimleri tarafından ışığın hasat edilmesi için kullanılırlar. Bu sistemleri kullanarak ışık, alıcı birime aktarılır ve alıcıda belirli bir dalgaboyunda daha fazla yoğunlaştırılmış enerji toplanır. Bu çalışmada, büyük Stokes kaymasına sahip olan ve yakın kızılötesi bölgesinde ışığı soğuran iki farklı yeni Förster-tipi enerji transfer kaseti tasarlandı ve sentezlendi. Birinci kaset dört adet BODİPY vericisine ve bir adet tetra-stiril BODİPY alıcısına sahip. İkinci kaset dört tane di-sitiril BODİPY vericisine ve bir tane tetra-stiril BODİPY alıcısına sahip. Verici ve alıcı grupları birleştirmek için Klik kimyası başarılı bir şekilde kullanıldı. Emisyon spektrumunu, kuantum verimleri ve emisyon ömürleri kullanılarak iki kasette de etkili enerji transferi karakterize edildi. Enerji transfer verimi ve enerji transfer hızı hesaplandı ve Förster-tipi enerji transfer kasetleri için bir gereklilik olan alıcı absorpsiyonu ile verici emisyonu arasında daha iyi spektral örtüşme olan kasette daha iyi enerji transferi olduğu gösterildi.

*Anahtar Kelimeler:* Boradiazaindasen, enerji hasadı, Förster-tipi enerji transferi, tetra-sitiril BODİPY

*Dedicated to my family*

## ACKNOWLEDGEMENT

I would like to express my gratitude to my supervisor Prof. Dr. Engin U. Akkaya for his guidance, support, patience and for teaching us how to become a good scientist. I will never forget his support throughout my life.

I would like to thank Tuğba Özdemir, Yusuf Çakmak, Safacan Kölemen, Onur Büyükcakır, Şeyma Öztürk for their partnership in this research. I owe a special thank to Ruslan Guliyev for his support, friendship and guidance to improve my skills in the field of supramolecular chemistry.

I want to thank our group members, Sündüs Erbaş Çakmak, Bilal Kılıç, Seda Demirel, Sencer Selçuk, Nisa Yeşilgül, Taha Bilal Uyar, Ahmet Atılgan, Elif Ertem, Merve Türkşanlı, Eser İden, Dr. O. Altan Bozdemir, Fazlı Sözmen, Fatma Pir, Gizem Çeltek, Yiğit Altay, Tuğçe Durgut, Tuba Yaşar, Ahmet Bekdemir, Muhammed Büyüktemiz, Hande Boyacı and rest of the SCL (Supramolecular Chemistry Laboratory) members for valuable friendships, wonderful collaborations, and great ambiance in the laboratory. They are very precious for me. It was wonderful to work with them.

I would like to thank Ali Ekrem Deniz, Ruslan Garifullin for their valuable friendship.

Finally, I want to express my gratitude to my family for their love, support, and understanding. I owe them a lot.

## LIST OF ABBREVIATIONS

FRET: Fluorescence Resonance Energy Transfer

LH: Light Harvesting

DSSC: Dye sensitized solar cell

LHE: Light harvesting efficiency

BODIPY: Boradiazaindacene

TLC: Thin layer chromatography

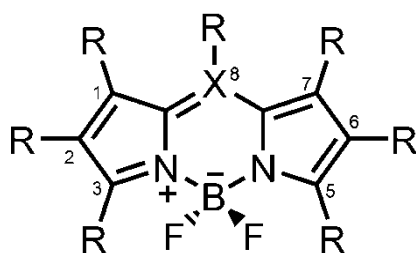
NMR: Nuclear magnetic resonance

DMF: Dimethylformamide

THF: Tetrahydrofuran

TFA: Trifluoroacetic acid

DDQ: Dichlorodicyanoquinone



R = H or any other group  
X = C or N

## TABLE OF CONTENTS

<b>CHAPTER 1</b> .....	1
<b>INTRODUCTION</b> .....	1
1.1. Supramolecular Chemistry .....	1
1.2. Fundamentals of Fluorescence .....	3
1.3. BODIPY Dyes.....	6
1.3.1. Applications of BODIPY Dyes.....	7
1.4. Light Harvesting and Energy Transfer .....	10
1.4.1. Energy Transfer Mechanisms in Light Harvesting systems .....	13
1.4.2. Literature Examples of Light Harvesting Systems.....	20
1.5 Tetrastaryl- Bodipy dyes and Knoevenagel condensation reaction .....	26
<b>CHAPTER 2</b> .....	30
<b>EXPERIMENTAL</b> .....	30
2.1. General.....	30
2.2. Syntheses .....	31
2.2.1. Synthesis of Compound 29 .....	31
2.2.2. Synthesis of Compound 30 .....	32
2.2.3. Synthesis of Compound 32 .....	32
2.2.4. Synthesis of Compound 35 .....	33
2.2.5. Synthesis of Compound 36 .....	34
2.2.6. Synthesis of Compound 37 .....	35
2.2.7. Synthesis of Compound 39 .....	36
2.2.8. Synthesis of Compound 40 .....	38
2.2.9. Synthesis of Compound 41 .....	39
<b>CHAPTER 3</b> .....	42
<b>RESULTS and DISCUSSION</b> .....	42

<b>CHAPTER 4</b> .....	54
<b>CONCLUSION</b> .....	54
<b>REFERENCES</b> .....	55
<b>APPENDIX A</b> .....	59
<b>NMR SPECTRA</b> .....	59
<b>APPENDIX B</b> .....	76
<b>MASS SPECTRA</b> .....	76

## LIST OF FIGURES

Figure 1. Comparison between molecular and supramolecular chemistry according to Lehn ..	2
Figure 2. Physical deactivation pathways of excited state .....	3
Figure 3. Structures of some fluorescent substances in literature .....	4
Figure 4. Jablonski Diagram .....	5
Figure 5. Graphical representation of Stokes' shift.....	5
Figure 6. Application areas and chemistry of BODIPY.....	7
Figure 7. Structures of some selective BODIPY-based chemosensors in literature .....	8
Figure 8. Structures of some Photosensitizers for photodynamic therapy in literature .....	9
Figure 9. Structures of some molecular logic gates in literature.....	10
Figure 10. Schematic representation of Light-harvesting antenna system .....	11
Figure 11. Schematic representation Light-harvesting antenna system.....	11
Figure 12. Schematic view of antenna system in purple bacteria. ....	12
Figure 13. Schematic representation Dexter-type (through-bond) energy transfer .....	13
Figure 14. Representation of exchange of electrons in Dexter-type energy transfer.....	14
Figure 15. Structure of some Molecular photonic wire in literature .....	15
Figure 16. Structure of Dexter type of energy transfer cassettes having different number of donor groups in literature .....	16
Figure 17. Schematic representation Förster-type (through-space) energy transfer .....	17
Figure 18. Representation of exchange of electrons in Förster-type energy transfer .....	17
Figure 19. Representation of artificial antenna system showing the form of slipped-cofacial array of chromophores .....	21
Figure 20. Structure of Cascade type energy transfer system in literature .....	22
Figure 21. Structure of Förster-type of light harvesting dendrimer in literature.....	23
Figure 22. Representation of self-assembling Förster-type energy transfer system from literature .....	24
Figure 23. Representation of self-assembling Förster-type energy transfer system from literature .....	25
Figure 24. Structures of Tetramethyl- and pentamethyl-Bodipy derivatives with relevant <sup>1</sup> H NMR chemical shifts in CDCl <sub>3</sub> .....	26
Figure 25. Structures of mono-, di-, tri-, and tetrasteryl-Bodipy derivatives of a compound from literature.....	27

Figure 26. <sup>1</sup> H NMR spectra and structures of distyryl (top) and the tetrasteryl-Bodipy (bottom).....	28
Figure 27. Example of Knoevenagel reaction from literature.....	29
Figure 28. Synthesis of compound <b>29</b> .....	31
Figure 29. Synthesis of Compound <b>30</b> .....	32
Figure 30. Synthesis of Compound <b>32</b> .....	33
Figure 31. Synthesis of Compound <b>35</b> .....	34
Figure 32. Synthesis of Compound <b>36</b> .....	35
Figure 33. Synthesis of Compound <b>37</b> .....	36
Figure 34. Synthesis of Compound <b>39</b> .....	37
Figure 35. Synthesis of Compound <b>40</b> .....	39
Figure 36. Synthesis of Compound <b>41</b> .....	41
Figure 37. Schematic view of energy transfer in Cassestte 1.....	43
Figure 38. Schematic view of energy transfer in Cassestte 2.....	44
Figure 39. Absorption spectrum of compounds <b>36</b> , <b>37</b> and <b>39</b> .....	45
Figure 40. Emission spectrum of compounds <b>36</b> , <b>37</b> and <b>39</b> .....	45
Figure 41. Excitation spectrum of compounds <b>40</b> and <b>41</b> .....	48
Figure 42. Absorption spectrum of compounds <b>36</b> , <b>39</b> and <b>40</b> .....	49
Figure 43. Emission spectrum of compounds <b>36</b> , <b>39</b> and <b>40</b> .....	50
Figure 44. Absorbance spectrum of compounds <b>37</b> , <b>39</b> and <b>41</b> .....	51
Figure 45. Emission spectrum of compounds <b>37</b> , <b>39</b> and <b>41</b> .....	51
Figure 46. <sup>1</sup> H NMR spectrum of compound <b>29</b> .....	59
Figure 47. <sup>13</sup> C NMR spectrum of compound <b>29</b> .....	60
Figure 48. <sup>1</sup> H NMR spectrum of compound <b>30</b> .....	61
Figure 49. <sup>1</sup> H NMR spectrum of compound <b>32</b> .....	62
Figure 50. <sup>13</sup> C NMR spectrum of compound <b>32</b> .....	63
Figure 51. <sup>1</sup> H NMR spectrum of compound <b>35</b> .....	64
Figure 52. <sup>13</sup> C NMR spectrum of compound <b>35</b> .....	65
Figure 53. <sup>1</sup> H NMR spectrum of compound <b>36</b> .....	66
Figure 54. <sup>13</sup> C NMR spectrum of compound <b>36</b> .....	67
Figure 55. <sup>1</sup> H NMR spectrum of compound <b>37</b> .....	68
Figure 56. <sup>13</sup> C NMR spectrum of compound <b>37</b> .....	69
Figure 57. <sup>1</sup> H NMR spectrum of compound <b>39</b> .....	70
Figure 58. <sup>13</sup> C NMR spectrum of compound <b>39</b> .....	71

Figure 59. $^1\text{H}$ NMR spectrum of compound <b>40</b> .....	72
Figure 60. $^{13}\text{C}$ NMR spectrum of compound <b>40</b> .....	73
Figure 61. $^1\text{H}$ NMR spectrum of compound <b>41</b> .....	74
Figure 62. $^{13}\text{C}$ NMR spectrum of compound <b>41</b> .....	75
Figure 63. ESI-HRMS of compound <b>36</b> .....	76
Figure 64. ESI-HRMS of compound <b>37</b> .....	77
Figure 65. ESI-HRMS of compound <b>39</b> .....	78
Figure 66. MALDI-MS of compound <b>40</b> .....	79
Figure 67. MALDI-MS of compound <b>41</b> .....	80

## LIST OF TABLES

Table 1. Photophysical properties of compounds .....	47
Table 2. Lifetimes and FRET efficiencies of compounds.....	52

# CHAPTER 1

## INTRODUCTION

### 1.1. Supramolecular Chemistry

Supramolecular chemistry is ‘chemistry of molecular assemblies and of the intermolecular bond’ as Jean- Marie Lehn stated, who is the one of its leading proponents. He was awarded with the Nobel Prize in 1987 for his studies in this field.<sup>1</sup> Although there are other definitions of this new branch of chemistry including ‘non molecular chemistry’ and ‘the chemistry of non covalent bond’, ‘chemistry beyond the molecule’ stated by J.M. Lehn is accepted definition.<sup>1</sup> Originally, non-covalent interactions between host and guest molecules were studied. However the rapid development in this field over the 25 years has provided in creation of modern supramolecular chemistry field, which includes self organization systems, self assembly, molecular recognition, molecular devices and machines. Now, supramolecular chemistry is an interdisciplinary field in terms of synthetic work and application fields. In that sense, inorganic and organic chemistry are used in the synthesis of target compounds and physical chemistry helps to characterize and explore the features of supramolecular systems.<sup>1</sup>

Supramolecular chemistry has many application areas including cation binding hosts, anion binding, ion pair receptors, solid-state inclusion compounds, crystal engineering, network solids, self-assembly, molecular devices, biological mimics, supramolecular catalysis, interfaces and liquid assemblies, and nanochemistry. Natural ionophores such as enniatins, valinomycin can be mimicked and modeled by supramolecular chemists and these artificial ionophores can selectively exhibit complexation with alkali metal cations, the most of the *s*, *p* *d* and *f* block metals and also nonmetallic cations such as organic ammonium salts and  $\text{NH}_4$ .<sup>1,2,3</sup> Solution-state inclusion chemistry is being used in important applications containing separation of mixtures of closely related compounds and enantiomers, storage of gases and toxic substances, stabilization of reactive compounds, slow release of drugs under physiological conditions. Self-assembled structures were synthesized to simplify chemical

syntheses as much as possible.<sup>4</sup> Molecular machines composed of units that carry certain functions for a beneficial task were successfully synthesized and studied. These systems have predefined task as V. Balzani mentioned ‘A machine, or device, differs from a chemical substance in that it is useful for what it *does*, rather than for what it *is*.<sup>5</sup> To mimic the structure or function of complex biological agents such as enzymes, DNA,<sup>6, 7</sup> artificial supramolecular systems were used.<sup>8</sup> Light harvesting energy transfer cassettes,<sup>9, 10</sup> sensitizers for solar cells<sup>11,12</sup> and chemical logic elements<sup>13,14</sup> are being studied under the hot topics of supramolecular chemistry.

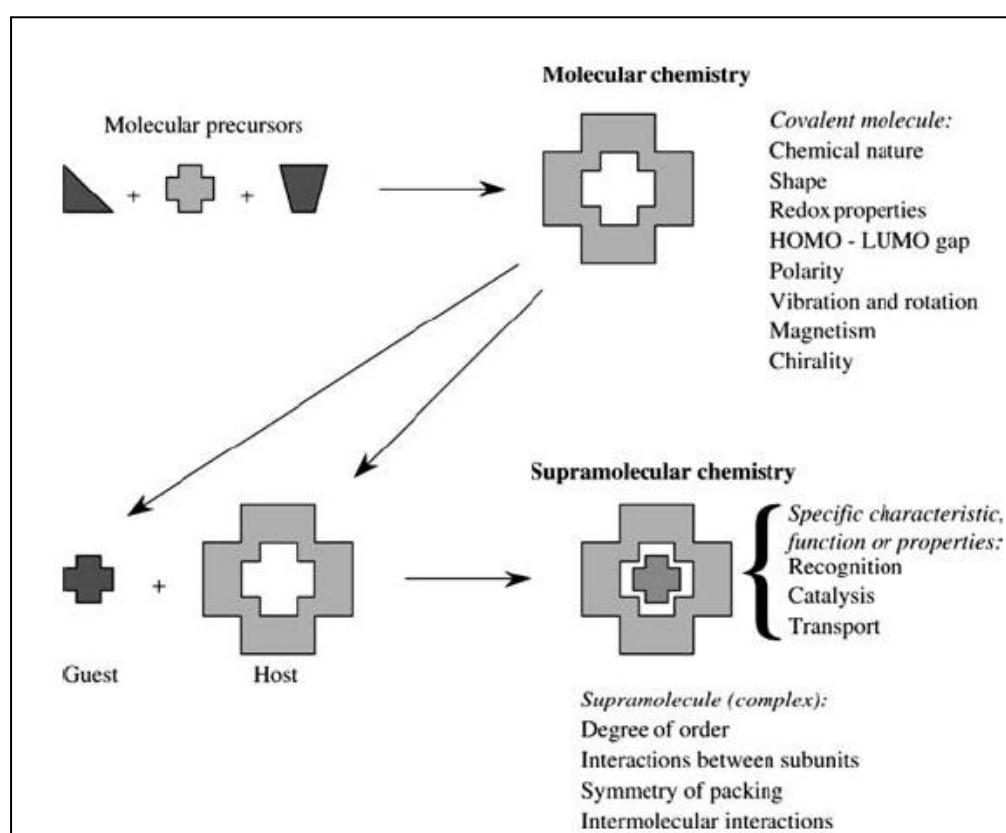


**Figure 1.** Comparison between molecular and supramolecular chemistry according to Lehn<sup>1</sup>

For most of the supramolecular models mentioned above, nature is the source and scientist tries to mimic natural processes in biological systems. Supramolecular chemistry and nanotechnology intersects at molecular level to achieve macroscopic functions of biological systems.

## 1.2. Fundamentals of Fluorescence

All photochemical and photophysical processes start with the absorption of a photon of visible or ultraviolet radiation. This radiation leads the formation of an electronically-excited state in molecules.<sup>15</sup> After excitation of electrons in a molecule, electronically excited molecule goes to ground state through a variety of relaxation pathways which can be intramolecular or intermolecular processes (figure 2). In intramolecular processes, there are radiative and radiationless transitions. Luminescence is a radiative transition, which involves the emission of electromagnetic radiation as excited molecule relaxes the ground state. It has two different categories depending on relaxation process between electronic states; fluorescence and phosphorescence. In radiationless transition, there is no emission of electromagnetic radiation in deactivation process.

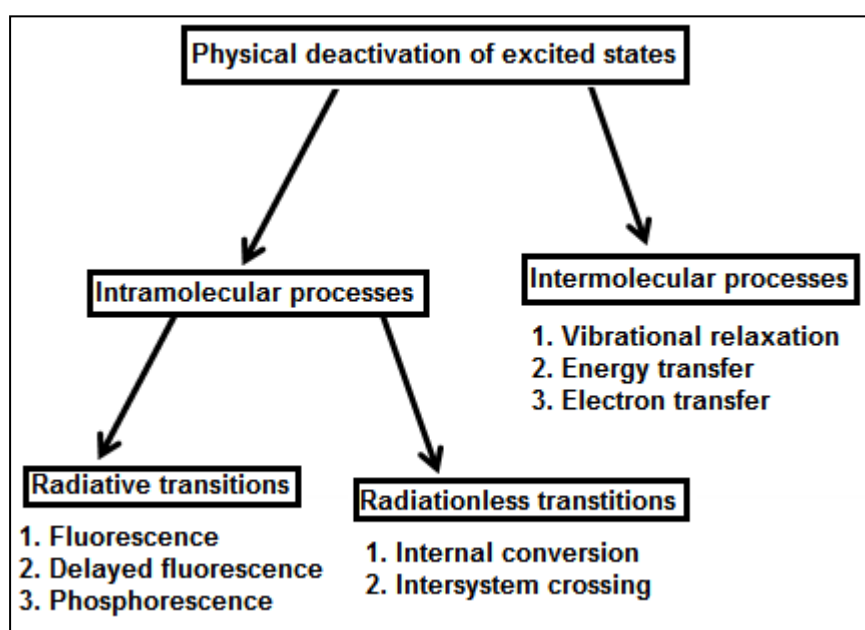


**Figure 2.** Physical deactivation pathways of excited state

Fluorescence is a radiative transition from excited state to the ground state of molecule, and it is a spin allowed process because transition occurs between the same spin multiplicities. As a result of strongly allowed transition between energy states, fluorescence has relatively short lifetimes in order of picoseconds to microseconds. Lifetime of a fluorophore is described as the average time that passes in excitation and relaxation to the

ground state. In phosphorescence, there is a spin forbidden radiative transition between different multiplicity states usually from vibrational level of the lowest excited triplet state,  $T_1$  to ground state,  $S_0$ . Because of this forbidden transition, it has relatively lower lifetimes in order of milliseconds to seconds. Some of the fluorescent molecules in literature are shown in figure 3.

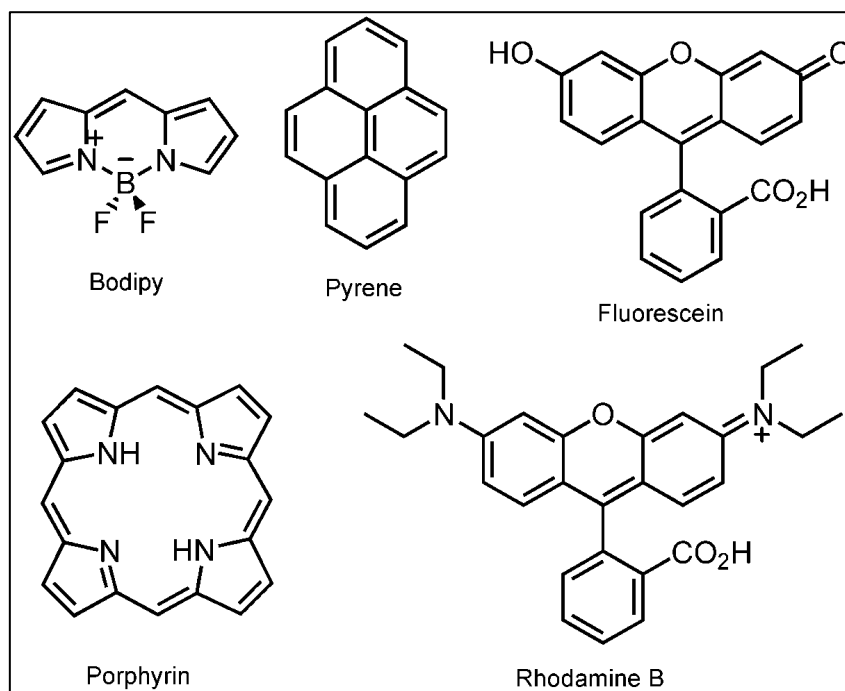


**Figure 3.** Structures of some fluorescent substances in literature

There are radiationless transitions which are internal conversion and intersystem crossing. If the transition occurs from singlet excited state to triplet excited state which is a forbidden transition, the transition is called intersystem crossing. Heavy atoms like bromine and iodine causes intersystem crossing. For the internal conversion, there is transition between excited states,  $S_2$  to  $S_1$ . Internal conversion has much more faster transition than intersystem crossing.

Jablonski diagram represents the properties of excited state and their relaxation process (figure 4). In Jablonski diagram, it is seen that energy of emission is smaller than energy of absorption. As a result, fluorescence occurs at higher wavelength and this is called as Stokes' shift (figure 5). The reason of Stokes' shift is rapid decay of excited electron to the

vibrational level of  $S_1$ . Excess vibrational energy is lost due to the decay to the higher vibrational levels of  $S_0$ . Stokes' shift is affected by solvent, complex formation, and energy transfer.

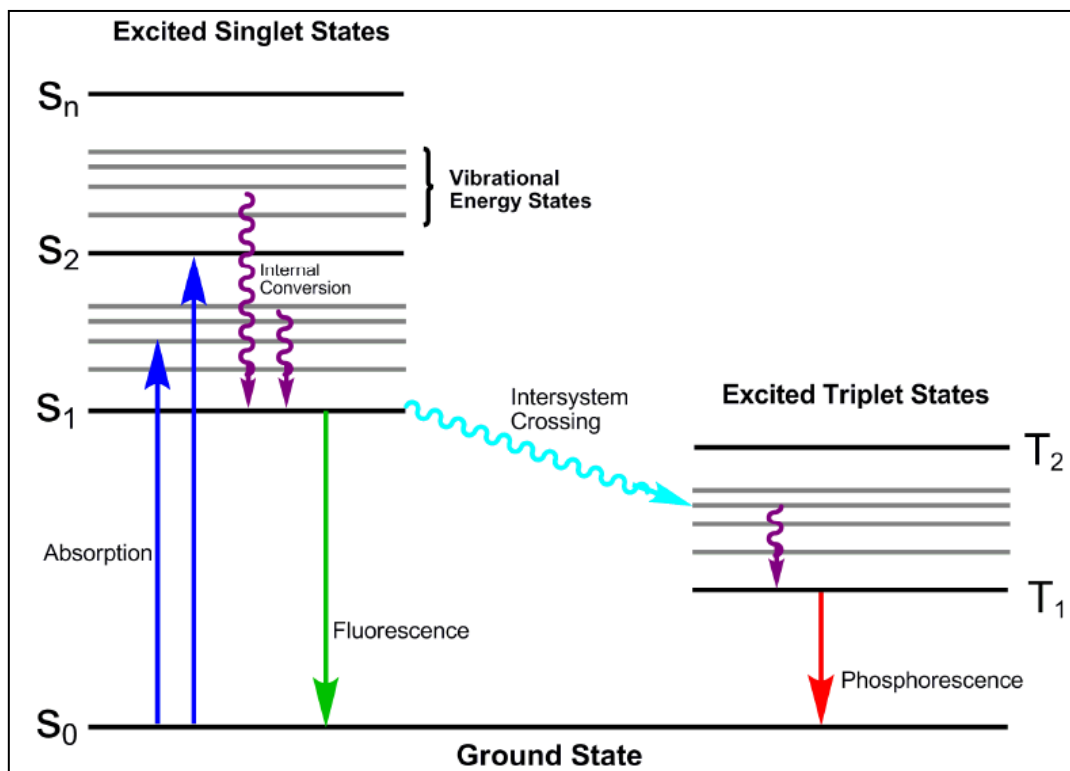


Figure 4. Jablonski Diagram

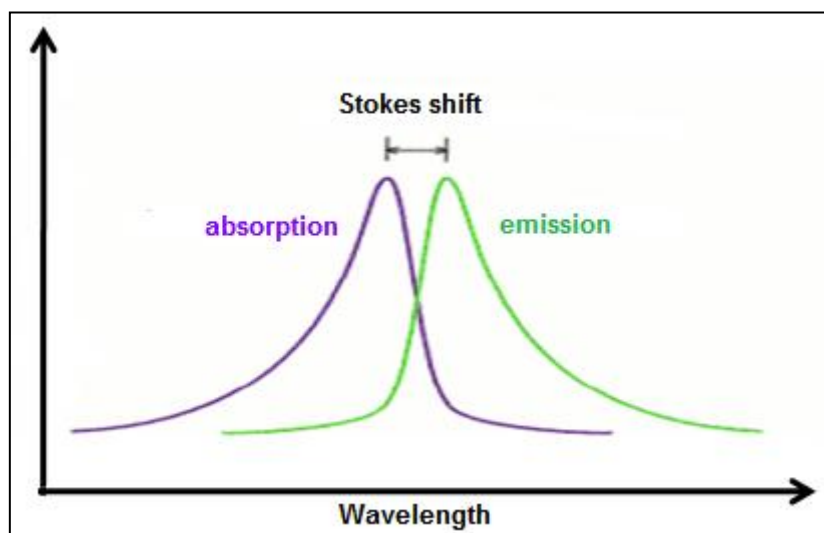


Figure 5. Graphical representation of Stokes' shift

Quantum yield is an important property of a fluorophore and it is used to compare different fluorophores in terms of fluorescence character. Quantum yield is the ratio of photons emitted to the photons absorbed. When there is much smaller non-radiative decay compared to radiative decay, quantum yield approaches the unity. To calculate quantum yield of a molecule, standard samples are used such as Rhodamine 6G,<sup>16</sup> rhodamine 101,<sup>17</sup> cresyl violet,<sup>18</sup> fluorescein,<sup>19</sup> and zinc phthalocyanine<sup>20</sup>. The selection criterion for a standard sample is that it should have similar absorption to the compound that is measured.

### 1.3. BODIPY Dyes

Many improvements were progressed with the help of fluorescent probes in biological imaging techniques. Fluorescent probes can be attached to the biological molecules such as antibodies and biological molecules can be observed inside living cells.<sup>21-23</sup> Many fluorescent probes were published in literature but there are limited fluorescent probes for biological imaging. For example, there are few probes that emit light at 800 nm or above at which the tissues are most transparent to light.<sup>24</sup> Among these limited fluorescent probes, the difluoroborindacene family (4,4-difluoro-4-borata-3a-azonia-4a-aza-s-indacene, abbreviated as BODIPY) has acquired popularity as being one of the most versatile fluorophores. BODIPY was first reported by Treibs and Kreuzer in 1968.<sup>25</sup> Till 1980, little attention was given to that dye but since 1980 the potential use of this fluorescent dye in biological labeling was recognized, and several new Bodipy-based compounds were synthesized and commercialized for biological labeling.<sup>26-28</sup> Now, BODIPY is being used in a wide range of fields such as biomolecular labeling,<sup>29,30</sup> ion sensing,<sup>31-33</sup> drug delivery systems, chemical logic gates,<sup>34-36</sup> light harvesting systems,<sup>37</sup> DSSC and photodynamic therapy<sup>38</sup>.

BODIPY has high fluorescence quantum yields and molar extinction coefficients. They also have excellent thermal and photochemical stability. They are stable to physical conditions because they have low sensitivity to pH and solvent polarity. Simple synthesis methods, good solubility in organic solvents, intense absorption band and negligible transition to triplet state are the other advantages of BODIPY dyes.<sup>24</sup> BODIPYs' photophysical properties such as emission and excitation wavelengths can be tuned via easy modification. Especially, functionalization of 1-3 and 5-7 positions extends the conjugation, which provides the tuning in visible spectrum (figure 6). Different functional units can also be attached to the



and emission wavelengths of BODIPY can be tuned with modifications. Akkaya research group published red-emitting BODIPY-based chemosensors<sup>39-41</sup> and some literature examples of chemosensors,<sup>39-43</sup> are shown in figure 7.

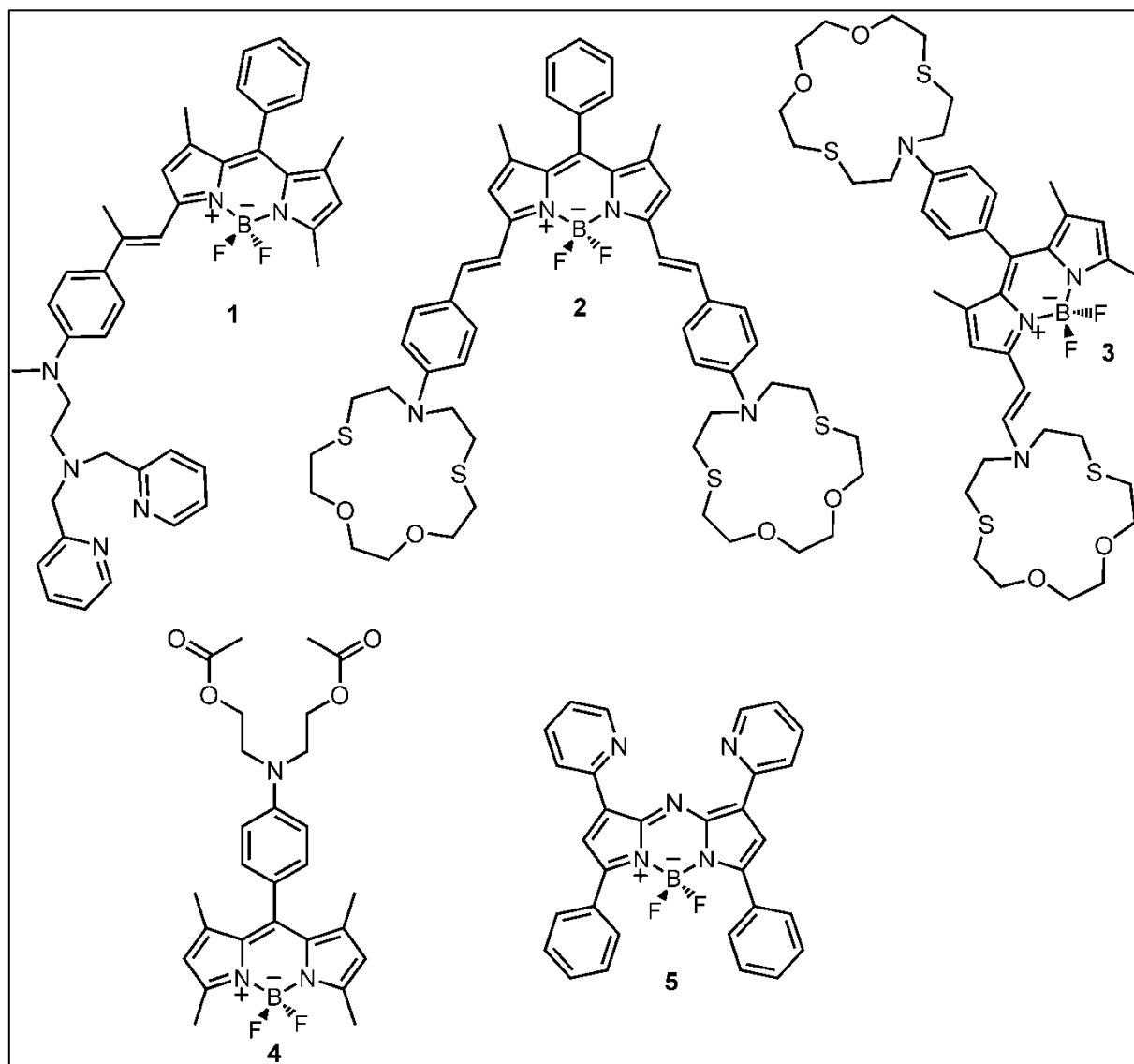


**Figure 7.** Structures of some selective BODIPY-based chemosensors in literature

Photodynamic therapy used for the treatment age related macular degeneration and tumors is another application area of BODIPY dyes. The treatment needs a combined application of red to near IR light and a sensitizer which produces singlet oxygen that kills tumor tissues. In examples (figure 8), published by Akkaya's research group, heavy atom such as Br or I are attached to 2 and 6 position of BODIPY, and these heavy atoms causes

intersystem crossing thus increase the triplet yield of dyes resulting with singlet oxygen generation.<sup>44,45</sup> Quantum yield decreases significantly in case of intersystem crossing. In compound 6, quantum yield decreases from 0.70 to 0.02 and high efficiency of singlet oxygen generation was measured.<sup>44</sup> In second example, conjugation from 3 and 5 positions is extended by condensation reaction and this conjugation provides emission at longer wavelength, 650-680 nm compared to peripheral BODIPY which has absorption at about 500 nm.<sup>45</sup>

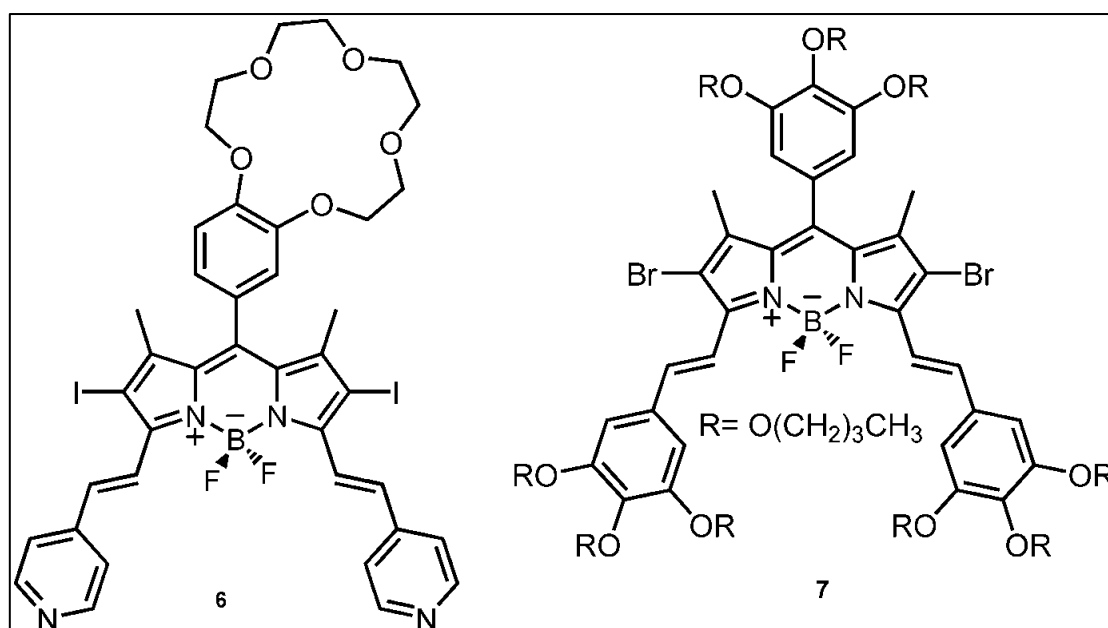


**Figure 8.** Structures of some Photosensitizers for photodynamic therapy in literature

Molecular logic gates try to mimic logic functions using molecules. In conventional computers, data processing is based on silicon circuitry, and it has binary encoding of information in electrical signals. However binary logic is a general concept and can be applied to any type of signal such as chemical and optical ones. Fluorescent molecules such as BODIPY have been promising for the realization of digital processing and they accomplished a range of molecular logic gates systems such as YES, NOT, AND, OR that each involves chemical input(s) and emitted light as an output. These logic elements can be combined with other applications such as photodynamic therapy, drug delivery. Many examples of logic elements shown in figure 9 were published by different research groups.<sup>34-36</sup>

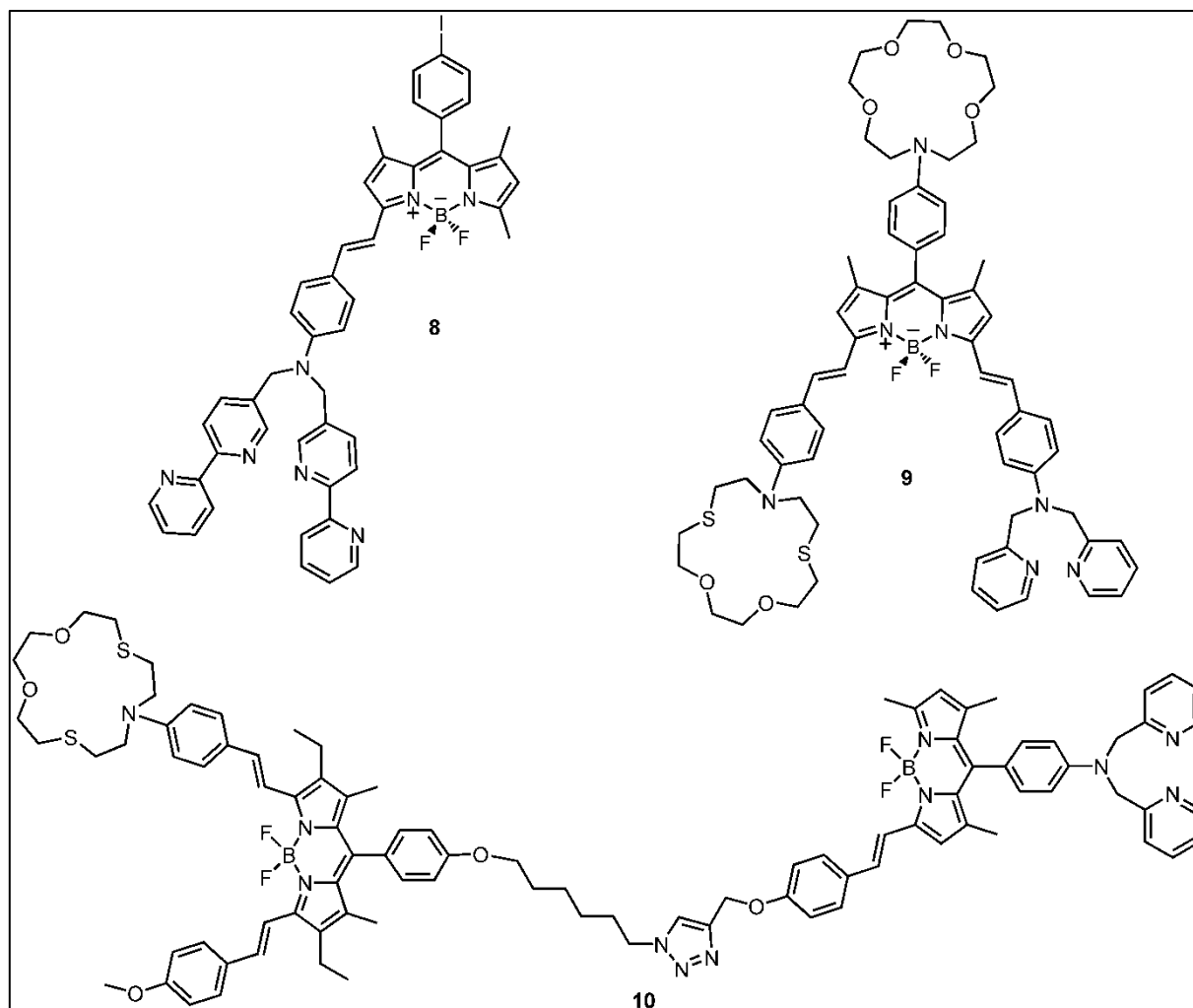


**Figure 9.** Structures of some molecular logic gates in literature

Addition to these areas, BODIPY is being used in many other areas containing solar cells, liquid crystals, DNA labeling.<sup>29,30,38</sup> These application areas and examples show that BODIPY chemistry have high versatility. Applications to light harvesting energy transfer cassettes were discussed in following sections.

#### 1.4. Light Harvesting and Energy Transfer

Light harvesting antenna system is being used in photosynthesis process. In chlorophyl, there are light harvesting chromophores that effectively collect sunlight and absorbed energy is channeled to a single reaction center. In nature, this system is used to

accomplish the light-harvesting efficiency problem.<sup>46</sup> Figure 10 and figure 11 show different representation of light harvesting systems. In first system, there are donor groups (D) at outside absorbing light at a specific wavelength than absorbed sunlight is transferred to inner donor groups, and final destination of absorbed sunlight is acceptor unit (A), core. As a result, much more concentrated energy is collected in the core.

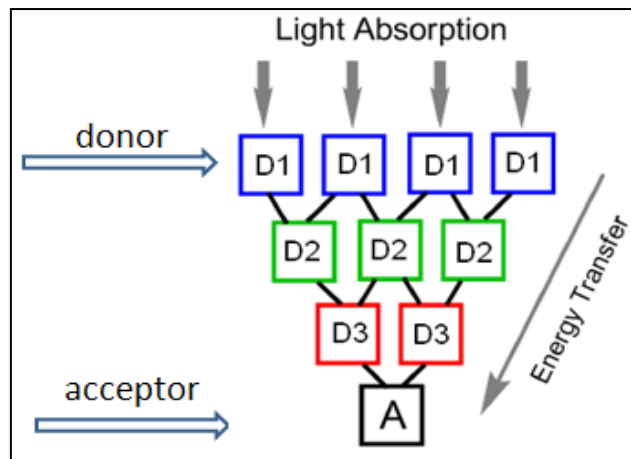


**Figure 10.** Schematic representation of Light-harvesting antenna system

In second light harvesting system, figure 11, there are different donor groups absorbing light at different wavelengths, and donor groups directly transfer this absorbed energy to the acceptor group. As a result, sunlight is tuned over a wide range by collecting light at different wavelengths, and energy is concentrated in the core.

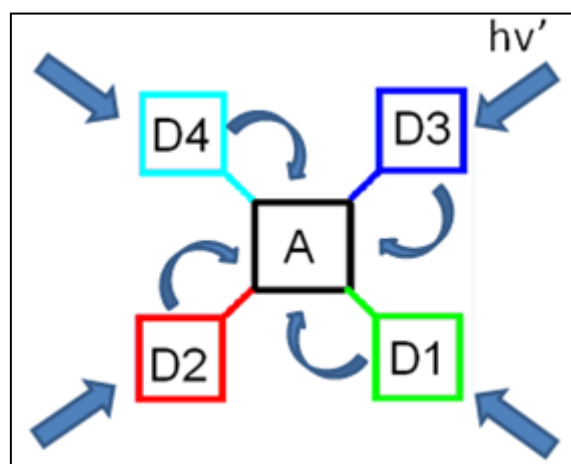


**Figure 11.** Schematic representation Light-harvesting antenna system

Photosynthetic purple bacteria is the most widely studied example of natural light harvesting antenna system.<sup>46</sup> Antenna system of photosynthetic purple bacteria has approximately 250 chlorophyll (BChl *a*) pigments and carotenoids having slightly different spectroscopic properties.<sup>46</sup> Figure 12 shows the representation of antenna system in purple bacteria. In this antenna system, there are donor groups called LH-II at outside which absorbs sunlight and they transfer this absorbed energy to the LH-I. LH-I surrounds inner reaction center and it gives this energy to the inner reaction center. Reaction takes place with this transferred energy. As a result of femtosecond energy transfer between LH units, absorbed energy is channeled to single reaction center which initiates the redox process leading to generation of proton gradient and release of oxygen at the end.<sup>47</sup> Most purple bacteria have LH-I, LH-II complexes and reaction center, but not all have LH-III complex.<sup>46</sup>

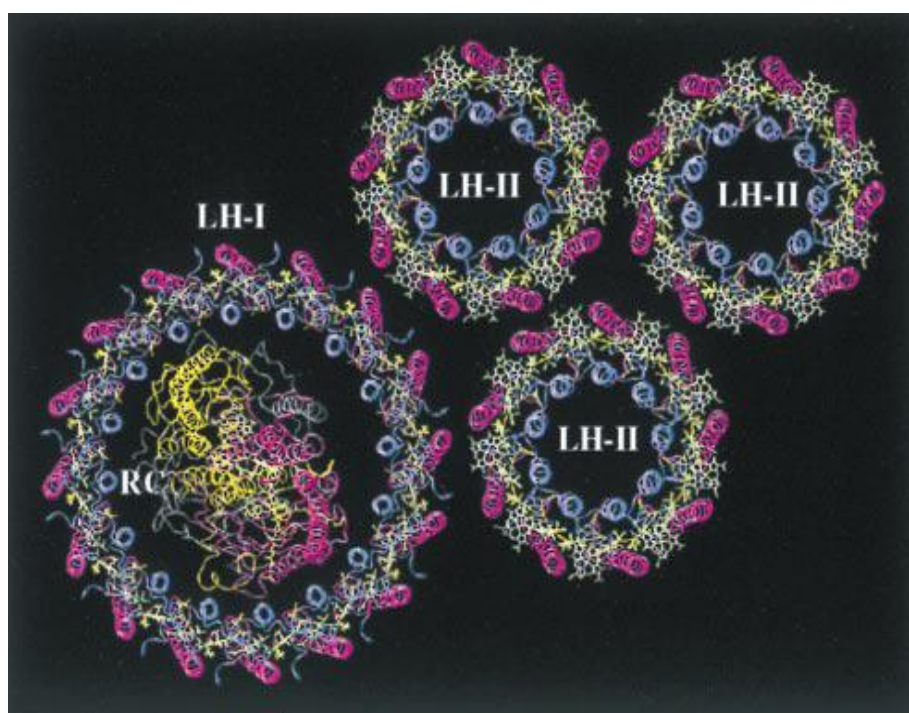


**Figure 12.** Schematic view of antenna system in purple bacteria.<sup>46</sup>

Artificial light harvesting antenna systems can be designed and synthesized with the assistance of supramolecular systems. These models can be used in light emitting diodes,<sup>48</sup> signal amplifiers,<sup>49</sup> and DSCC<sup>50</sup>. There are three important parameters to observe the antenna effect in artificial supramolecular models, dimensions of time, energy and space.<sup>51</sup> Energy transfer must occur to the other unit before having radiative or non-radiative deactivation of

donor part for the time dimension. The energy of the acceptor in excited state should be lower or equal to the energy of donor in excited state for energy dimension. Also, overall excitation energy transfer direction should be towards a selected component of system, which is space dimension. In light harvesting antenna systems, there are different type of energy transfer mechanisms; Dexter and Förster type of energy transfers.

### 1.4.1. Energy Transfer Mechanisms in Light Harvesting systems

Simple energy transfer cassette is composed of donor (D) and acceptor (A) chromophores. In energy transfer process, energy is transferred from excited chromophore of donor species to the acceptor, chromophore, which is in its ground state. Donor part is excited via light source at the absorption wavelength of donor group. When excited donor group returns to the ground state, it gives its energy to the acceptor group and acceptor group is excited with this energy. This energy transfer may occur through bond (Dexter-type)<sup>50</sup> or through space (Förster-type)<sup>51,52</sup>, which are theoretically confirmed and experimentally proved. Using different approaches, energy transfer type and efficiency can be detected and calculated. These approaches are comparison of relative lifetimes, quantum yields, and decrease in donor emission or enhancement in acceptor emission.

#### 1.4.1.1. Dexter-type Energy Transfer

In this type of energy transfer, there is conjugation between donor and acceptor units (figure 13). Therefore energy transfer is through bond. Orbital overlap is the key parameter for energy transfer between units. However, orbital overlap requirement for energy transfer restricts the energy transfer to very short distances usually less than  $10\text{\AA}$ . Also, the structure of donor, acceptor and linker units, the orientation of donor and acceptor units affect the energy transfer rate.

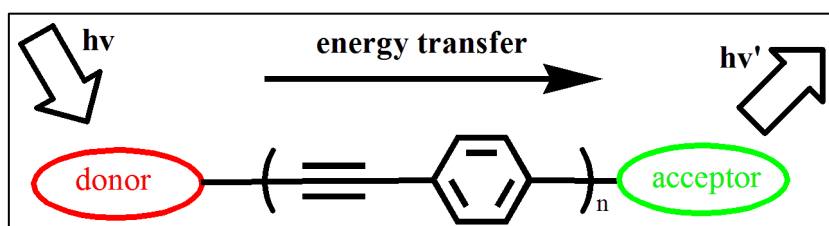


**Figure 13.** Schematic representation Dexter-type (through-bond) energy transfer

Figure 14 shows the representation of electrons in HOMO-LUMO of donor and acceptor units in Dexter-type energy transfer. When donor group electron is excited, its electron goes LUMO of donor group and from LUMO of donor, this excited electron goes to LUMO (excited state) of acceptor group. At the same time, electron of acceptor group at HOMO goes HOMO of donor group. As a result, there are simultaneous exchanges of electrons between HOMO-LUMO of donor and acceptor groups. In this type of conjugated energy transfer cassettes, it is not possible to measure or calculate how much energy is transferred via through bond mechanism and how much is transferred through space mechanism.

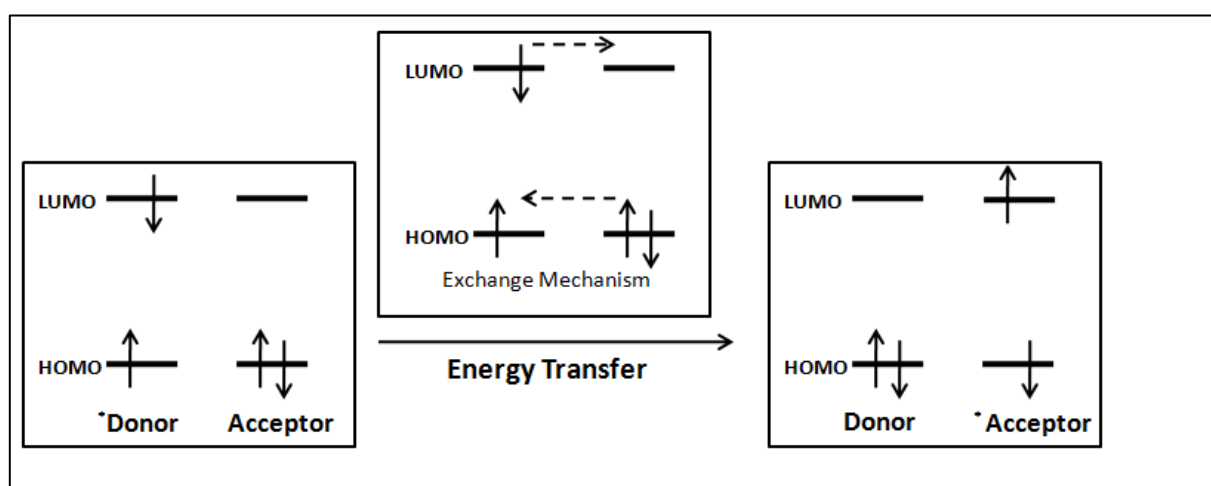


**Figure 14.** Representation of exchange of electrons in Dexter-type energy transfer

Energy transfer rate constant can be calculated the formula shown below.

$$k_{ET} = K J \exp(-2R_{DA} / L) \quad (1)$$

where K is orbital interaction, J represents the overlap integral between donor emission and acceptor absorbance,  $R_{DA}$  is the donor acceptor separation and L is the van der Waals radii.<sup>55</sup> As donor-acceptor separation increases, energy transfer rate constant decreases.

Different energy transfer cassettes were designed and synthesized in literature. Lindsey and coworkers published an interesting example of energy transfer cassette, compound 11, having Dexter-type of energy transfer mechanism (figure 15).<sup>56</sup> In this

example, they synthesized a linear molecular photonic wire composed of BODIPY as donor chromophore, three Zn-porphyrins as transmission and free base porphyrin as acceptor chromophore. When there is Zinc ion in first two porphyrins, transferred energy is emitted from last porphyrin, non-metalated one, (compound 11) but when there is Mg in last porphyrin, transferred energy is emitted from third porphyrin which has no ion, free one (compound 12). The distance between donor and acceptor is 90 Å. Upon excitation at 485 nm, which is the absorption wavelength of donor, there is efficient energy transfer from donor to acceptor and energy transfer efficiency is 76 %.

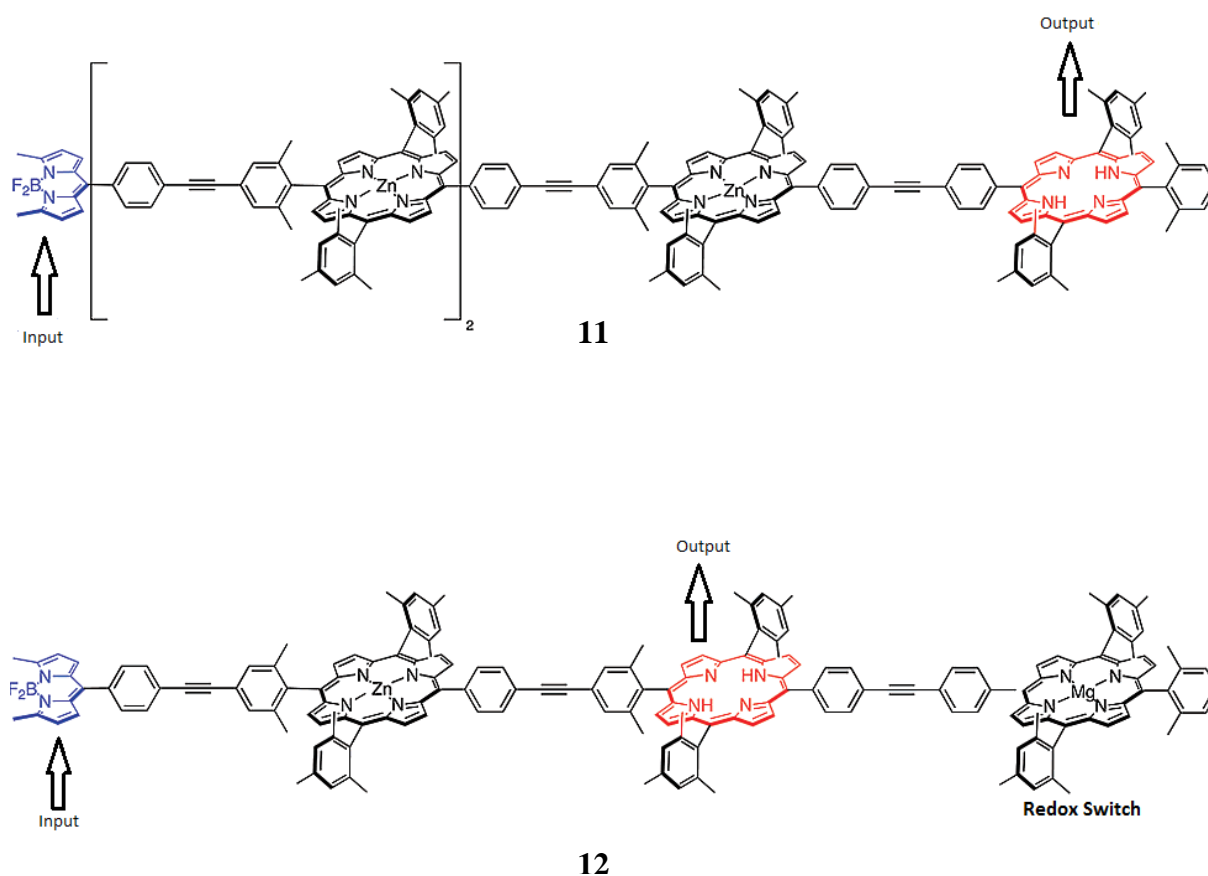


**Figure 15.** Structure of some Molecular photonic wire in literature

In other literature example of Lindsey and coworkers, they studied the effect of number of donor groups on energy transfer efficiency.<sup>57</sup> Figure 16 shows energy transfer cassettes having different number of donor groups. All cassettes have the same acceptor group but the first one has one donor, the second one has two donor groups, and the last one has eight donor groups. In these cassettes, as number donor groups increases, energy transfer

efficiency increases from 68 to 94% for free porphyrin and it increases from 91 to 99% for Zn-porphyrins.<sup>57</sup>

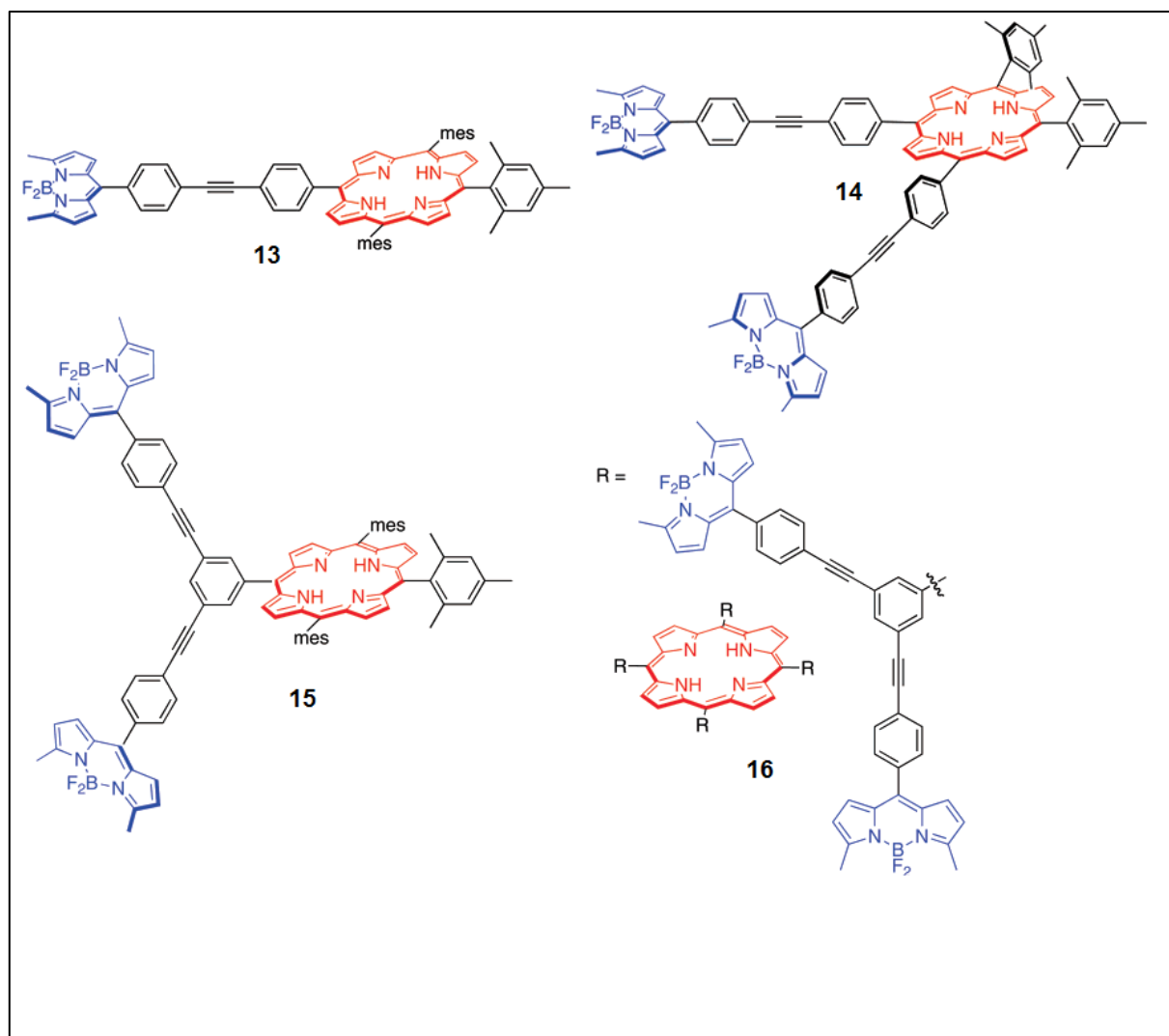


**Figure 16.** Structure of Dexter type of energy transfer cassettes having different number of donor groups in literature

#### 1.4.1.2. Förster-type Energy Transfer

In contrast to Dexter-type energy transfer, there is no conjugation between donor and acceptor units in Förster-type energy transfer systems (figure 17).<sup>58</sup> Therefore, energy transfer is through space which actually is linked to long-range dipole-dipole interactions. There is no requirement between donor and acceptor to be connected covalently to each other. There can

be this type of through space energy transfer in self-assembly systems and they are also called Förster-type Energy Transfer.

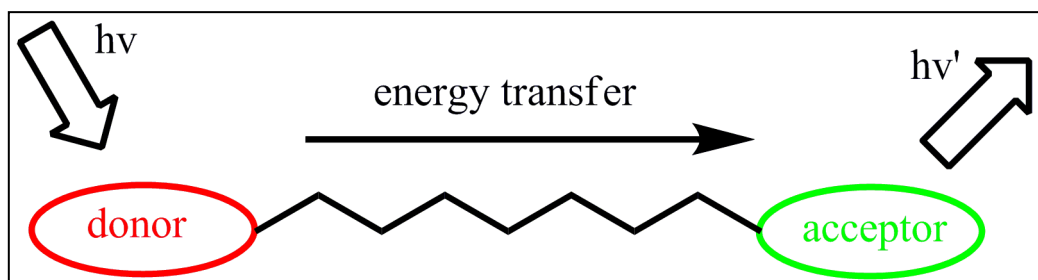


**Figure 17.** Schematic representation of Förster-type (through-space) energy transfer

Figure 18 shows the representation of electrons in HOMO-LUMO of donor and acceptor units in Förster-type energy transfer systems. When donor group electron is excited, it goes to higher level LUMO orbital, at the excited state. When excited electron of donor group goes to ground state, it gives its energy to the acceptor group and acceptor electron is excited with this energy. There is no exchange of electrons. Because of this reason, energy transfer can be made to a farther distance compared to Dexter-type energy transfer systems.

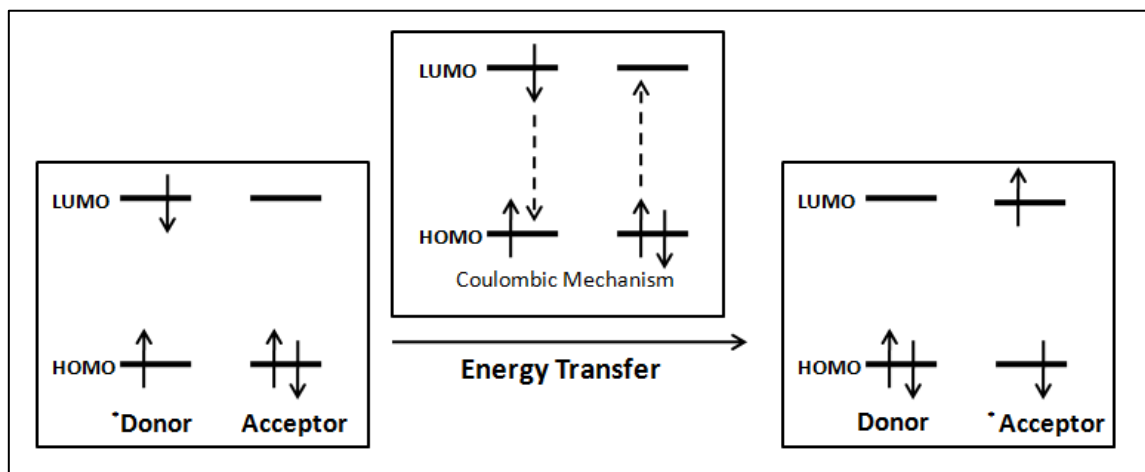


**Figure 18.** Representation of exchange of electrons in Förster-type energy transfer

In this type of energy transfer, the key parameters are the spectral overlap of donor emission and acceptor absorption, the distance between donor and acceptor units and the relative orientation of the transition dipoles.<sup>59</sup> In a simple Förster-type of energy transfer

system having a single pair of donor (D) and acceptor (A) units separated by a distance of  $R$ , energy transfer rate ( $k_{\text{FRET}}$ ) can be expressed in terms of Förster distance ( $R_0$ ) using the equation 2. There may be other deactivation radiative and nonradiative pathways other than energy transfer such as internal conversion. Förster distance,  $R_0$ , can be formulated as below and it is the distance between donor and acceptor units at which half of excited molecules decay by energy transfer (eqn 3).

$$k_{\text{FRET}} = [ 900 (\ln 10) \kappa^2 \Phi_{\text{D}} J(\lambda) ] / [ 128 \pi^5 n^4 N \tau_{\text{D}} R_{\text{DA}}^6 ] \quad (2)$$

$$R_0 = 9.78 \times 10^3 [\kappa^2 n^{-4} Q_{\text{D}} J(\lambda) ] \quad (3)$$

In equation 2 and 3,  $\kappa$  is the orientation factor between excited state donor and ground state acceptor. It is related to dipole-dipole interaction of donor and acceptor units.  $n$  represents the refractive index of the solvent,  $Q_{\text{D}}$  is the quantum yield of donor unit in the absence of acceptor unit,  $J$  is the Förster overlap integral of donor emission and acceptor absorbance,  $\tau_{\text{D}}$  represents lifetime of excited donor in the absence of acceptor unit, and lastly  $R_{\text{DA}}$  is the distance between donor and acceptor. FRET efficiency calculation will be explained in the following part.

#### 1.4.1.2.1. FRET Efficiency Calculation

There are many approaches to calculate Förster energy transfer rate. However, generally, two approaches are being used in calculation: time-resolved and steady state approaches.<sup>59</sup>

In time-resolved approach, time-resolved emission of any acceptor or donor is used. This method gives more accurate results compared to steady state because there is no inner

filter effect or integration error. FRET efficiencies and FRET rate constant can be calculated by using formula given below.

$$k_{\text{FRET}} = 1/\tau_{\text{DA}} - 1/\tau_{\text{D}} \quad (4)$$

$$E = \tau_{\text{D}} k_{\text{FRET}} / (1 + \tau_{\text{D}} k_{\text{FRET}}) \quad (5)$$

where  $k_{\text{FRET}}$  is the FRET rate and  $E$  is the energy transfer efficiency.  $\tau_{\text{D}}$  and  $\tau_{\text{DA}}$  represents the excited state lifetime of donor in the absence and presence of acceptor respectively. FRET efficiency can be calculated more simply using equation stated below.

$$E = 1 - \tau_{\text{DA}}/\tau_{\text{D}} \quad (6)$$

In steady state approach, in contrast to time resolved approach, decrease in donor quantum yield is used. In this method, very dilute solutions should be used in measurement process because there is a problem of self quenching which is the reabsorption of emitted light by the same or other molecules. This problem is also called inner filter effect.<sup>60,61</sup> Energy transfer efficiency can be calculated using equation 7.

$$E = 1 - \Phi_{\text{DA}} / \Phi_{\text{D}} \quad (7)$$

where  $\Phi_{\text{DA}}$  and  $\Phi_{\text{D}}$  represents quantum yield of donor in the presence and absence of acceptor respectively. There is one more equation which is stated below (eqn 8) to calculate energy transfer efficiency in steady state. In this equation, excitation spectra or enhancement in fluorescence emission of the acceptor can be used.

$$E = A_{\text{A}}(\lambda_{\text{D}}) / A_{\text{D}}(\lambda_{\text{D}}) * [I_{\text{AD}}(\lambda_{\text{A}}^{\text{em}}) / I_{\text{A}}(\lambda_{\text{A}}^{\text{em}}) - 1] \quad (8)$$

where  $A_{\text{A}}$  and  $A_{\text{D}}$  is absorbance values of acceptor and donor at the maximum absorbance wavelength of donor.  $I_{\text{AD}}$  and  $I_{\text{A}}$  represent the integrated emission area of acceptor in the presence and absence of donor at  $\lambda_{\text{A}}^{\text{em}}$ . Quantum yield can be calculated using equation 9 stated below.

$$Q = Q_{\text{R}} (I/I_{\text{R}}) * (A_{\text{R}}/A) * (n^2/n_{\text{R}}^2) \quad (9)$$

where  $Q_R$  is quantum yield of reference,  $I$  and  $I_R$  represents integrated area of emission spectrum for specific wavelength for sample and for standard, respectively,  $A$  and  $A_R$  are absorbance of corresponding wavelength for sample and standard,  $n$  and  $n_R$  are the refractive indices of solvents in which sample and standard compounds were dissolved, respectively. Refractive index values were taken as 1.329 for methanol, 1.3624 for ethanol and 1.333 for water. All measurements of the samples except standards were done with chloroform which has an  $n$  value of 1.49.

Förster type of energy systems are being used in many areas of supramolecular chemistry. Some of these areas are artificial antenna systems, cascade systems, fluorescent signaling systems for biological purposes. Some literature examples of Förster type energy transfer systems will be given in next parts.

## **1.4.2. Literature Examples of Light Harvesting Systems**

### **1.4.2.1. Artificial Light Harvesting Antenna Systems**

There are many examples of artificial photosynthetic antenna systems in literature published by different groups because photosynthesis process is one of the most important natural events for plants and humans. Such systems try to mimic the circular arrangement of pigments in LH-II complex of purple bacteria via noncovalent bonds, covalent bonds, or metal coordination bonds.<sup>62-64</sup>

System shown in figure 19 is an interesting example of artificial photosynthetic antenna system.<sup>65</sup> In this system, there are twelve porphyrins which are combined noncovalently to form assembled circular array in which it has maximum separation and this separation is named radius of antenna which is 4.1 nm.<sup>66</sup>

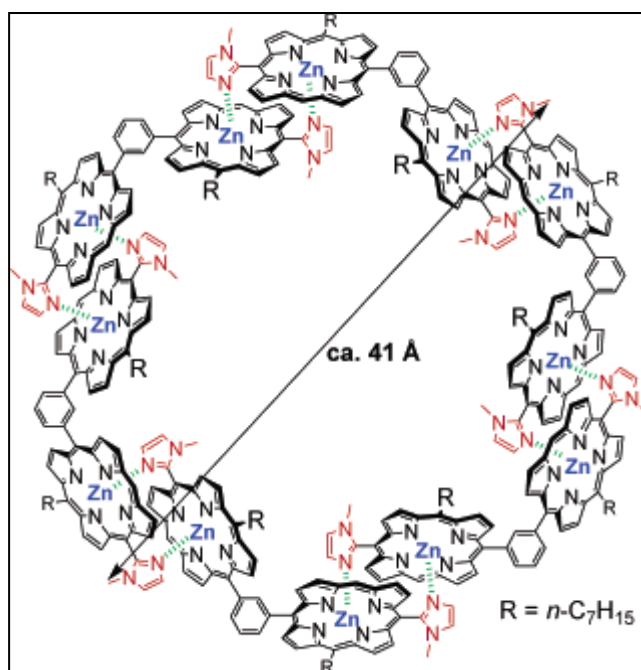


**Figure 19.** Representation of artificial antenna system showing the form of slipped-cofacial array of chromophores.<sup>66</sup>

### 1.4.2.2. Light Harvesting Cascade Systems

Cascade systems are light harvesting energy transfer systems that have many chromophores. They absorb light at different wavelengths from each other and make energy transfer to a final chromophore. Actually, this is the case for photosynthesis process because plants tune and absorb sunlight in wide range of spectrum.

Frechet and his co-workers published an interesting example of cascade energy transfer system (figure 20).<sup>67</sup> This cascade system have three different chromophores which are coumarin 2 (blue) absorbing at 350 nm, fluorol 7GA (green) absorbing at 415 nm, and perylene core (red) absorbing at 555 nm. In this system, there are two different energy transfer pathways which coumarin can make. The first one is energy transfer from coumarin to the perylene core and the second one is energy transfer from coumarin groups to fluorol 7GA units. Also, there is another energy transfer pathways which is energy transfer from fluorol 7GA units to perylene core. The energy transfer from coumarin groups to fluorol 7GA units has the lowest energy transfer efficiency (79%) due to poor spectral overlap between emission of coumarin and absorption of perylene. Other energy transfer efficiencies are 99% from coumarin groups to fluorol 7GA units and 96% fluorol 7GA units to perylene core.

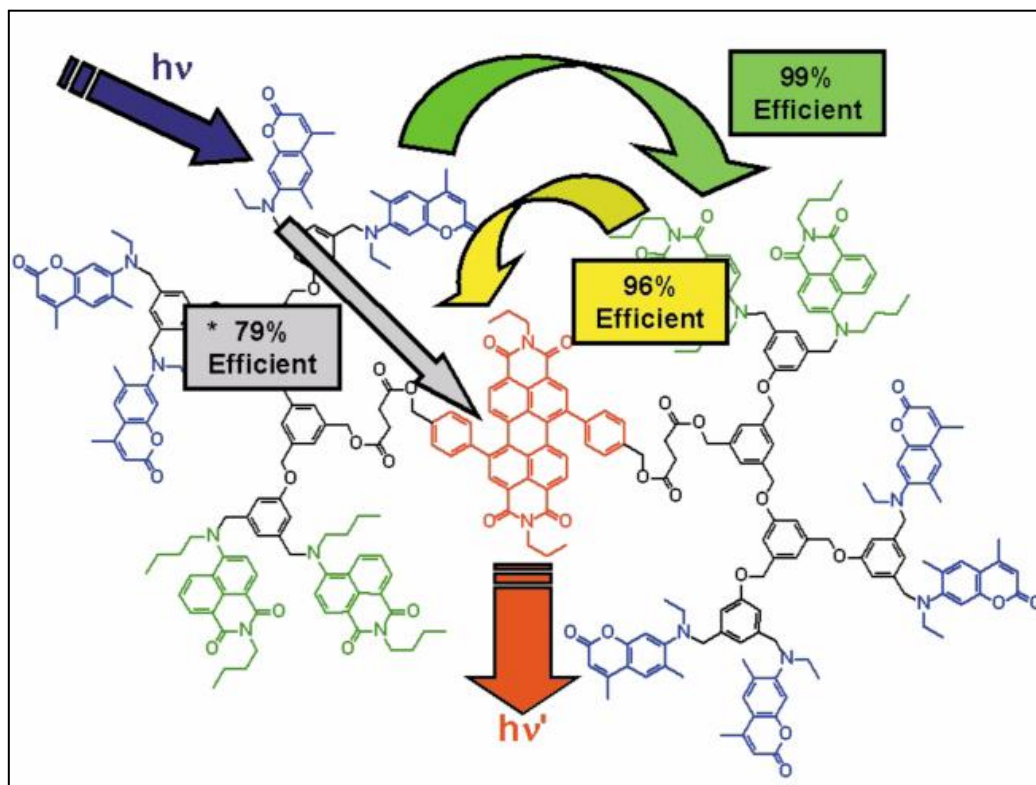


**Figure 20.** Structure of Cascade type energy transfer system in literature<sup>67</sup>

### 1.4.2.3. BODIPY dyes in Light Harvesting Systems

BODIPY dyes can be modified easily and its photophysical properties such as absorption and emission wavelength can be tuned over a wide range via easy modifications. Because of easy modification in photophysical properties, many examples of light harvesting energy transfer systems that use BODIPY dyes as donor or acceptor group were published in literature. Compound 17 was synthesized by Akkaya research group.<sup>68</sup> It has 8 BODIPY groups at the corners as donor group and one perylene diimide (PDI) group as acceptor at the core. Absorption of donor and acceptor groups is shown in absorbance spectrum. Upon excitation of BODIPY donor groups at 526 nm, no emission is observed in emission spectrum at 550 nm which is the emission wavelength of the donor groups. Quenching of emission at that wavelength is the indication of efficient energy transfer (99%) between donor and acceptor groups. Also, there is enhancement in core emission compared to direct excitation of core at 588 nm which is the absorption wavelength of acceptor unit and this is caused by antenna effect.

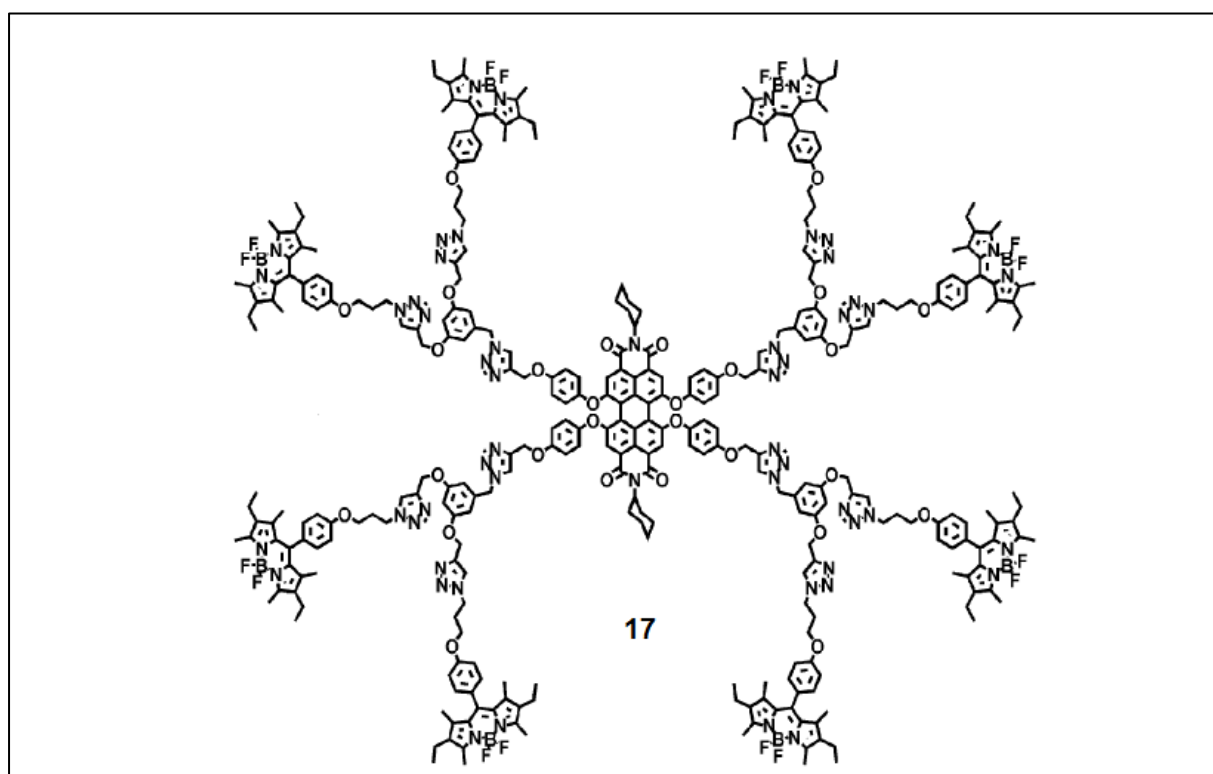


**Figure 21.** Structure of Förster-type of light harvesting dendrimer in literature

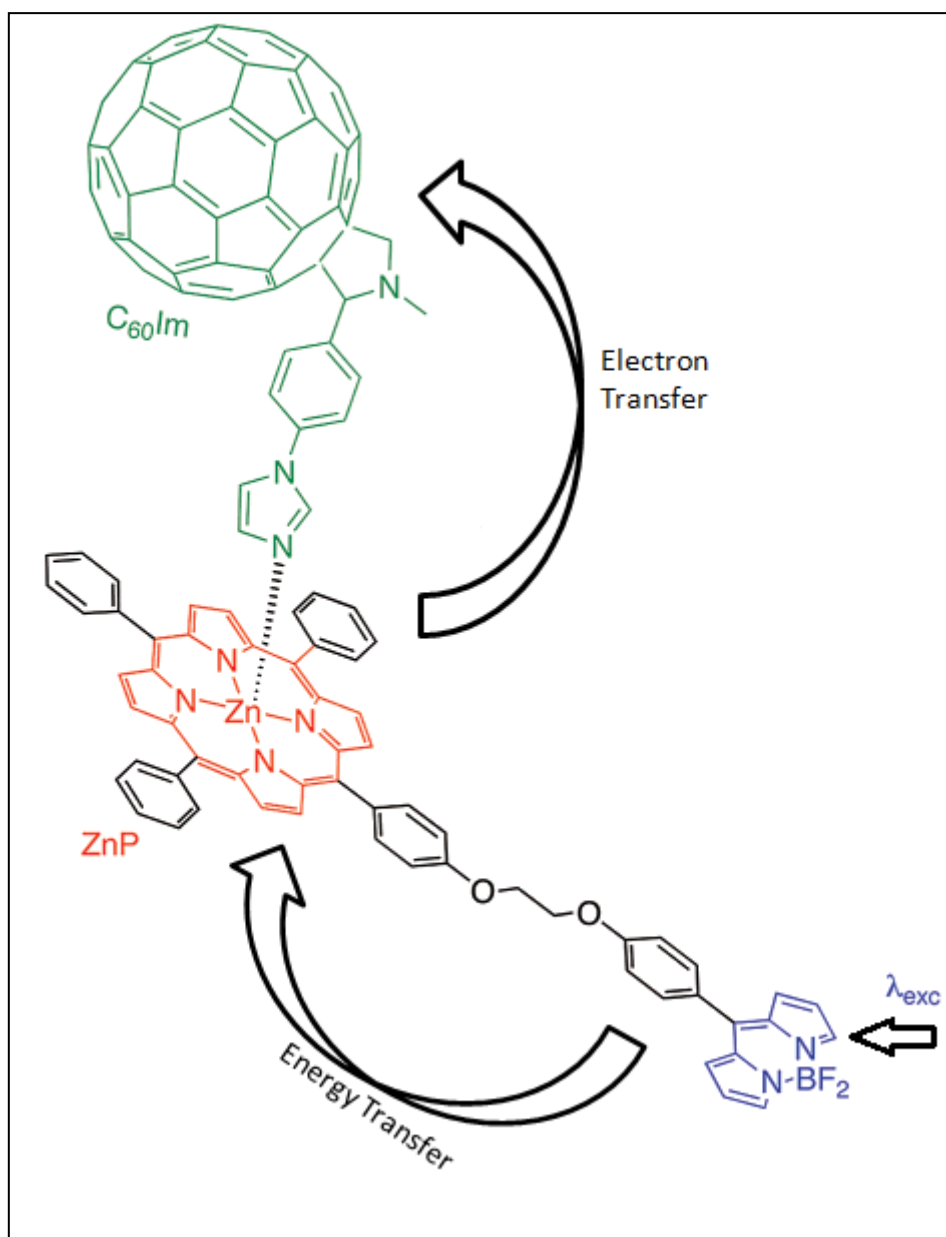


**Figure 22.** Representation of self-assembling Förster-type energy transfer system from literature

Artificial light harvesting system in figure 22 called a “supramolecular triad” was published by Ito et. al.<sup>69</sup> This system is a bit different compared to system in figure 21. In this system, there are energy transfer and electron transfer. There are BODIPY dyes as donor, zinc porphyrin (ZnP) as station for energy transfer and fullerene (C<sub>60</sub>-Im) as station for

electron transfer. Upon excitation from BODIPY donor, there is energy transfer from this donor unit to zinc porphyrin (ZnP) followed by electron transfer to a fullerene (C60-Im) unit. Because of this mechanism, this system is called as “supramolecular triad”. Overall system mimics processes in natural photosynthesis because system has “combined antenna-reaction center” having Zn-porphyrin combined to the fullerene component via metal to axial-ligand coordination and system works efficiently.

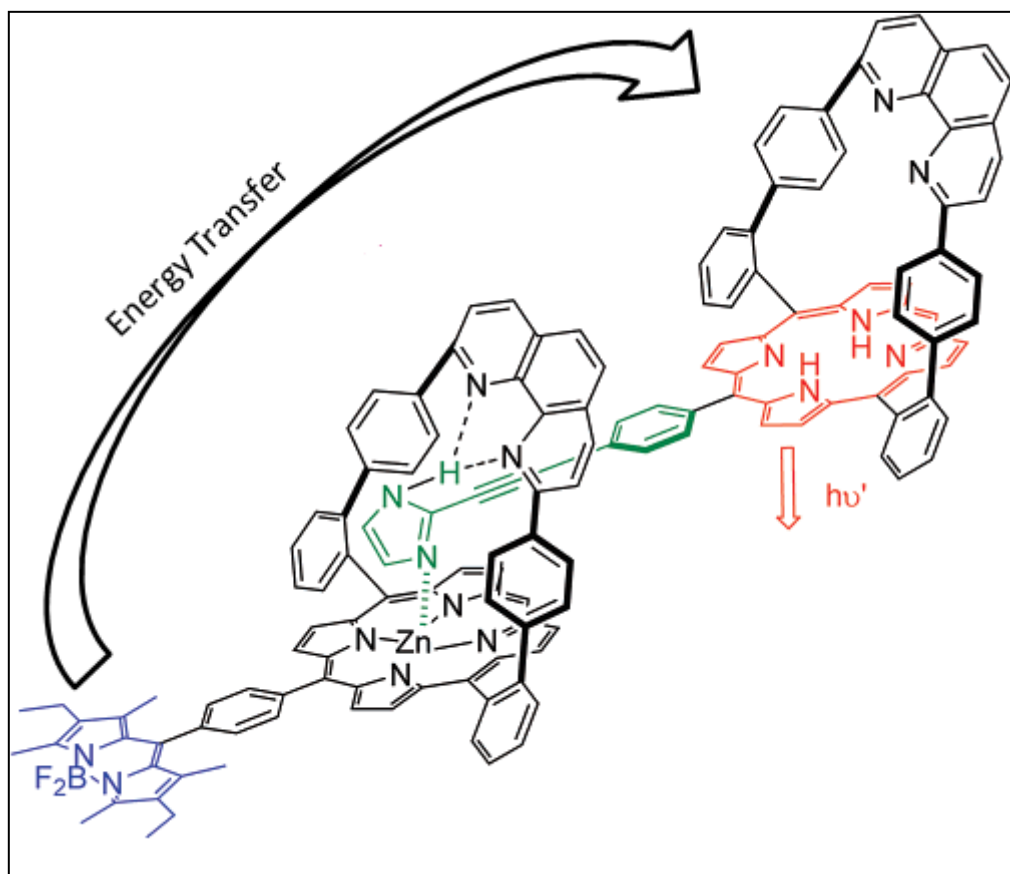


**Figure 23.** Representation of self-assembling Förster-type energy transfer system from literature

Complex in figure 23 was published by Weiss et al.<sup>70</sup> There is self-assembling system provided by the affinity of phenanthroline-strapped zinc porphyrins for *N*-unsubstituted imidazoles. In this system, upon excitation of BODIPY donor at 495 nm, there is energy transfer from two different points to the free porphyrin. Donor makes efficient net energy transfer (80%) to the free porphyrin and also the excited ZnP-Im makes energy transfer (85%) to the free porphyrin.

## 1.5 Tetrasteryl- Bodipy dyes and Knoevenagel condensation reaction

Many important properties have been added to BODIPY dyes after their initial synthesis by Kreuzer in 1968.<sup>71</sup> The peripheral BODIPY dye has absorption peak around 500 nm and this wavelength can be shifted into red region of the visible spectrum by increasing the conjugation of bodipy core via incorporation of fused aromatic rings or aryl substituents to the meso (8) position.<sup>72-77</sup> However, mono- and distyryl modifications via Knoevenagel condensation added greater versatility to BODIPY dyes in tuning of absorption and emission wavelengths.<sup>78-83</sup> Using Knoevenagel reaction, different aldehydes having different characteristics can be incorporated to methyl groups of 1, 3, 5 and 7 positions of Bodipy unit. The 3- and 5-methyls are the positions that yield first in Knoevenagel reaction because they are the most acidic ones which was resulted from Mulliken-charge analysis on the core carbon atoms of tetramethyl- BODIPY and electron density of the carbon atoms varies in the following order: 2,6 >> 1,7 > 3,5.<sup>84</sup> Also, <sup>1</sup>H NMR gives additional information about acidity of methyl substituents shown in figure 24.

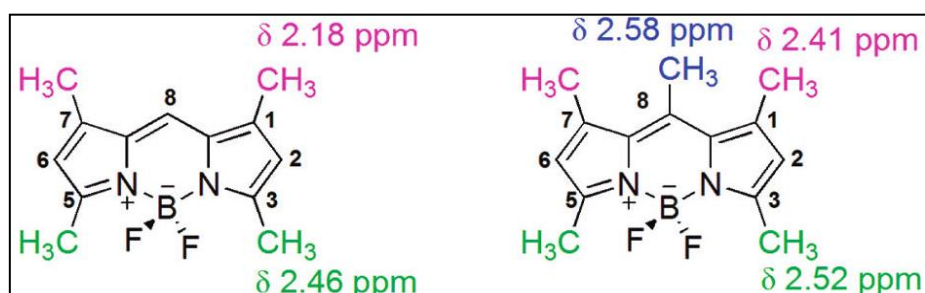


**Figure 24.** Structures of Tetramethyl- and pentamethyl-Bodipy derivatives with relevant <sup>1</sup>H NMR chemical shifts in CDCl<sub>3</sub><sup>84</sup>

Akkaya research group has many studies and published important results about functionalization of methyl groups on 3 and 5 of positions of BODIPY.<sup>85</sup> Until 2009, only methyls on 3 and 5 positions of BODIPY could be functionalized. Because of this reason, absorption and emission wavelength of BODIPY dye were restricted to 700 nm. In 2009, Akkaya group published first example of tetrasteryl BODIPY and they successively achieved the synthesis and isolation of mono-, di-, tri-, and tetrasteryl derivatives of different BODIPYs.<sup>84</sup>

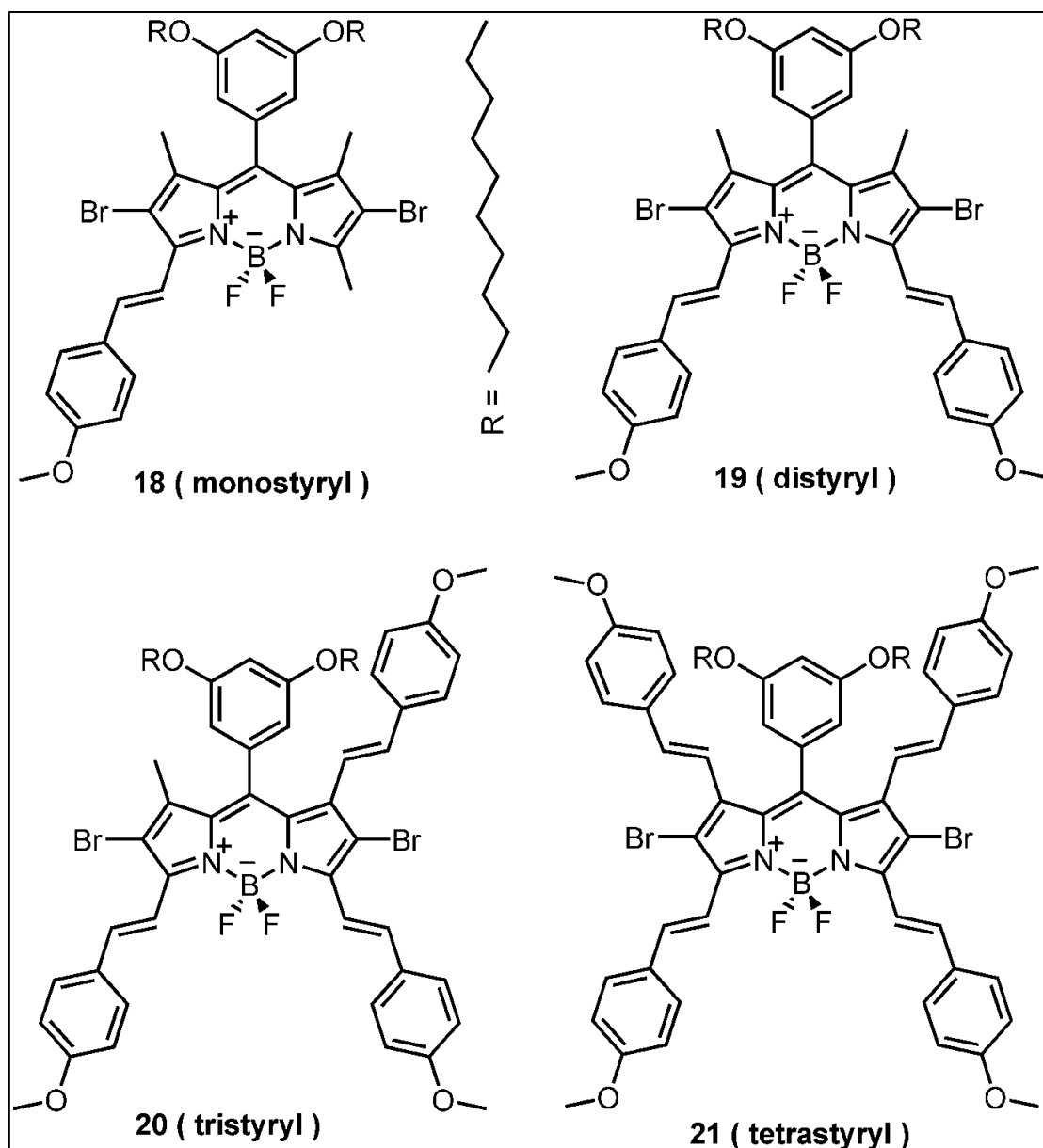


**Figure 25.** Structures of mono-, di-, tri-, and tetra-styryl-Bodipy derivatives of a compound from literature

Mono-, di-, tri-, and tetra-styryl structures of one compound from this paper are shown in figure 25. This straightforward functionalization opened new page in BODIPY chemistry and its applications. Because, by simple condensation reaction, BODIPY dye absorption can be pushed from 500 to 800 nm which is true near IR dye having large extinction coefficient. After this first tetra-styryl- BODIPY study, similar studies were published by Ziessel group.<sup>86</sup> Reaction condition of Knoevenagel condensation for tetra-styryl- BODIPY synthesis will be explained at the end of this part.

$^1\text{H}$  NMR spectrum is used to characterize the tetrastyryl- BODIPY and it has specific peaks that belong to *trans*-vicinally coupled protons of methyl groups on positions 1 and 7. Figure 26 shows  $^1\text{H}$  NMR spectra of the distyryl (top) and the tetrastyryl- BODIPY (bottom). The protons that look Fluorine atoms shifts to the downfield ( to the 8.6 ) in both spectra because of electron withdrawing ability of Fluorine. The *trans* protons of this downfield shifted ones of both compounds give peak in similar region ( 7.8 ) because they are not affected from Fluorine atoms and they have 16 Mhz coupling constant showing that they are *trans* coupling. However, there is a significant upfield shift of one proton ( red) to the 6.05 of *trans*-vicinally coupled protons due to shielding zone of the meso-phenyl ring in tetrastyryl-bodipy. For the other proton ( green) of *trans*-vicinally coupled protons, there is no shift and it gives peak at about 7.8 which is similar with *trans* coupled protons ( blue ones ) of distyryl bodipy showing that there is no effect of meso-phenyl ring. Also they have 16 Mhz coupling constant showing that they are *trans* coupling, too. These results show that tetrastyryl-BODIPY dyes can be characterized easily using NMR data.

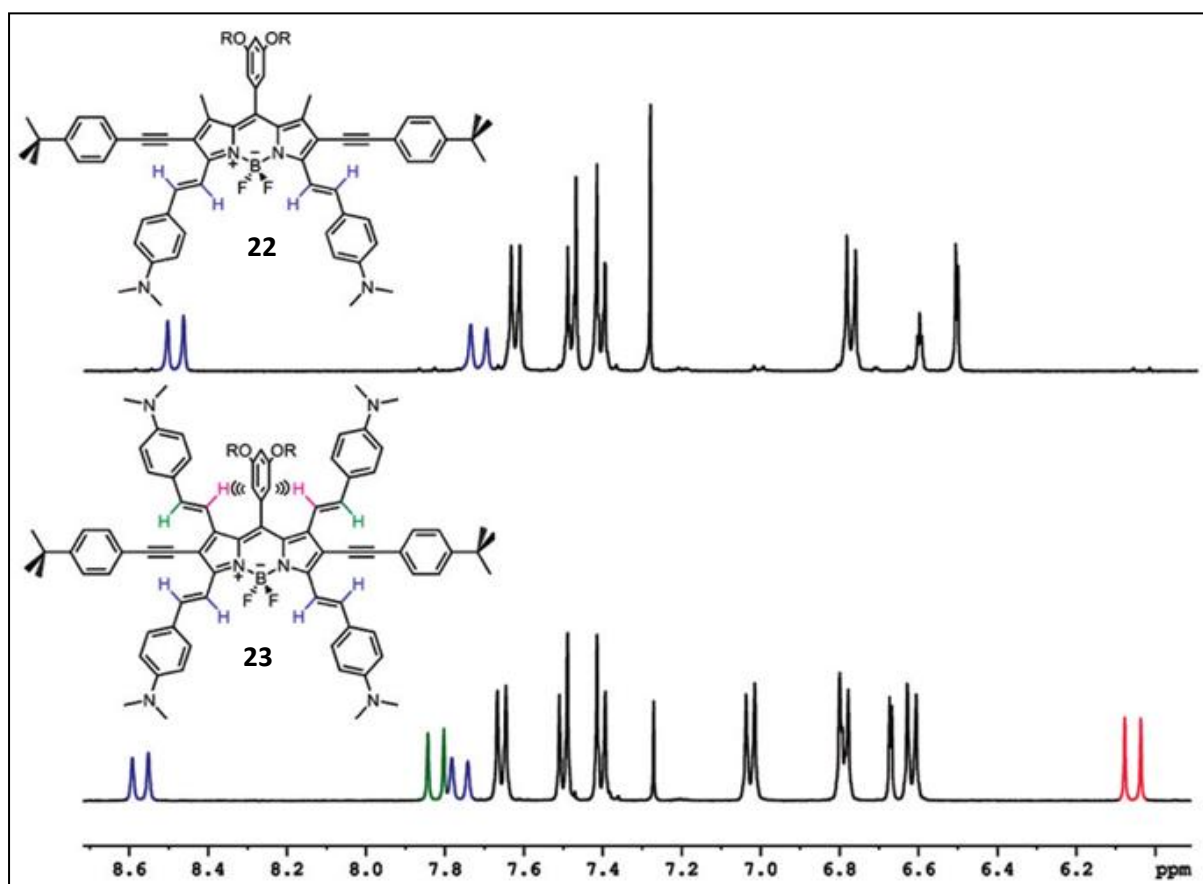


**Figure 26.**  $^1\text{H}$  NMR spectra and structures of distyryl (top) and the tetrastyryl-Bodipy (bottom)<sup>84</sup>

Knoevenagel condensation reaction is frequently being used in modification of Bodipy. It is the dehydration reaction which resulted from a nucleophilic addition of an active hydrogen compound to a carbonyl group. Water is eliminated in this type of reaction and product of this reaction is often an alpha, beta conjugated enone. Aldehyde or a ketone can be used as carbonyl group and a weak base is used as catalyst. Figure 27 shows an example of Knoevenagel condensation used in synthesis of monostyryl- BODIPY compound. Mono-, di-, tri-, and tetrasteryl derivatives of BODIPY can be synthesized ( figure 25) using Knoevenagel reaction at same reaction conditions. Piperidine is used as a base, acetic acid is used to increase the acidity of reactivity of carbonyl group of aldehyde and benzene or toluene can be used as solvent. In Knoevenagel reaction of BODIPY, acidity of methyl substituents is very important because proton should have enough acidity to be abstracted with a mild base which is piperidine in this case. If strong base is used, self-condensation of the aldehyde would proceed. Although increasing electron withdrawing ability of 2 and 6 positions of BODIPY via coupling electron withdrawing units by Suzuki or Sonagashira coupling which increases the acidity of methyl substituents on 1, 3, 5, and 7 positions, most of the peripheral BODIPY has enough acidity for the synthesis of mono- and distyryl derivatives. However, for tetrasteryl derivatives, strong electron withdrawing units such as 4-*t*-butylphenylethynyl should be coupled to the 2,6-positions of BODIPY. Without these couplings, tetrasteryl-bodipy can not be obtained, mono styryl and di styryl one is obtained. Also, solvent should all be removed using deanstark apparatus, reaction media should be dry in tetrasteryl-Bodipy synthesis. It is difficult to stop reaction at tristyryl product, generally, tetra styryl or di styryl product is obtained.

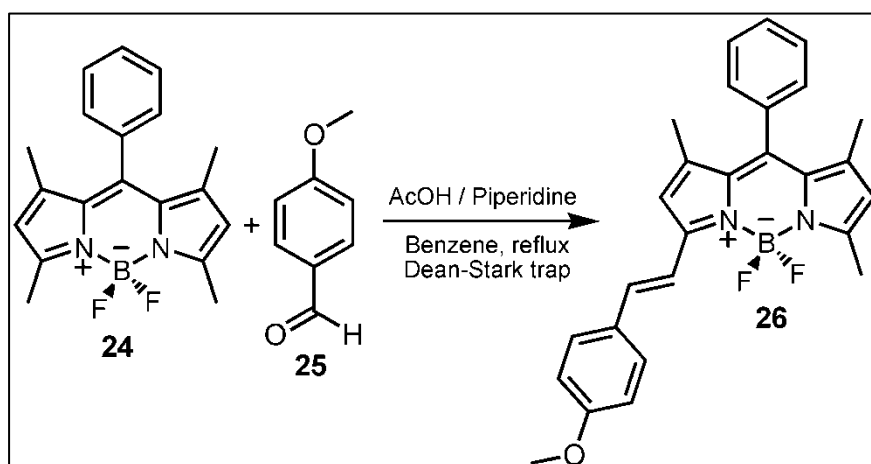


**Figure 27.** Example of Knoevenagel reaction from literature

## CHAPTER 2

### EXPERIMENTAL

#### 2.1. General

All chemicals and solvents obtained from Sigma-Aldrich were used without further purification. Thin layer chromatography (Merck TLC Silica gel 60 F<sub>254</sub>) were used to monitor reactions. Chromatography on silica gel was done with Merck Silica gel 60 (particle size: 0.040-0.063 mm, 230-400 mesh ASTM).

<sup>1</sup>H NMR and <sup>13</sup>C NMR spectra were taken on Bruker DPX-400 working at 400 MHz for <sup>1</sup>H NMR and 100 MHz for <sup>13</sup>C NMR in CDCl<sub>3</sub> with tetramethylsilane as internal standard. All spectra were taken at 25 °C and coupling constants (*J values*) are given in Hz. Chemical shifts are given in parts per million (ppm) and splitting patterns are shown as s (singlet), d (doublet), t (triplet), q (quartet), m (multiplet), and p (pentet).

Absorption spectra were performed by using a Varian Cary-100 spectrophotometer. Fluorescence measurements were taken on a Varian Eclipse spectrofluorometer. Mass spectra were recorded on Agilent Technologies 6530 Accurate-Mass Q-TOF LC/MS. MALDI mass spectra were recorded at the Izmir Institute of Technology, Izmir, Turkey and at the University of Sheffield, Mass Spectrometry Service Laboratory, Sheffield, United Kingdom.

## 2.2. Syntheses

Compounds **28** and **38** were synthesized according to literature procedure.<sup>84,68</sup> Tetrahydrofuran was dried by refluxing it over sodium/benzophenone. All other solvents and reagents were purchased from Sigma-Aldrich and used without further purification.

### 2.2.1. Synthesis of Compound **29**

Argon gas was bubbled through 200 mL CH<sub>2</sub>Cl<sub>2</sub> for 30 min then 2,4-dimethyl pyrrole (**27**) (15.8 mmol, 1.5 g) and 3,5-bis(decyloxy)phenylbenzaldehyde (**28**) (7.17 mmol, 3.0 g) were dissolved in it under argon atmosphere. 1-2 drop of TFA was added and stirred at room temperature nearly 3-4 h and Argon is removed. After 3-4 h, a solution of DDQ (7.17 mmol, 1.63 g) in 40 ml CH<sub>2</sub>Cl<sub>2</sub> was added and stirred for 30 min followed by the addition of 5 mL Et<sub>3</sub>N and 5 mL BF<sub>3</sub>.OEt<sub>2</sub>. After stirring 30 min. the resulting mixture was washed three times with water and dried over Na<sub>2</sub>SO<sub>4</sub>. The solvent was evaporated and the residue was purified by column chromatography on silica gel using CHCl<sub>3</sub> as the eluant. Red solid (1.38 g, 30%).

<sup>1</sup>H NMR (400 MHz, CDCl<sub>3</sub>): δ<sub>H</sub> 6.47 (s, 1H ), 6.36 (s, 2H ), 5.89 (s, 2H ), 3.84 (t, 4H, *J* = 6.50 Hz ), 2.48 (s, 6H ), 1.70 (m, 4H ), 1.50 (s, 6H ), 1.36 (m, 4H ), 1.19 (s, 24H ), 0.81 (t, 6H, *J* = 6.5 Hz ).

<sup>13</sup>C NMR (100 MHz, CDCl<sub>3</sub>): δ<sub>C</sub> 161.3, 155.5, 143.1, 136.4, 131.2, 120.9, 106.5, 102.4, 68.4, 32.0, 29.7, 29.5, 29.4, 29.3, 26.1, 22.6, 14.5, 14.3, 14.0 ppm.

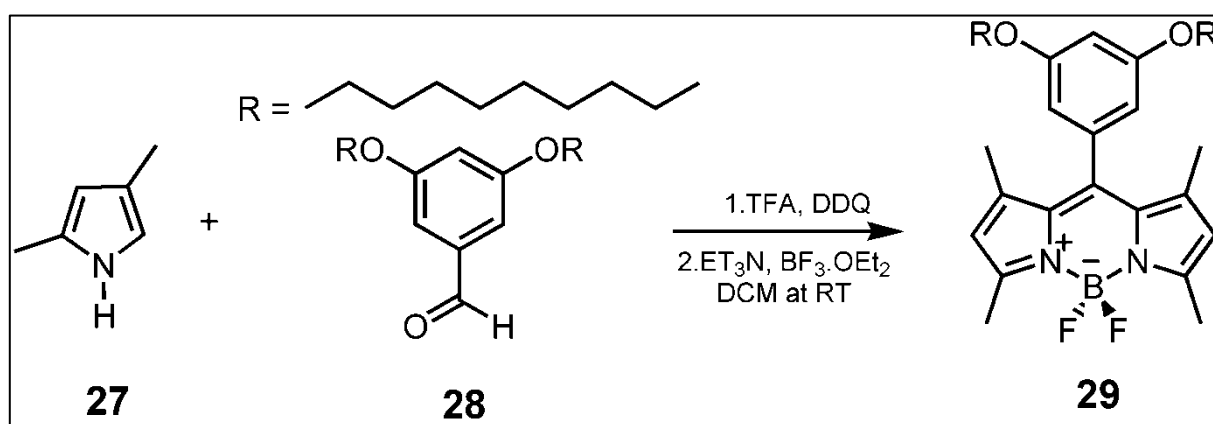
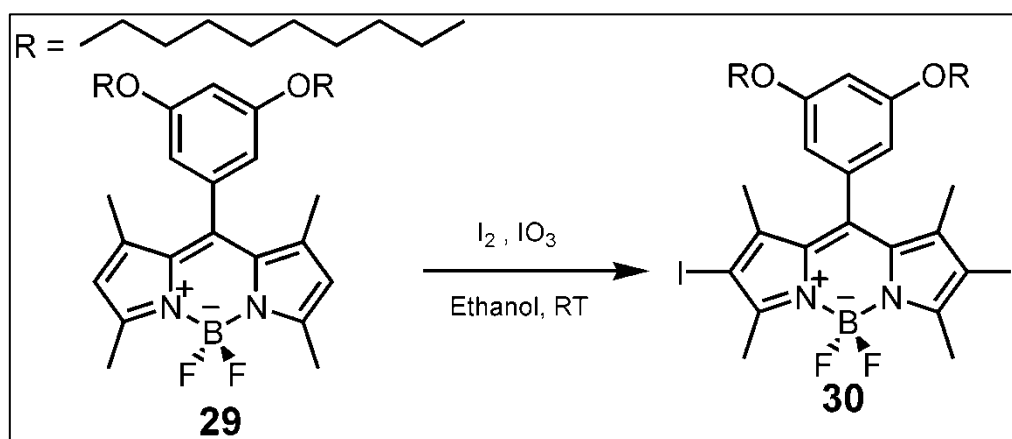


Figure 28. Synthesis of compound **29**

## 2.2.2. Synthesis of Compound 30

**29** (0.218 mmol, 0.133 g) was dissolved in 250 mL EtOH. To this solution I<sub>2</sub> (0.545 mmol, 0.138 g) was added. After 5 min., HIO<sub>3</sub> (0.436 mmol, 0.077 g) which was dissolved in 2 mL H<sub>2</sub>O were added and reaction mixture was stirred at 60°C. The reaction was monitored by TLC (CHCl<sub>3</sub>). When all the starting material had been consumed, saturated Na<sub>2</sub>S<sub>2</sub>O<sub>3</sub> solution in water was added and the product was extracted with chloroform. Solvent was concentrated *in vacuo*. Red waxy solid (0.26 g, 90%).

<sup>1</sup>H NMR (400 MHz, CDCl<sub>3</sub>): δ<sub>H</sub> 6.50 (s, 1H), 6.30 (s, 2H), 3.84 (t, 4H, *J* = 6.50 Hz), 2.58 (s, 6H), 1.70 (m, 4H), 1.50 (s, 6H), 1.3 (m, 4H), 1.2 (s, 24H), 0.81 (t, 6H, *J* = 6.5 Hz).



**Figure 29.** Synthesis of Compound 30

## 2.2.3. Synthesis of Compound 32

**30** (0.296 mmol, 263 mg) and 5 mL of diisopropylamine were added in 10 mL of freshly distilled THF in 50 mL Schlenk tube. After 5 min., (PPh<sub>3</sub>)<sub>2</sub>PdCl<sub>2</sub> (0.0293 mmol, 20.6 mg) and CuI (0.047 mmol, 8.88 mg) were added. After 5 min., 4-*t*-butyl-ethynylbenzene, **31**, (0.888 mmol, 140.4 mg). Resulting mixture was excessively deaerated by bubbling with Argon for 40 min. After degassing, the reaction mixture was stirred at 60 °C for 24 h. Solvent was concentrated *in vacuo* and the residue was washed with water (100 mL) and extracted

into  $\text{CHCl}_3$ . The residue was purified by column chromatography on silica gel using 1:1  $\text{CHCl}_3$  : Hexane as the eluant yielded the desired product as a violet solid. (347 mg, 80%).

$^1\text{H}$  NMR (400 MHz,  $\text{CDCl}_3$ ):  $\delta = 7.53$  (4H, d;  $J = 8.1$  Hz ),  $7.33$  (4H, d;  $J = 8.1$  Hz ),  $6.56$  (1H, t;  $J = 2.3$  Hz ),  $6.41$  (2H, d;  $J = 2.3$  Hz ),  $3.96$  (4H, t;  $J = 6.6$  Hz ),  $2.71$  (6H, s ),  $1.83$ - $1.73$  (4H, m ),  $1.69$  (6H, s ),  $1.50$ - $1.40$  (4H, m ),  $1.40$ - $1.30$  (24H, m ),  $1.25$  (18H s ),  $0.89$  (6H, t;  $J = 6.9$  Hz ).

$^{13}\text{C}$  NMR (100 MHz,  $\text{CDCl}_3$ ):  $\delta = 161.3$ ,  $158.0$ ,  $151.4$ ,  $143.5$ ,  $142.0$ ,  $135.9$ ,  $131.1$ ,  $125.3$ ,  $120.4$ ,  $116.5$ ,  $108.1$ ,  $102.6$ ,  $96.5$ ,  $80.9$ ,  $68.5$ ,  $34.8$ ,  $31.9$ ,  $31.2$ ,  $29.6$ ,  $29.5$ ,  $29.4$ ,  $29.3$ ,  $29.1$ ,  $26.0$ ,  $22.9$ ,  $14.1$ ,  $13.7$ ,  $13.2$ .

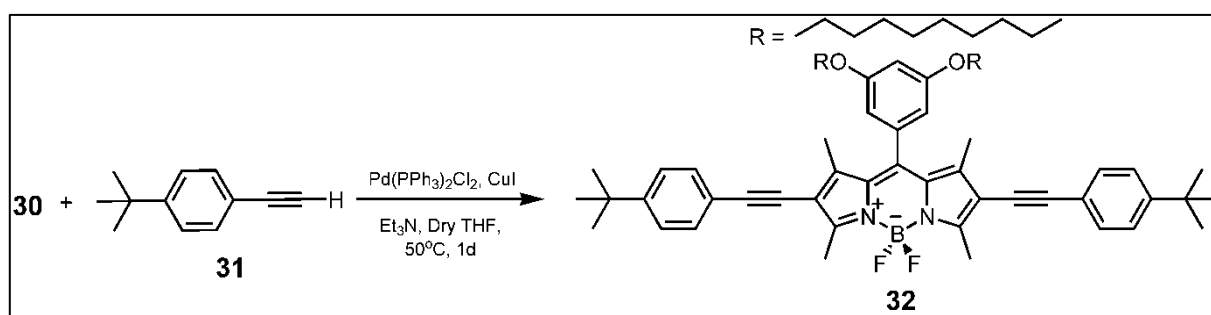


**Figure 30.** Synthesis of Compound 32

#### 2.2.4. Synthesis of Compound 35

Argon gas was bubbled through 200ml  $\text{CH}_2\text{Cl}_2$  for 30 min then 3-ethyl-2,4-dimethyl pyrrole (8.41 mmol, 1035 mg) and compound 35 (3.5 mmol, 1000 mg) were dissolved in it under argon atmosphere. 1-2 drop of TFA was added and the solution stirred at room temperature nearly 3-4 h and Argon is removed. At this point, a solution of DDQ (3.5 mmol, 794.5 mg) in 50 ml  $\text{CH}_2\text{Cl}_2$  was added, stirring was continued for 30 min followed by the addition of 3 ml  $\text{Et}_3\text{N}$  and 3 ml  $\text{BF}_3 \cdot \text{OEt}_2$ . After stirring 30 min. the reaction mixture was washed three times with water and dried over  $\text{Na}_2\text{SO}_4$ . The solvent was evaporated and the residue was purified by column chromatography on silica gel using  $\text{CHCl}_3$  as the eluant. Dark red solid (606.9 mg, 31%).

$^1\text{H}$  NMR (400 MHz,  $\text{CDCl}_3$ ):  $\delta$  = 1.0 (t,  $J$  = 7.52, 6H), 1.35 (s, 6H), 1.50-1.60 (m, 4H), 1.81-1.92 (m, 4H), 2.3 (q,  $J$  = 7.56, 4H), 2.55 (s, 6H), 3.59 (t,  $J$  = 6.64 Hz, 2H), 4.05 (t,  $J$  = 6.45 Hz, 2H), 7.0 (d,  $J$  = 8.56 Hz, 2H), 7.15 (d,  $J$  = 8.56 Hz, 2H).

$^{13}\text{C}$  NMR ( $\text{CDCl}_3$ , 100 MHz,  $\delta$  ppm) 11.9, 12.5, 14.6, 17.1, 25.4, 26.7, 29.1, 32.5, 44.9, 67.9, 114.9, 127.8, 129.4, 130.1, 132.6, 138.4, 140.0, 153.5, 159.5

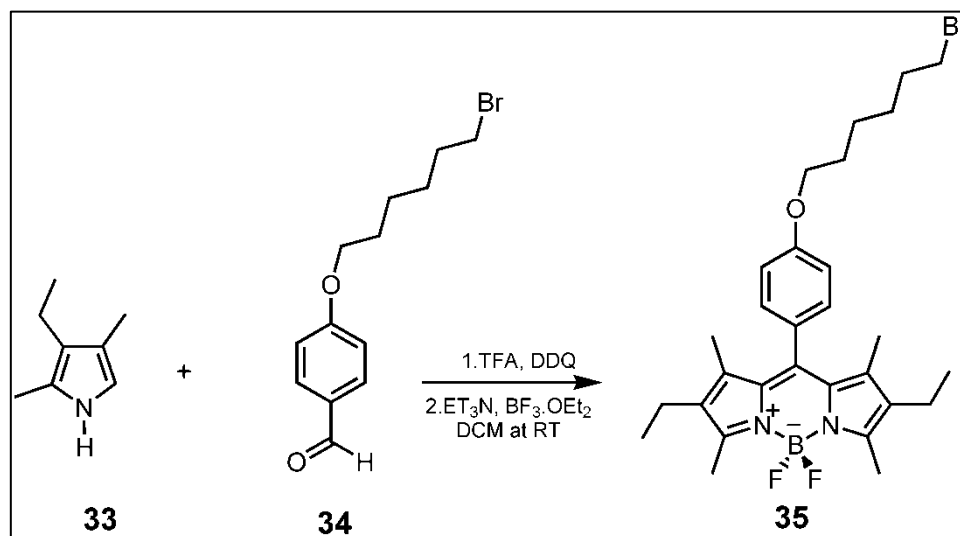


**Figure 31.** Synthesis of Compound 35

### 2.2.5. Synthesis of Compound 36

A mixture of compound 35 (1.43 mmol, 800 mg) and  $\text{NaN}_3$  (3.576 mmol, 232 mg) in 20 ml DMSO was heated at 100 °C for 2h and controlled with TLC. When the reaction was completed, water (100 mL) added to the residue and the product was extracted into the chloroform (3 x 100 mL). Organic phase dried over  $\text{Na}_2\text{SO}_4$ , evaporated and residue was used without further purification. Dark red solid (702.4 g, 97 %).

$^1\text{H}$  NMR ( $\text{CDCl}_3$ , 400 MHz,  $\delta$  ppm)  $\delta$  = 1.0 (t,  $J$  = 7.52 Hz, 6H), 1.35 (s, 6H), 1.50-1.60 (m, 4H), 1.62-1.71 (m, 2H), 1.80-1.91 (m, 2H), 2.3 (q,  $J$  = 7.56 Hz, 4H), 2.55 (s, 6H), 3.32 (t,  $J$  = 6.64 Hz, 2H), 4.05 (t,  $J$  = 6.45 Hz, 2H), 7.0 (d,  $J$  = 8.56 Hz, 2H), 7.15 (d,  $J$  = 8.56 Hz, 2H).

$^{13}\text{C}$  NMR ( $\text{CDCl}_3$ , 100 MHz,  $\delta$  ppm) 11.8, 12.5, 14.6, 17.1, 25.7, 26.6, 28.8, 29.1, 51.4, 67.9, 115.0, 127.8, 129.4, 131.2, 132.6, 138.4, 140.3, 153.5, 159.5

MS (TOF- ESI):  $m/z$  : Calcd: 521.3137  $[\text{M}]^+$ , Found: 520.30651 $[\text{M}-\text{H}]^+$ ,  $\Delta=1.6$  ppm.

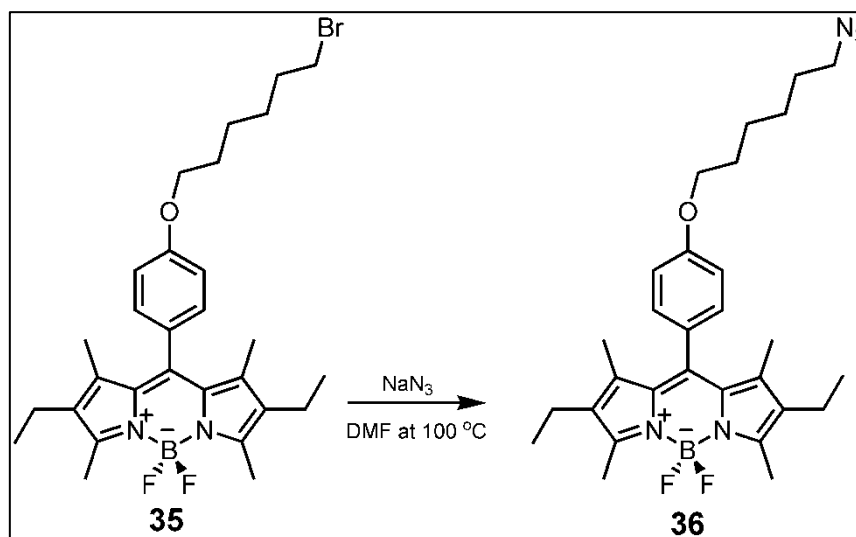


**Figure 32.** Synthesis of Compound **36**

### 2.2.6. Synthesis of Compound **37**

Compound **36** (0.384 mmol, 200 mg) and 4-Methoxybenzaldehyde, **25**, (0.844 mmol, 115 mg) were added to a 100 mL round-bottomed flask containing 50 mL benzene and to this solution, piperidine (0.3 mL) and acetic acid (0.3 mL) were added. The mixture was heated under reflux by using a Dean Stark trap and it is monitored by TLC. When all the starting compounds had been finished, the mixture was cooled to room temperature and solvent was evaporated. Water (120 mL) added to the residue and the product was extracted with chloroform (3 x 100 mL). The organic phase dried over  $\text{Na}_2\text{SO}_4$ , evaporated. The residue was poured into 2:1 EtOAc : Hexanes solution and dissolved by heating then it is cooled to  $0\text{ }^\circ\text{C}$ . Compound **37** precipitated at that temperature then it was filtered and Compound **37** was obtained as pure product. Green solid (155.1 mg, 53%).

$^1\text{H}$  NMR ( $\text{CDCl}_3$ , 400 MHz,  $\delta$  ppm) 1.20 (t,  $J= 7.46$  Hz, 6H), 1.40 (s, 6H), 1.50-1.60 (m, 4H), 1.65-1.75 (m, 2H), 1.85-1.95 (m, 2H), 2.65 (q,  $J= 7.62$  Hz, 4H), 3.35 (t,  $J= 6.84$  Hz, 2H), 3.89 (s, 6H), 4.10 (t,  $J= 6.40$  Hz, 2H), 6.95 (d,  $J= 8.56$  Hz, 2H), 7.05 (d,  $J= 8.44$  Hz,

2H), 7.23 (d,  $J=8.44$  Hz, 2H), 7.25 (d,  $J=16.70$  Hz, 2H), 7.62 (d,  $J=8.60$  Hz, 2H), 7.70 (d,  $J=16.70$  Hz, 2H).

$^{13}\text{C}$  NMR ( $\text{CDCl}_3$ , 100 MHz,  $\delta$  ppm) 11.70, 14.08, 18.40, 25.73, 26.58, 28.82, 29.16, 51.40, 55.39, 67.90, 114.22, 115.00, 118.24, 128.14, 128.76, 129.86, 130.35, 133.34, 133.48, 135.23, 138.15, 138.80, 150.31, 159.54, 160.15.

MS (HRMS-ESI):  $m/z$  : Calcd: 757.397 [M], Found: 757.533 [M-H] $^+$ ,  $\Delta=197$  ppm.

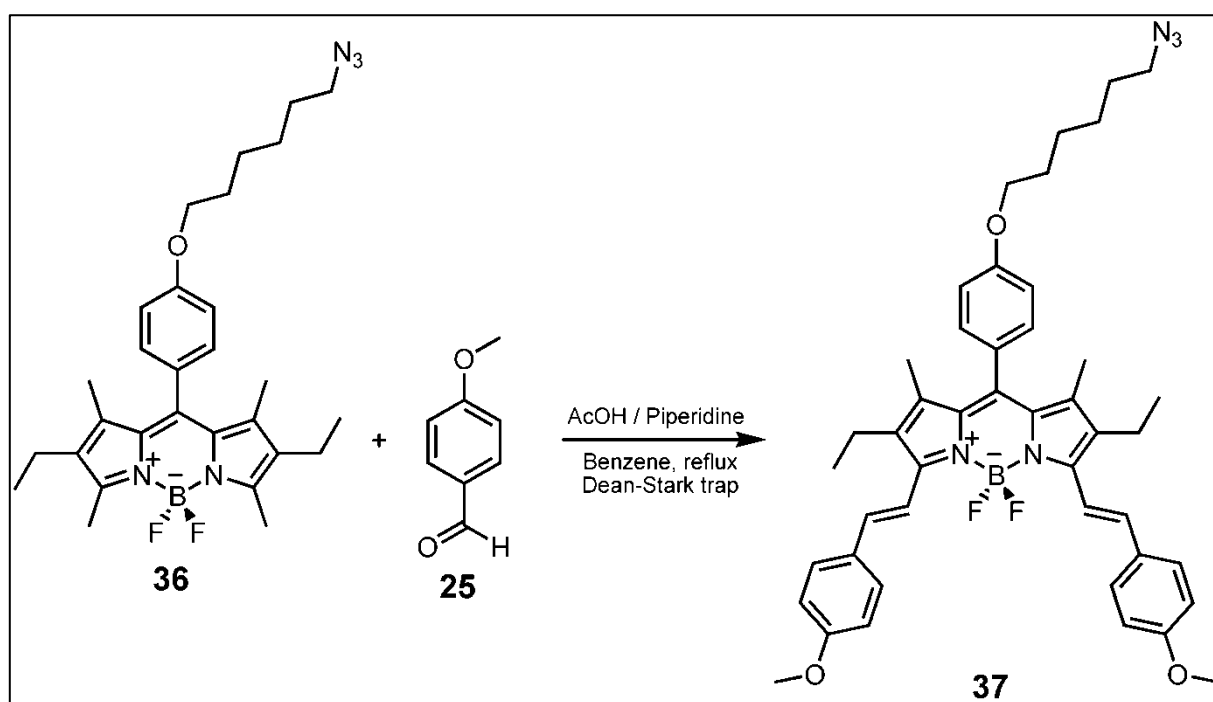


**Figure 33.** Synthesis of Compound 37

### 2.2.7. Synthesis of Compound 39

Compound 32 (0.42 mmol, 400 mg) and compound 38 (2.95 mmol, 472 mg) were added to a 100 mL round-bottomed flask containing 50 mL benzene and to this solution, piperidine (0.3 mL) and acetic acid (0.3 mL) were added. The mixture was heated under reflux by using a Dean Stark trap and it is monitored by TLC in Chloroform. When all the starting compounds had been finished, the mixture was cooled to room temperature and solvent was evaporated. Water (120 mL) added to the residue and the product was extracted

with chloroform (3 x 100 mL). Organic phase dried over Na<sub>2</sub>SO<sub>4</sub>, evaporated and residue was purified by silica gel column chromatography using 3:2 CHCl<sub>3</sub> : Hexanes as the eluant. Dark green solid (416 mg, 65%).

<sup>1</sup>H NMR (400 MHz, CDCl<sub>3</sub>): δ = 0.88 (t; *J* = 6.8 Hz, 6H), 1.18-1.32 (m; 28H), 1.35 (s; 18H), 1.55-1.65 (m; 4H), 2.55 (t; *J* = 2.4 Hz, 1H), 2.60 (t; *J* = 2.4 Hz, 1H), 3.83 (t; *J* = 6.5 Hz, 4H), 4.70 (d; *J* = 2.4 Hz, 4H), 4.80 (d; *J* = 2.4 Hz, 4H), 6.10 (d; *J* = 16.2 Hz, 2H), 6.61 (d; *J* = 16.2 Hz, 2H), 6.72 (d; *J* = 2.2 Hz, 1H), 6.89 (d; *J* = 8.8 Hz, 4H), 7.02-7.10 (m; 8H), 7.42 (d; *J* = 8.7 Hz, 4H), 7.48 (d; *J* = 8.7 Hz, 4H), 7.70 (d; *J* = 8.8 Hz, 4H), 7.78 (d; *J* = 16.3 Hz, 2H), 7.82 (d; *J* = 17.0 Hz, 2H), 8.59 (d; *J* = 16.3 Hz, 2H).

<sup>13</sup>C NMR (100 MHz, CDCl<sub>3</sub>): δ = 14.1, 22.7, 25.9, 29.0, 29.3, 29.6, 31.2, 31.9, 34.9, 55.8, 55.9, 68.7, 75.6, 75.9, 78.4, 78.5, 85.7, 98.9, 103.2, 108.3, 109.0, 114.9, 115.3, 117.4, 119.7, 120.7, 125.7, 128.0, 129.3, 130.5, 130.9, 131.2, 132.9, 133.7, 136.7, 137.6, 138.8, 142.1, 151.7, 153.4, 157.7, 158.6, 161.6.

MS (HRMS-ESI): *m/z* : Calcd: 1516.819 [M], Found: 1516.798 [M], Δ=14 ppm

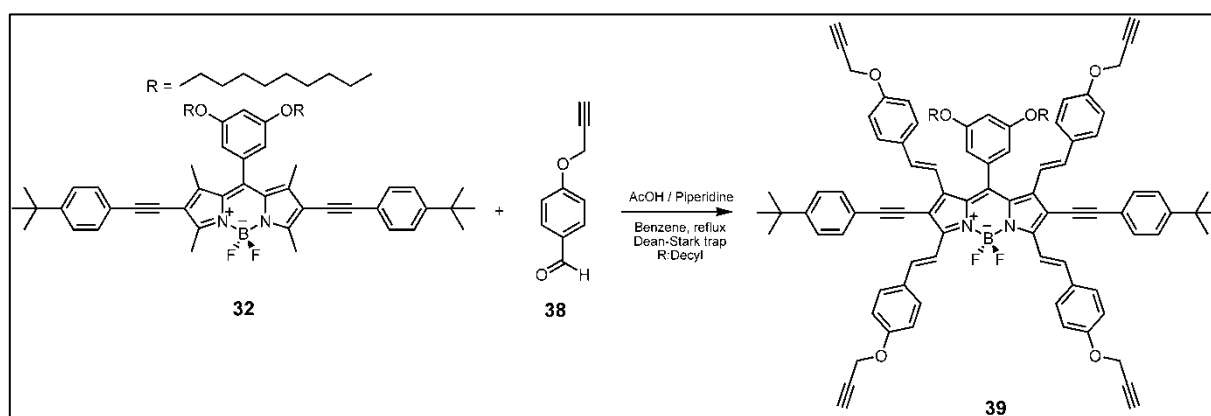


**Figure 34.** Synthesis of Compound 39

## 2.2.8. Synthesis of Compound 40

To the solution of the compound **36** (0.238 mmol, 124 mg) in a 12:1:1 mixture of CHCl<sub>3</sub>, EtOH and water (14 ml); compound **39** (0.040 mmol, 60 mg), sodium ascorbate (0.0237 mmol, 4.7 mg), CuSO<sub>4</sub> (0.0118 mmol, 2.9 mg) and 3-4 drop Et<sub>3</sub>N are added and it was stirred at room temperature for 24 h. Water (50 mL) added to the residue and the product was extracted into the chloroform (3 x 50 mL). After evaporation of the solvents, the crude product was purified by column chromatography (CHCl<sub>3</sub>). Black solid (122 mg, 85%).

<sup>1</sup>H NMR (CDCl<sub>3</sub>, 400 MHz, δ ppm) 0.75 (t, *J* = 6.76 Hz, 6H), 0.89 (t, *J* = 8.3 Hz, 24H), 1.05-1.20 (m, 28H), 1.24 (s, 18H), 1.26 (s, 24H), 1.36 (p, *J* = 8.39 Hz, 4H), 1.43-1.55 (m, 16H), 1.74 (p, *J* = 7.01 Hz, 8H), 1.92 (p, *J* = 7.34 Hz, 8H), 2.16-2.26 (m, 16H), 2.44 (s, 24H), 3.75 (t, *J* = 6.42 Hz, 4H), 3.91 (t, *J* = 6.24 Hz, 8H), 4.31 (t, *J* = 6.66 Hz, 8H), 5.14 (s, 4H), 5.22 (s, 4H), 6.00 (d, *J* = 16.20 Hz, 2H), 6.53 (s, 2H), 6.62 (s, 1H), 6.80 (d, *J* = 8.64 Hz, 4H), 6.89 (d, *J* = 8.52 Hz, 8H), 6.96 (d, *J* = 8.72 Hz, 4H), 6.99 (d, *J* = 8.64 Hz, 4H), 7.02-7.08 (m, 8H), 7.32 (d, *J* = 8.60 Hz, 4H), 7.37 (d, *J* = 8.48 Hz, 4H), 7.52 (s, 2H), 7.56 (s, 2H), 7.58 (d, *J* = 8.68 Hz, 4H), 7.69 (d, *J* = 16.12 Hz, 4H), 8.46 (d, *J* = 16.40, 2H).

(CDCl<sub>3</sub>, 100 MHz, δ ppm) 11.88, 12.48, 14.14, 14.21, 14.65, 17.08, 21.07, 22.69, 25.62, 25.66, 25.90, 26.36, 26.41, 28.97, 29.07, 29.12, 29.33, 29.58, 30.24, 30.28, 31.21, 31.90, 50.37, 60.40, 62.21, 62.25, 67.76, 68.66, 98.91, 114.81, 114.95, 115.29, 120.59, 122.44, 122.58, 125.77, 127.77, 127.83, 128.13, 129.32, 129.48, 130.49, 131.20, 132.62, 132.66, 136.66, 137.44, 138.39, 138.44, 138.68, 138.83, 140.31, 140.36, 142.09, 144.06, 153.43, 153.48, 158.43, 159.32, 159.43, 161.61.

MS (MALDI): *m/z* : Calcd: 3602.074 [M]<sup>+</sup>, Found: 3711.572 [M-Ag]<sup>+</sup>

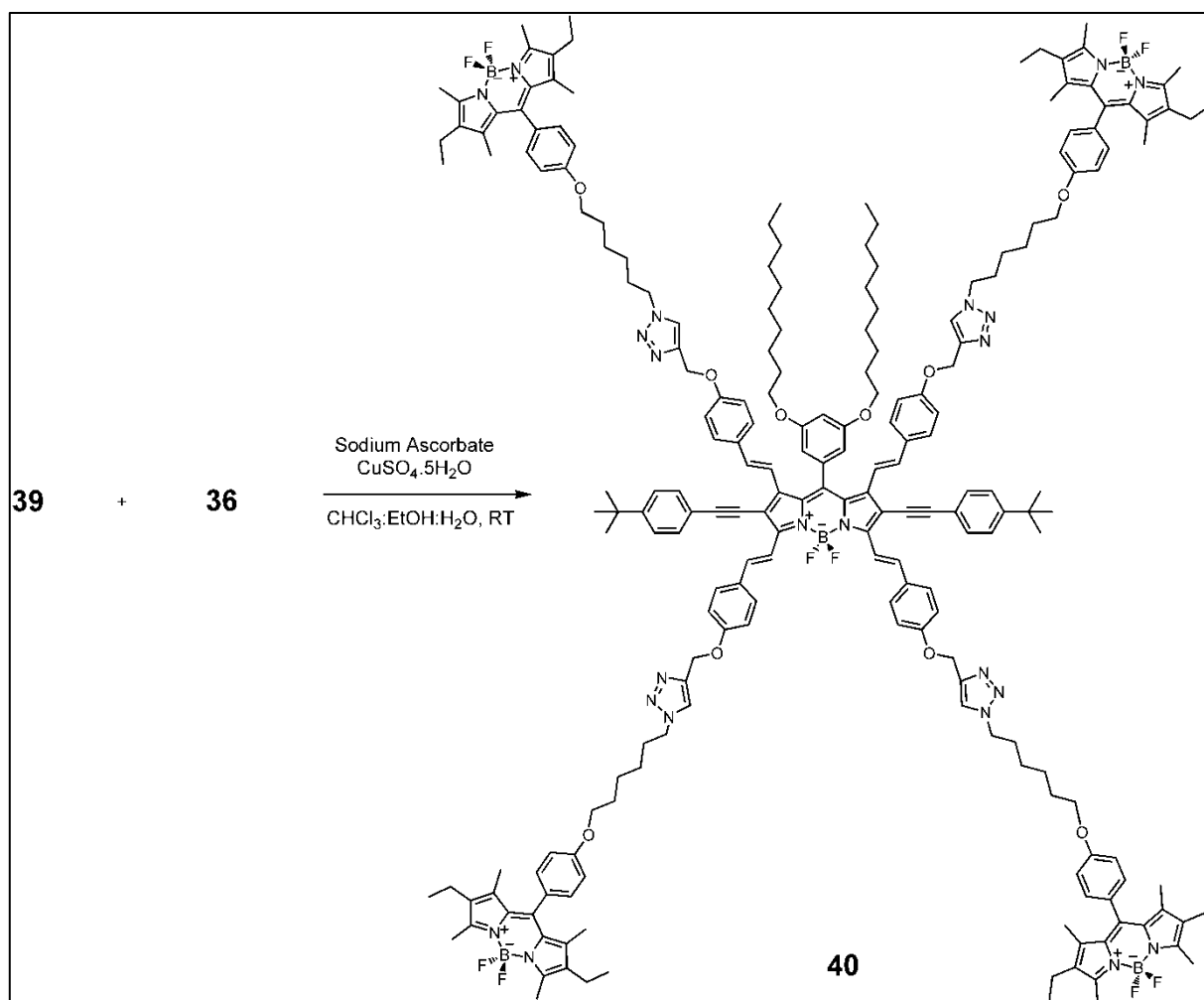


**Figure 35.** Synthesis of Compound **40**

### 2.2.9. Synthesis of Compound **41**

To the solution of the compound **37** (0.237 mmol, 335 mg) in a 12:1:1 mixture of  $\text{CHCl}_3$ , EtOH and water (14 ml); compound **39** (0.0396 mmol, 60 mg), sodium ascorbate (0.0237 mmol, 4.7 mg),  $\text{CuSO}_4$  (0.0118 mmol, 2.9 mg) and 3-4 drop  $\text{Et}_3\text{N}$  are added and it was stirred at room temperature for 24 h. Water (50 mL) added to the residue and the product was extracted into the chloroform (3 x 50 mL). After evaporation of the solvents, the crude product was purified by column chromatography ( $\text{CHCl}_3$ ). Black solid (144 mg, 80%).

$^1\text{H}$  NMR ( $\text{CDCl}_3$ , 400 MHz,  $\delta$  ppm) 0.90 (t,  $J= 6.90$  Hz, 6H), 1.18 (t,  $J= 7.60$  Hz, 24H), 1.19-1.30 (m, 28H), 1.37 (s, 18H), 1.40 (s, 24H), 1.41-1.50 (m, 4H), 1.52-1.69 (m, 16H), 1.79-1.90 (m, 8H), 1.95-2.07 (m, 8H), 2.55-2.65 (m, 16H), 3.86-3.90 (m, 28H), 4.09 (t,  $J= 6.20$  Hz, 8H), 4.42 (t,  $J= 7.00$  Hz, 8H), 5.25 (s, 4H), 5.32 (s, 4H), 6.11 (d,  $J= 16.13$  Hz, 2H), 6.65 (d,  $J= 2.04$  Hz, 2H), 6.75 (s, 1H), 6.92 (d,  $J= 8.56$  Hz, 4H), 6.95 (d,  $J= 8.84$  Hz, 16H), 7.01 (d,  $J= 8.50$  Hz, 8H), 7.06 (d,  $J= 8.72$  Hz, 4H), 7.10 (d,  $J= 8.00$  Hz, 4H), 7.16-7.25 (m, 16H), 7.43 (d,  $J= 8.52$  Hz, 4H), 7.48 (d,  $J= 8.52$  Hz, 4H), 7.59 (d,  $J= 8.72$  Hz, 16H), 7.63-7.74 (m, 16H), 7.78 (s, 2H), 7.83 (s, 2H), 8.58 (d,  $J= 16.13$ , 2H).

( $\text{CDCl}_3$ , 100 MHz,  $\delta$  ppm) 11.74, 14.05, 14.16, 18.41, 22.71, 25.62, 25.69, 25.93, 26.32, 26.40, 28.99, 29.14, 29.34, 29.59, 30.22, 30.28, 31.22, 31.92, 34.93, 50.39, 55.43, 62.14, 62.21, 62.26, 67.78, 68.68, 85.74, 98.97, 108.28, 114.25, 114.82, 114.92, 114.99, 115.32, 118.13, 118.23, 119.52, 120.61, 122.49, 122.67, 122.76, 125.77, 128.05, 128.11, 128.16, 128.76, 129.34, 129.87, 130.39, 130.49, 133.22, 133.48, 133.81, 135.34, 138.20, 138.94, 142.13, 144.06, 150.31, 151.82, 153.38, 158.40, 159.17, 159.53, 160.25, 161.69. MS

MALDI:  $m/z$ : : Calcd: 4546.409  $[\text{M}]^+$ , Found: 4547.0  $[\text{M}]$

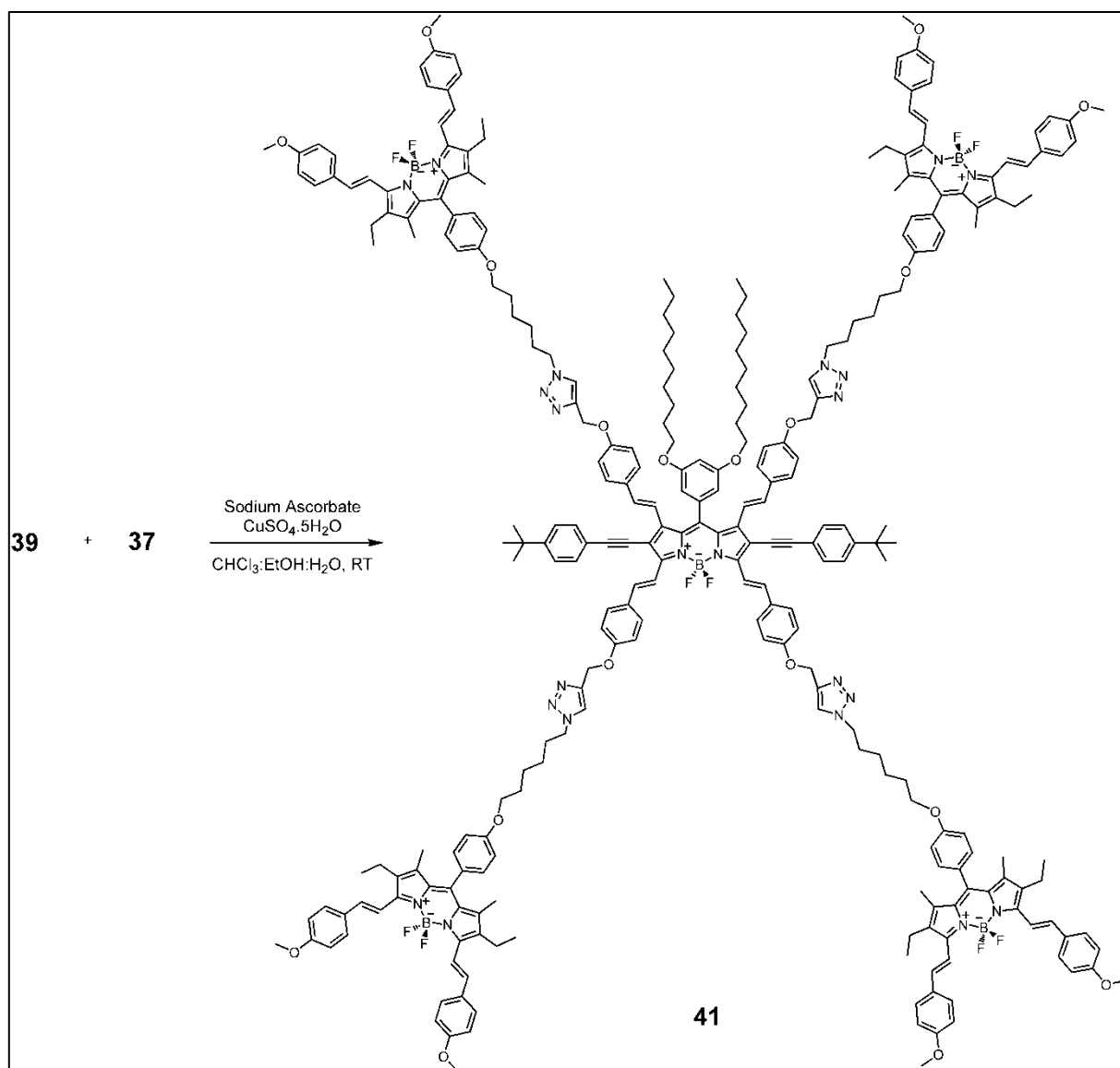


**Figure 36. Synthesis of Compound 41**

## CHAPTER 3

### RESULTS and DISCUSSION

Scientists make effort to understand and mimic the natural biological processes because understanding the working mechanisms of biological processes provide scientist to design and select certain parameters that are tuned to work efficiently under real life conditions. Photosynthesis is one of the natural processes that is tried to be mimicked by scientists. Supramolecular systems are being used to function as light harvesting energy transfer systems because they make photochemical conversion of solar energy.<sup>66,67</sup> In light harvesting systems, there are donor groups that can absorb sunlight at different wavelength then they transfer absorbed energy to the acceptor group, core, and acceptor emits this energy at a specific wavelength. As a result sun light energy is concentrated at the core.

In this study, two different light harvesting energy transfer cassettes (40 and 41) were designed and synthesized. Both energy transfer cassettes make Förster type (through space) of energy transfer. They have large Stokes' shift and emit in near-IR region. In the design of cassettes and selection of donor and acceptor chromophores, spectral overlap of donor emission and acceptor absorption were taken into account in order to have efficient energy transfer between donor and acceptor units. Tetra-styryl BODIPY (39) is selected as acceptor group, core and BODIPY (36) is selected as donor groups at the corners for cassette 1 (40) (figure 37). For the cassette 2 (41), again tetra-styryl BODIPY is selected as acceptor group and di-styryl-BODIPY (37) is selected as donor groups at the corners (figure 38). There is an alkyl chain which has 6 methylene (CH<sub>2</sub>) units between donor groups and acceptor as spacer for a bond energy transfer. The difference between two cassettes is in donor groups. Peripheral BODIPY is donor and it has emission at about 520 nm for cassette 1, distyryl-BODIPY is donor and it has emission about 650 nm for the cassette 2.

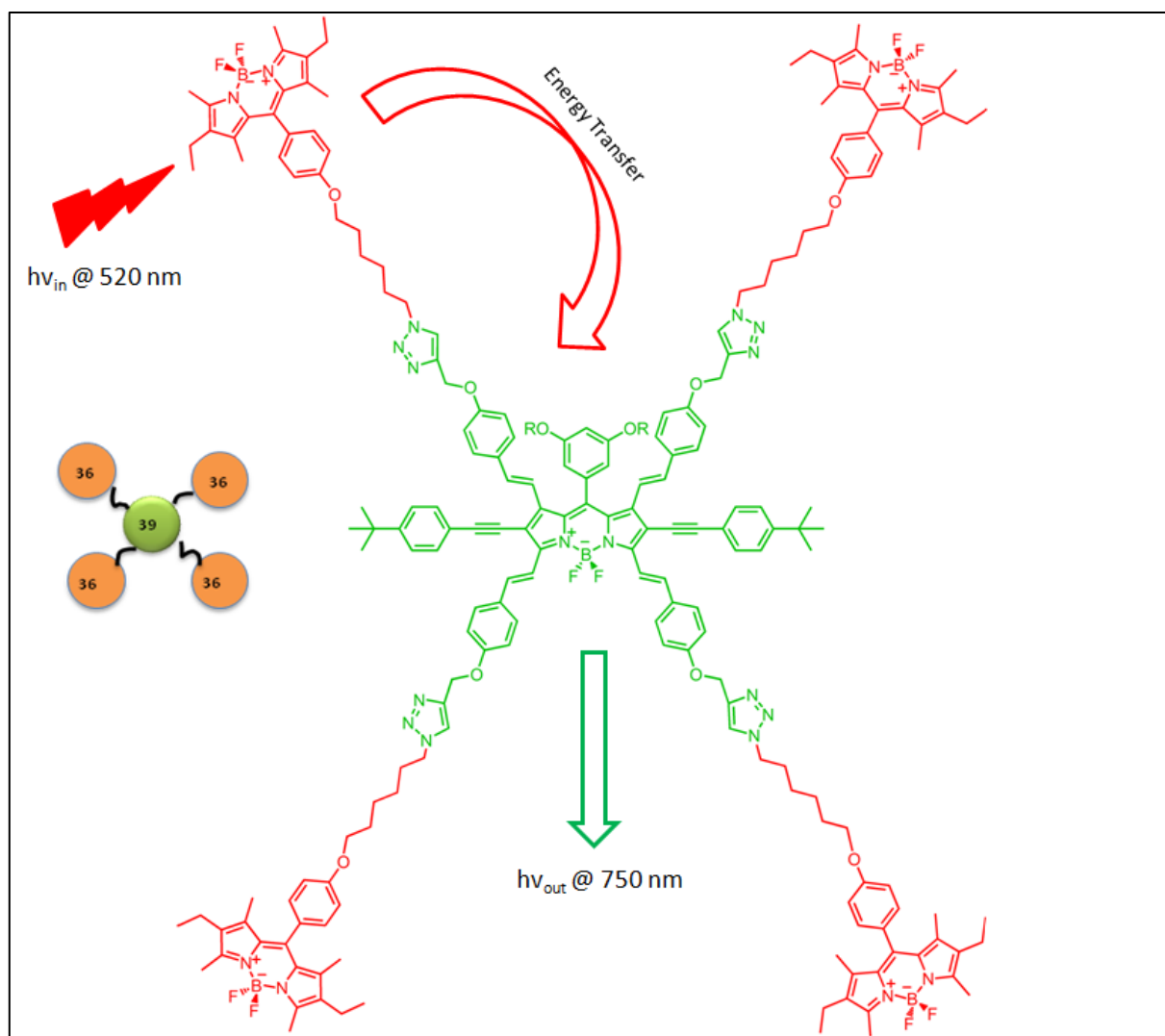


**Figure 37.** Schematic view of energy transfer in Cassette 1

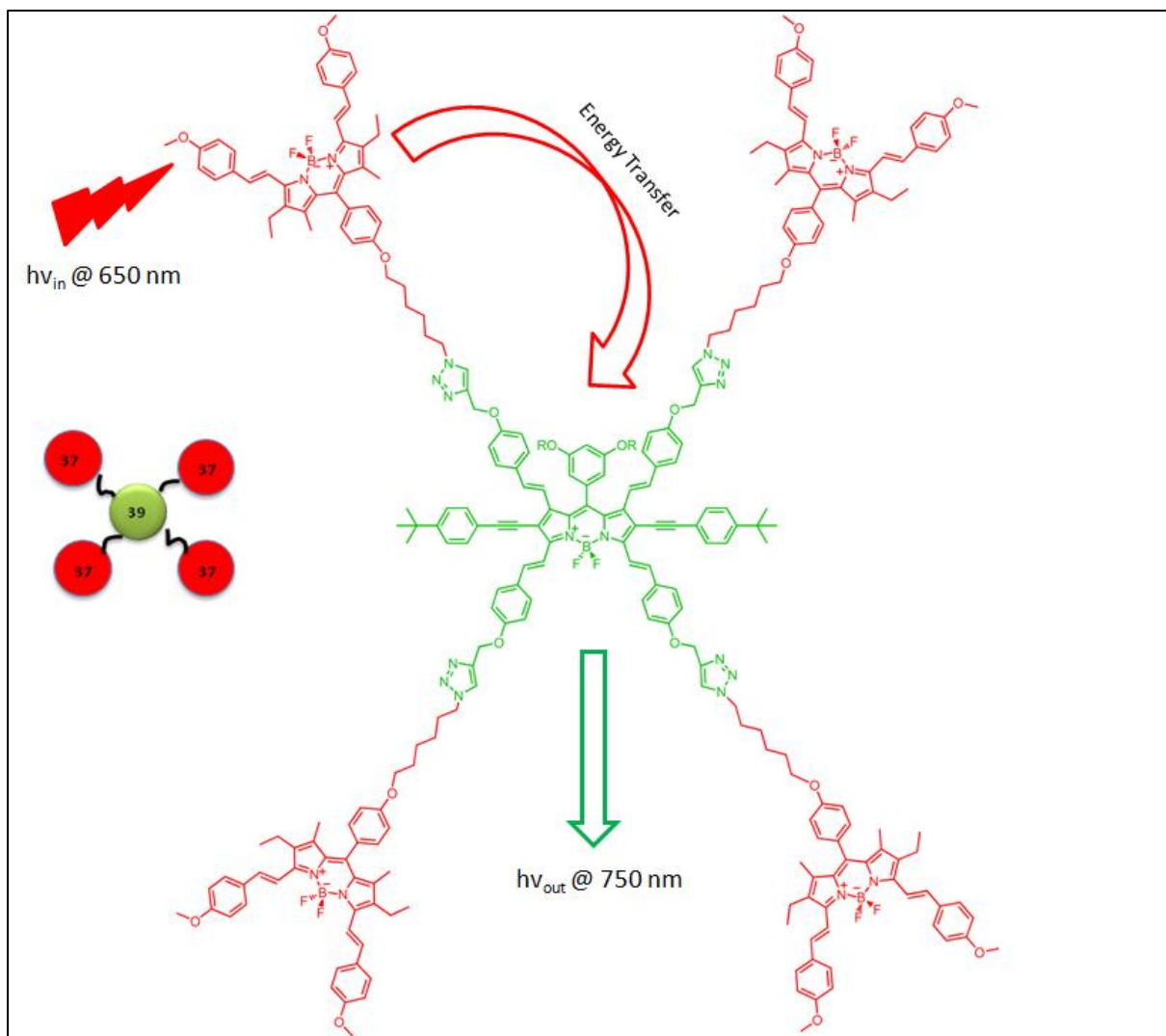


**Figure 38.** Schematic view of energy transfer in Cassette 2

The reason of such a design is to compare the energy transfer efficiencies in cassette 1 and 2. There is better overlap between donor emission and acceptor absorption in cassette 2 relative to cassette 1, so it is expected to see better energy transfer in cassette two. (figure 39 and 40)

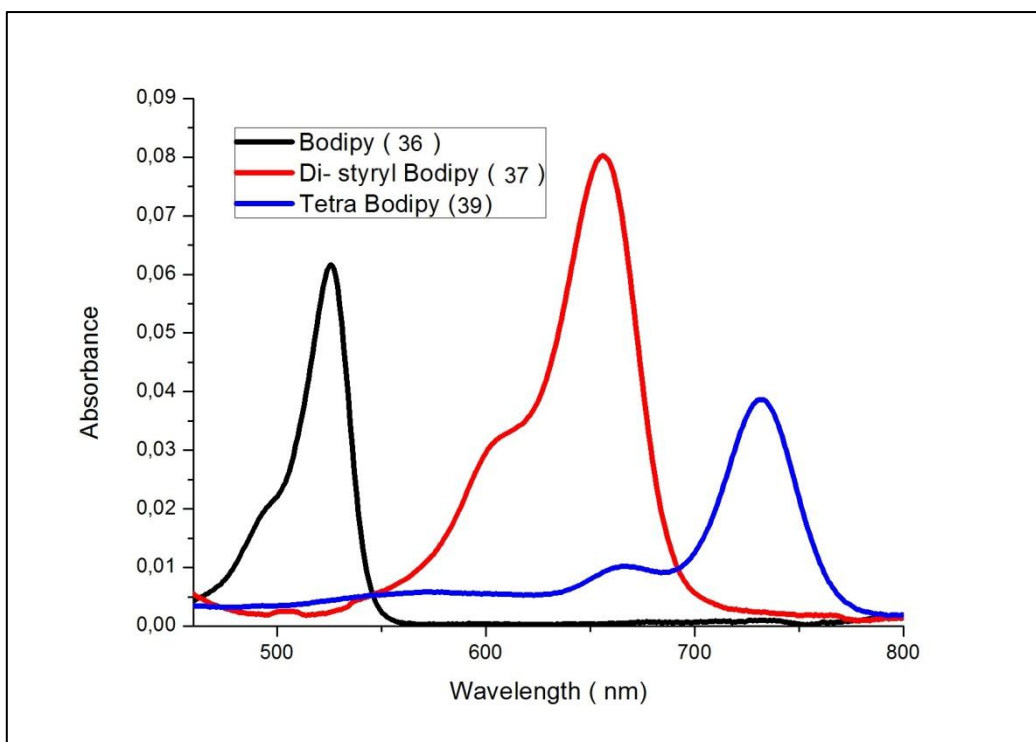


**Figure 39.** Absorption spectrum of compounds **36**, **37** and **39**

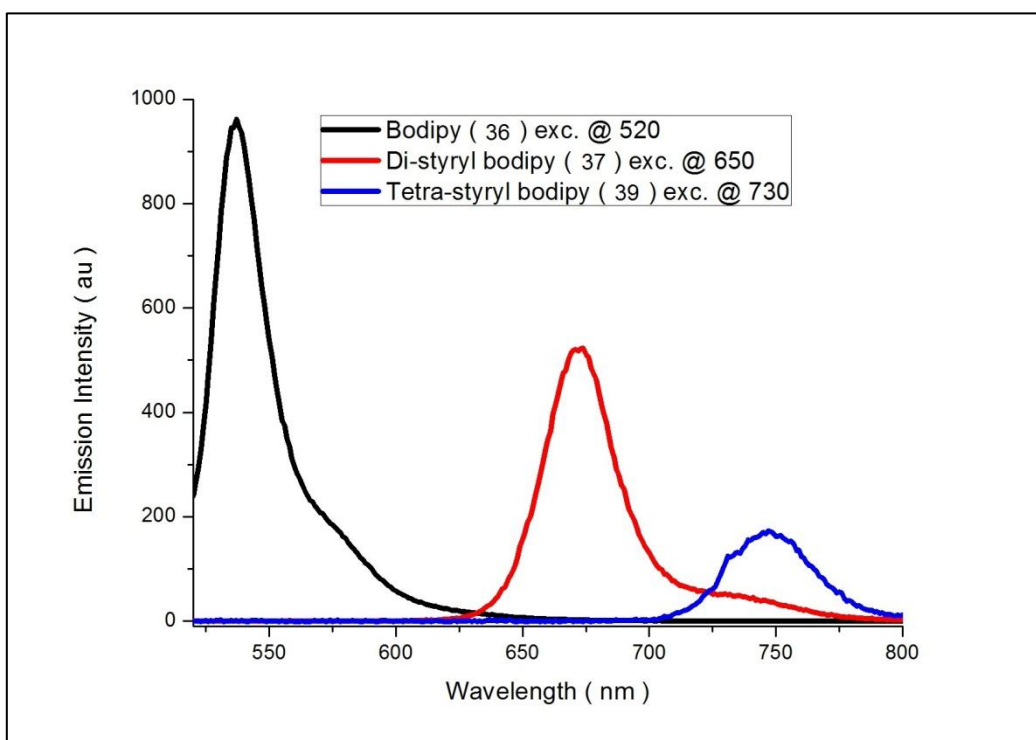


**Figure 40.** Emission spectrum of compounds **36**, **37** and **39**

BODIPYs in donor and acceptor groups were synthesized using standard BODIPY reaction procedures, which have an aldehyde and pyrrole in the presence of TFA and DDQ at room temperature, then the addition of  $\text{BF}_3 \cdot \text{Et}_2\text{O}$  and  $\text{Et}_3\text{N}$ . The reason for the use of 3,5-dioxy decyl aldehyde is to increase the solubility of BODIPY in organic solvents such as benzene. To increase the reactivity of 1, 3, 5 and 7 positions of BODIPY for Knoevenagel condensation reaction, electron withdrawing group is attached to BODIPY via Sonagashira coupling to synthesize tetra-styryl BODIPY. If decyl aldehyde and electron withdrawing group are not used in peripheral BODIPY, tetra-styryl BODIPY can not be obtained, instead of that product, di-styryl BODIPY is obtained because of solubility and reactivity problems. For tetra-styryl and di-styryl BODIPY which have extended conjugation resulting with the emission at higher wavelength, Knoevenagel condensation reaction was used. Donor and acceptor chromophores in cassette 1 and 2 were attached via copper (I) catalyzed click reactions between azido and ethynyl groups of the compounds. For the characterization of azide formation with brominated units,  $^1\text{H}$  NMR spectroscopy is used. There is a shift from  $\delta 3.5$  to  $\delta 3.3$  in hydrogens of  $\text{CH}_2$  attached to Br that shows bromo reagent is consumed and azido product is produced. For click reactions, again  $^1\text{H}$  NMR is used and there is distinct singlet peak at around  $\delta 7.6$  in  $^1\text{H}$  NMR which is the triazole hydrogen. The structures of other compounds were characterized by  $^1\text{H}$  NMR,  $^{13}\text{C}$  NMR and mass spectroscopy (Appendix A and B).

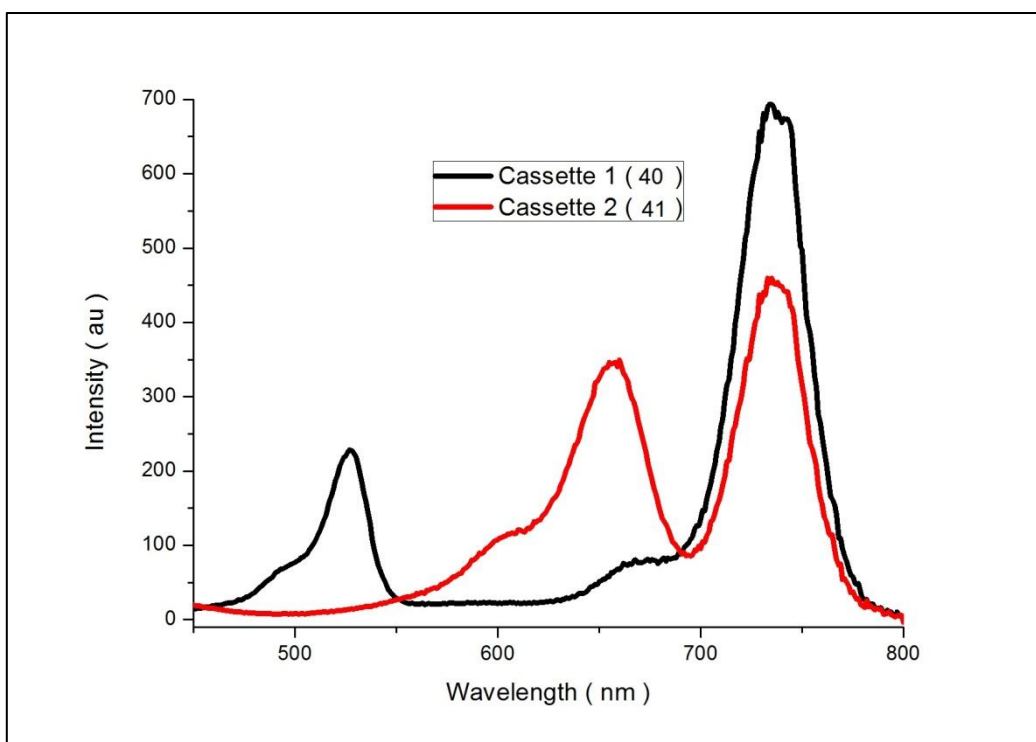
Photophysical characterization of **36**, **37**, **39**, **40** and **41** (extinction coefficient, absorbance wavelength and quantum yields) is shown in Table 1. BODIPY has extinction coefficient of 76000 at 525 nm, di-styryl BODIPY extinction coefficient is 48000 at 650 nm and tetra-styryl BODIPY has 143000 at 730 nm. Extinction coefficients of cassette 1 are 53000 at 525 nm and 32000 at 733 nm, cassette 2 are 357000 at 655 nm and 175000 at 734 nm. It is seen that as the number of specific BODIPY unit increases, extinction coefficient at that BODIPY's maximum absorbance wavelength increases.

**Table 1.** Photophysical properties of compounds

Compound	$\lambda_{\text{abs}}$ (nm)	$\Phi$ $I_{\text{exc}}(525\text{nm})$	$\Phi$ $I_{\text{exc}}(650\text{nm})$	$\Phi$ $I_{\text{exc}}(734\text{nm})$	Extinction coefficients
<b>36</b>	52	0.97	-	-	76000
<b>37</b>	650	-	0.67	-	48000
<b>39</b>	733	-	-	0.31	143000
<b>40</b>	525 733	0.089	-	-	53000 32000
<b>41</b>	650 734	-	0.058	-	357000 175000

Three different reference chromophores were used in quantum yield calculation shown in Table 2 and these reference chromophores are Rhodamine 6G (488 nm, water), Sulforhodamine 101 (550 nm, ethanol), tetra-styryl BODIPY (730 nm, chloroform). Quantum yields were calculated using equation 9 stated in introduction part.

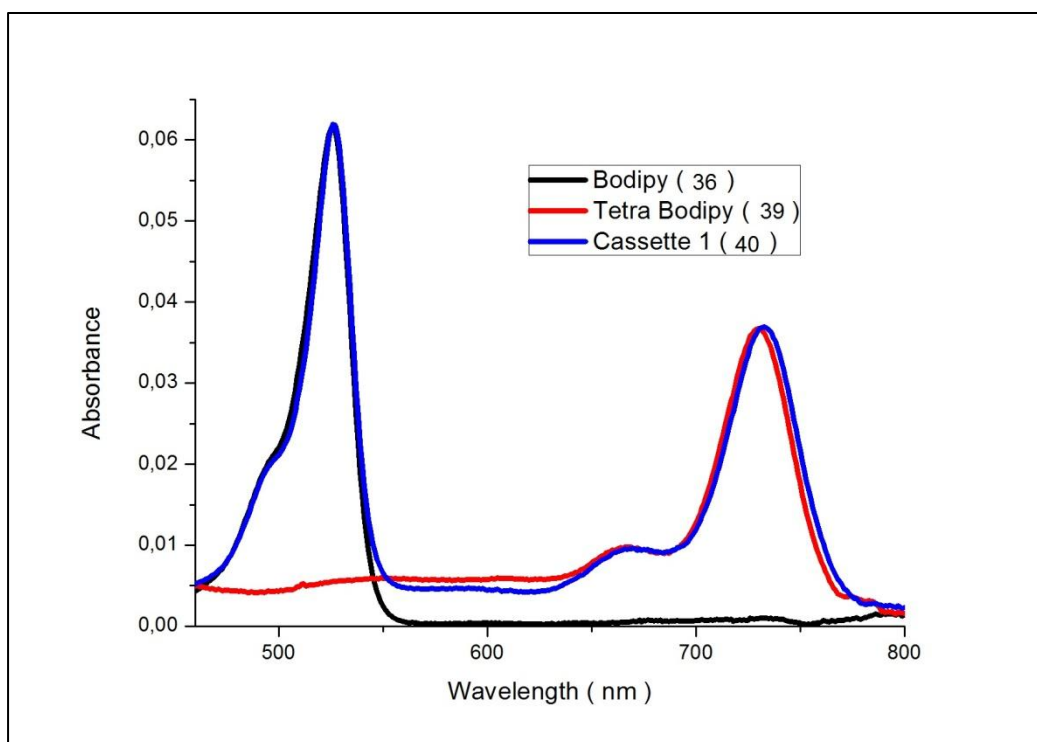
Excitation spectrum of compounds **40** and **41** is shown in figure 41. In this spectrum, there are two distinct peaks of compounds **40** and **41** at 525 nm, 650 nm and 740 nm. This proves that there are two individual chromophores in structure of both cassettes and also there are no ground state interactions between different units of cassettes.



**Figure 41.** Excitation spectrum of compounds **40** and **41**

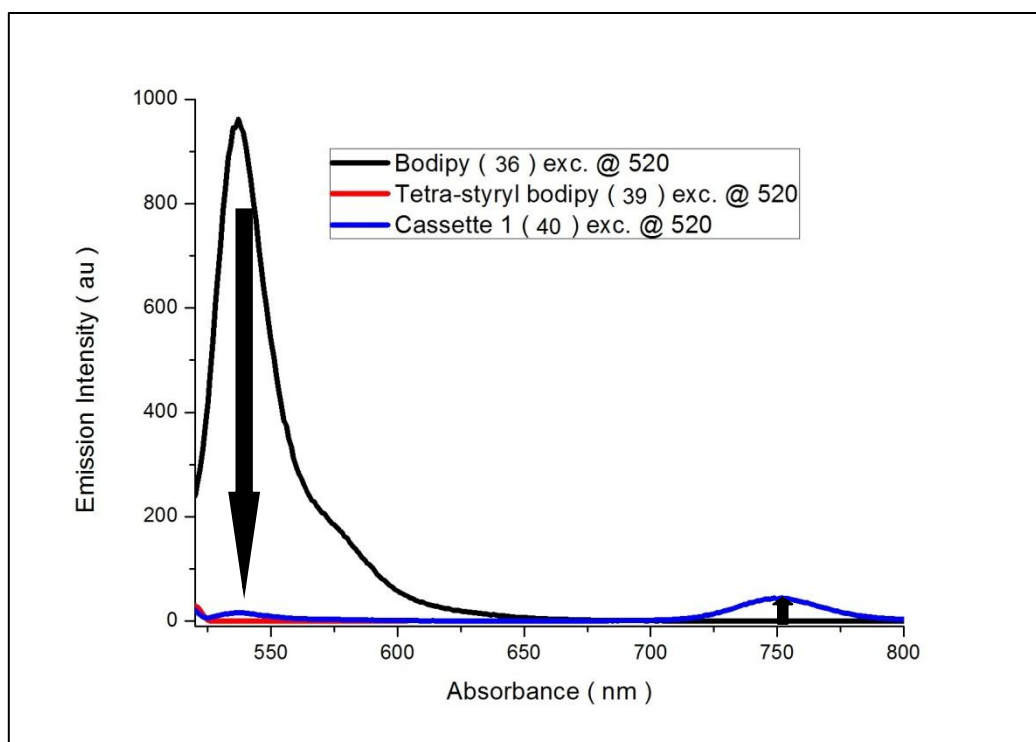
Energy transfer characterization can be made by interpreting absorbance and emission spectrum, comparing relative lifetimes and quantum yields. Representation in figure 37 and 38 show whole energy transfer process in cassette 1 and 2. In absorption spectra of both cassettes, there are two distinct absorbance peaks indicating that there are two non-interacting chromophores in each cassette with no-ground state interactions (figure 42 and 44).

Figure 38 shows the absorbance spectrum of peripheral BODIPY, tetra-styryl BODIPY and Cassette 1 at equally absorbing concentrations. Peripheral BODIPY has absorption at around 525 nm (black, donor chromophore) and tetra-styryl BODIPY has the band around 740 nm (blue, acceptor chromophore). Cassette has two distinct absorptions at around 525 nm and 740 nm (red). Energy transfer between donor and acceptor can be seen in emission spectrum of equally absorbing 36, 39 and 40 in chloroform.



**Figure 42.** Absorption spectrum of compounds **36**, **39** and **40**

In emission spectrum of cassette 1 (40) excited from peripheral BODIPY at 520 nm, it is seen that there is a significant quenching of donor emission at around 540 nm and enhancement in acceptor emission at around 750 nm (Figure 43). In addition to that, compound **39** excited at 520 nm which is absorbance wavelength of donor group has no emission at 750 nm. This shows that all increase in emission at 750 nm is coming from energy transfer from donor groups,. Also, quantum yield of **40** excited from peripheral BODIPY's absorbance wavelength decreases significantly from 0,97 to 0,089 which shows that there is energy transfer from outer BODIPY to core BODIPY (Table 1). Additionally, lifetime of BODIPY decreased consistently, from 5.02 ns to 0.15 ns which is the other evidence for energy transfer (Table 2).



**Figure 43.** Emission spectrum of compounds **36**, **39** and **40**

Absorbance spectrum of di-styryl BODIPY, tetra-styryl BODIPY and Cassette 2 at equally absorbing concentrations is shown in Figure 44. There are two distinct absorption peaks in spectrum, these are; absorption at around 650 nm (blue, donor chromophore) which belongs to di-styryl BODIPY and band around 740 nm (black, acceptor chromophore) which is tetra-styryl BODIPY. Energy transfer between donor and acceptor can be seen in emission spectrum of equally absorbing **37**, **39** and **41**. (Figure 45) In emission spectrum of cassette 2 excited from di-styryl BODIPY at 650 nm, it is seen that there is a significant quenching of donor emission at around 650 nm and enhancement in acceptor emission at around 750 nm (figure 45). Additionally, compound **39** excited at 650 nm which is absorbance wavelength of donor group has no emission at 750 nm indicating that all increase in emission at 750 nm is coming from energy transfer from donor groups, it is not acceptor emission. Also, quantum yield of **41** excited from BODIPY's absorbance wavelength decreases significantly from 0.67 to 0.058 which shows that energy transfer from outer di-styryl BODIPY to core tetra-styryl-BODIPY (Table 1). Lifetime of cassette 2 could not be measured accurately.

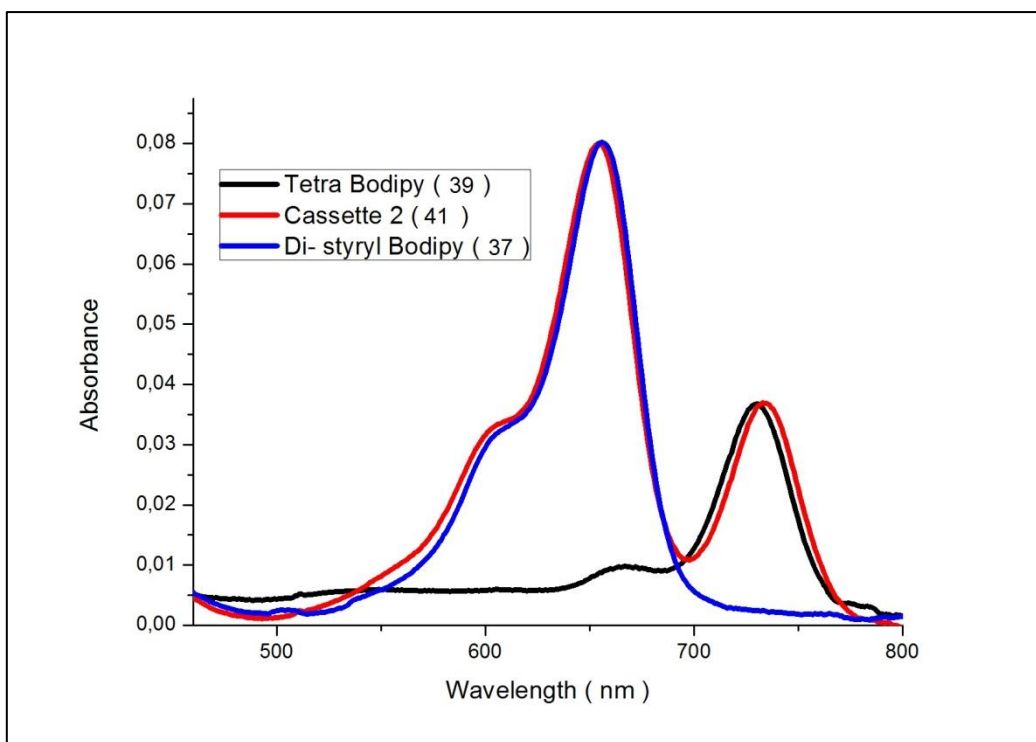


**Figure 44.** Absorbance spectrum of compounds **37**, **39** and **41**

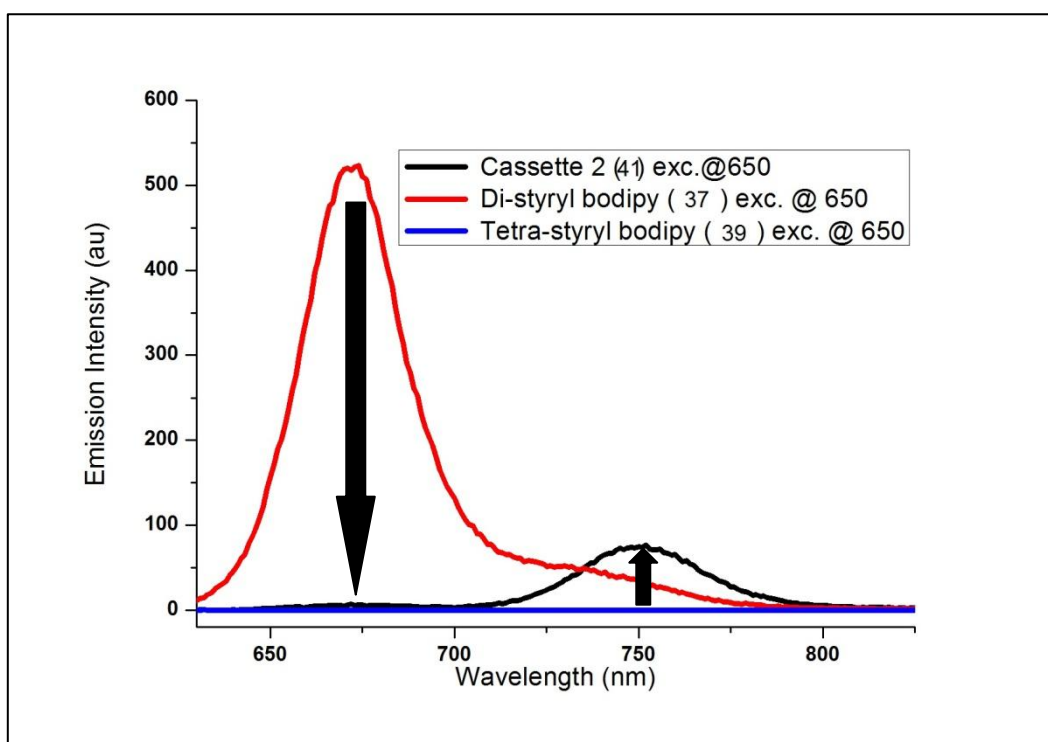


**Figure 45.** Emission spectrum of compounds **37**, **39** and **41**

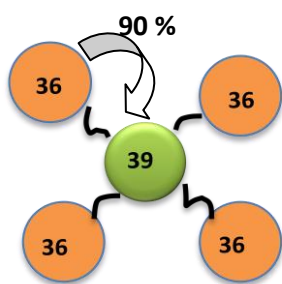
There are two different approaches to calculate energy transfer efficiency; time-resolved and steady state approaches. FRET efficiencies given in Table 2 were calculated using steady-state approach because in time-resolved approach, lifetimes of individual donor and cassettes are needed. However, lifetime of cassette **2** was not measured accurately. Also, in steady-state approach, there are no problems associated with inner filter effect and integration errors giving more accurate results compared to time-resolved approach. FRET efficiencies of cassette 1 and 2 were calculated as 90 % and 92% (Table 2). Rate constants were calculated using equation 4 and rate constant is calculated as  $1.97 \times 10^9$  for cassette 1 and for cassette 2, it is  $2.05 \times 10^9$  (Table 2).

**Table 2.** Lifetimes and FRET efficiencies of compounds

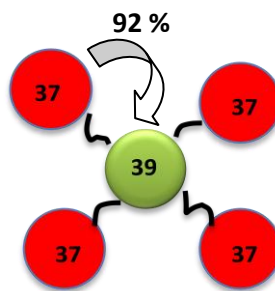
Compound	t (ns)			$k_{\text{FRET}}(\text{s}^{-1})$	$E_{\text{FRET}}$ (Steady state)
	$I_{\text{em}}(550)$	$I_{\text{em}}(652)$	$I_{\text{em}}(749)$		
<b>36</b>	5.02	-	-	-	-
<b>37</b>	-	4.55	-	-	-
<b>39</b>	-	-	3.41	-	-
<b>40</b>	-	-	0.15	$1.97 \times 10^9$	90 %
<b>41</b>	-	-	-	$2.05 \times 10^9$	92 %

In Table 2, it is seen that, cassette 2 has higher energy transfer efficiency and higher rate constant than cassette 1 as it is expected at the beginning. The reason is that there is better spectral overlap between donor emission and acceptor absorption in cassette 2 which is the requirement for Förster-type of energy transfer. Representation of cassettes is shown below.

-  BODIPY (36)
-  Distyryl-BODIPY (37)
-  Tetrasteryl-BODIPY (39)



**Cassete 1 (40)**



**Cassete 2 (41)**

## CHAPTER 4

### CONCLUSION

In this study, two different novel BODIPY-based Förster type light-harvesting energy transfer cassettes were designed and synthesized. Their fluorescence resonance energy transfer (FRET) characterization was successfully made using different techniques. FRET efficiency and rate constant were calculated.

Cassette 1 and 2 were synthesized and characterization of energy transfer between donor and acceptor chromophores were made using absorbance and emission spectrum, quantum yields and lifetimes. FRET efficiency was calculated as 90% for the cassette 1 and 92 % for cassette 2. Also cassettes were compared to each other in terms of efficiency. It is demonstrated that energy transfer efficiency is higher in cassette that has better spectral overlap between donor emission and acceptor absorption.

In conclusion, two novel energy transfer cassettes having large pseudo Stokes' shift and emissions in near-IR region were revealed to the literature. These light harvesters are likely to be useful in organic solar concentrators. Further improvement along this line is expected to yield unimolecular luminescent solar concentrators.

## REFERENCES

1. Lehn, J. M. *Angew. Chem. Int. Ed.* **1988**, 27, 89.
2. Cram, D. J. *Angew. Chem. Int. Ed.* **1988**, 27, 1009.
3. Pedersen, C. J. *Angew. Chem. Int. Ed. Engl.* **1988**, 27, 1021.
4. Whitesides, G. M.; Grzybowski, B. *Science* **2002**, 295, 2418.
5. Balzani, V.; Credi, A.; and Venturi, M. *Molecular Devices and Machines*, Wiley-VCH: Weinheim, **2003**.
6. Paul, D.; Suzumura, A.; Sugimoto, H.; Teraoka, J.; Shinoda, S.; Tsukube, H. *J. Am. Chem. Soc.* **2003**, 125, 11478.
7. Pauvert, M.; Laine, P.; Jonas, M.; Wiest, O. *J. Org. Chem.* **2004**, 69, 543.
8. Motherwell, W. B.; Bingham, M. J.; Six, Y. *Tetrahedron* **2001**, 57, 4663.
9. Sugou, K.; Sasaki, K.; Kitajima, K.; Iwaki, T.; Kuroda, Y. *J. Am. Chem. Soc.* **2002**, 124, 1182.
10. McQuade, D. T.; Hegedus, A. H.; Swager, T. M. *J. Am. Chem. Soc.* **2000**, 122, 12389.
11. Kim, S.; Choi, H.; Kim, D.; Song, K.; Kang, S.O.; Ko, J. *Tetrahedron* **2007**, 63, 9206.
12. Lo, S.-C.; Burn, P. L. *Chem. Rev.* **2007**, 107, 1097.
13. Pischel, U. *Angew. Chem. Int. Ed.* **2007**, 46, 4026.
14. Credi, A. *Angew. Chem. Int. Ed.* **2007**, 46, 5472.
15. Principles and Applications of Photochemistry Brian Wardle
16. Olmsted, J. *J. Phys. Chem.* **1979**, 83, 2581.
17. Karstens, T.; Kobs, K. *J. Phys. Chem.* **1980**, 84, 1871.
18. Magde, D.; Brannon, J.H.; Cremers, T.L.; Olmsted, J. *J. Phys. Chem.* **1979**, 83, 696.
19. Umberger, J.Q.; Lamer, V.K. *J. Am. Chem. Soc.* **1945**, 67, 1099.
20. Du, H.; Fuh, R. A.; Li, J.; Corkan, A.; Lindsey, J. S. " *Photochemistry and Photobiology*, **1998**, 68, 141.
21. Yamada, K.; Toyota, T.; Takakura, K.; Ishimaru, M.; Sugawara, T. *New J. Chem.* **2001**, 25, 667.
22. Frangioni, J. V. *Curr. Opin. Chem. Biol.* **2003**, 7, 626.
23. Ross, A. H.; Daou, M.-C.; McKinnon, C. A.; Condon, P. J.; Lachyankar, M. B.; Stephens, R. M.; Kaplan, D. R.; Wolf, D. E. *J. Cell Biol.* **1996**, 132, 945.
24. Loudet, A.; Burgess, K. *Chem. Rev.* **2007**, 107, 4891.
25. Treibs, A.; Kreuzer, F.H.; Liebig's *J. Ann. Chem.* **1968**, 718, 208.

26. Monsma, F. C.; Barton, A.C.; Kang, H.C.; Brassard, D.L.; Haugland, R. P.; Sibley, D.R. *J. Neurochem.* **1989**, *52*, 1641.
27. Registered trademark of Molecular Probes; <http://probes.invitrogen.com>.
28. Ulrich, G.; Ziessel, R.; Harriman, A. *Angew. Chem., Int. Ed.* **2008**, *47*, 1184.
29. Haugland, R. P. *Handbook of Fluorescent Probes and Research Chemicals*, 6th ed.; Molecular Probes: Eugene, OR, **1996**.
30. Yee, M.; Fas, S. C.; Stohlmeyer, M. M.; Wandless, T. J.; Cimprich, K. A. *J. Biol. Chem.* **2005**, *280*, 29053.
31. Rurack, K.; Kollmannsberger, M.; Resch-Genger, U.; Daub, J. *J. Am. Chem. Soc.* **2000**, *122*, 968.
32. Coskun, A.; Akkaya, E. U. *J. Am. Chem. Soc.* **2005**, *127*, 10464.
33. Coskun, A.; Deniz, E.; Akkaya, E. U. *Org. Lett.* **2005**, *7*, 5187.
34. Giannetto, A., Campagna, S., Ziessel, R. Bura, T., Nastasi, F., Puntoriero, F. *New J. Chem.*, 2011, **35**, 948-952
35. Bozdemir, O. A.; Guliyev, R.; Buyukcakir, O.; Selcuk, S.; Kolemen, S.; Gulseren, G.; Nalbantoglu, T.; Boyaci, H.; Akkaya, E. U. *J. Am. Chem. Soc.* **2010**, *132*, 8029.
36. Guliyev, R., Ozturk S., Kostereli, Z., *Angew. Chem.* (submitted on 16.05.2011)
37. Bozdemir, O. A.; Cakmak, Y.; Sozmen, F.; Ozdemir, T.; Siemiarczuk, A.; Akkaya, E. U. *Chem. Eur. J.* **2010**, *16*, 6346.
38. Yilmaz, M.D.; Akkaya, E. U. *Org. Lett.* **2005**, *7*, 5187.
39. Coskun, A.; Yilmaz, M.D.; Akkaya, E. U. *Org. Lett.* **2007**, *9*, 607.
40. Coskun, A.; Deniz, E.; Akkaya, E. U. *Tetrahedron. Lett.* **2007**, *48*, 5359.
41. Coskun, A.; Akkaya, E. U. *J. Am. Chem. Soc.* **2005**, *127*, 10464.
42. Yuan, M.; Li, Y.; Li, J.; Li, C.; Liu, X.; Lv, J.; Xu, J.; Liu, H.; Wang, S.; Zhu, D. *Org. Lett.*, **2007**, *9*, 2313.
43. Qi, X.; Jun, E. J.; Xu, L.; Kim, S.-J.; Joong Hong, J. S.; Yoon, Y. J.; Yoon, J. *J. Org. Chem.* **2006**, *71*, 2881.
44. Atilgan, S.; Ekmekci, Z.; Dogan, A.L.; Guc, D.; Akkaya, E.U. *Chem. Commun.* **2006**, 4398.
45. Ozlem, S.; Akkaya, E. U. *J. Am. Chem. Soc.* **2009**, *131*, 48.
46. Hu, X.; Damjanovic, A.; Ritz, T.; Schulten, K. *Proc. Natl. Acad. Sci. USA*, **1998**, *95*, 5935.
47. Lehninger, A.L.; Nelson, D.L.; Cox, M.M. *Principles of Biochemistry*, Worth Publishers Inc., New York, **1993**.

48. Balzani, V.; Credi, A.; Venturi, M. *Molecular Devices and Machines – A Journey into the Nano World*, Wiley-VCH, **2002**.
49. Balzani, V.; Ceroni, P.; Gestermann, S.; Kauffmann, C.; Gorka, M.; Vögtle, F. *Chem. Commun.* **2000**, 853.
50. Bignozzi, C.A.; Argazzi, R.; Kleverlaan, C.J. *Chem. Soc. Rev.* **2000**, 29, 87.
51. Dexter, D.L. *J. Chem. Phys.* **1953**, 21, 836.
52. Förster, T. *Ann. Phys.* **1948**, 2, 55.
53. Förster, T. *Z. Naturforsch.* **1949**, 4, 321.
54. Turro, N.J. *Modern Molecular Photochemistry*, University Science Books, Sausalito, **1991**.
55. Förster, T. *Disc. Faraday Soc.* **1959**, 27, 7.
56. Li, F.; Yang, S. I.; Ciringh, Y.; Seth, J.; Martin, C. H.; Singh, D. L.; Kim, D.; Birge, R. R.; Bocian, D. F.; Holten, D.; Lindsey, J. S. *J. Am. Chem. Soc.* **1998**, 120, 10001.
57. Wagner, R. W.; Lindsey, J. S. *J. Am. Chem. Soc.* **1994**, 116, 9759.
58. Lakowicz, J.R., *Principles of Fluorescence Spectroscopy*, 2nd ed., Kluwer/Plenum, New York, **1999**.
59. Valeur, B. *Molecular Fluorescence, Principles and Applications*, Wiley-WC, **2002**.
60. Lakowicz, J.R. *Principles of Fluorescence Spectroscopy*, Kluwer Academic, Plenum Publishers, **1999**.
61. Sharma, A.; Schulman, S.G. *Introduction to Fluorescence Spectroscopy*, Wiley Science, **1999**.
62. Burrell, A.K.; Officer, D.L.; Pleiger P.G.; Reid, D.C.W. *Chem. Rev.* **2001**, 101, 2751.
63. Wurthner, F.; You, C.-C.; Saha-Moller, C.R. *Chem. Soc. Rev.* **2004**, 33, 133.
64. Takahashi, R.; Kobuke, Y. *J. Am. Chem. Soc.*, **2003**, 125, 2372.
65. Burrell, A.K.; Officer, D.L.; Pleiger P.G.; Reid, D.C.W. *Chem. Rev.* **2001**, 101, 2751.
66. D'Souza, F.; Smith, P. M.; Zandler, M. E.; McCarty, A. L.; Itou, M.; Araki, Y.; Ito, O. *J. Am. Chem. Soc.* **2004**, 126, 7898.
67. Serin, J.M.; Brousmiche, D.W.; Frechet, J.M.J. *Chem. Commun.* **2002**, 2605.
68. Engin U. Akkaya *et al.*, *New J. Chem.* **2010**, 34, 151.
69. Koepf, M.; Trabolsi, A.; Elhabiri, M.; Wytko, J. A.; Paul, D.; Albrecht-Gary, A. M.; Weiss, J. *Org. Lett.* **2005**, 7, 1279.
70. Imamura, T.; Fukushima, K. *Coord. Chem. Rev.* **2000**, 198, 133.
71. Treibs, A.; Kreuzer, F. H. *Justus Liebigs Ann. Chem.* **1968**, 718, 208.

72. Rousseau, T.; Cravino, A.; Bura, T.; Ulrich, G.; Ziessel, R.; Roncali, J. *Chem. Commun.* **2009**, 1673.
73. Rousseau, T.; Cravino, A.; Bura, T.; Ulrich, G.; Ziessel, R.; Roncali, J. *J. Mater. Chem.* **2009**, *19*, 2298.
74. Liu, J.-Y.; Ermilov, E. A.; Roder, B. *Chem. Commun.* **2009**, 1517.
75. Niu, S. L.; Ulrich, G.; Ziessel, R.; Kiss, A.; Renard, P.-Y.; Romieu, A. *Org. Lett.* **2009**, *11*, 2049.
76. Wenwu, Q.; Baruah, M.; Sliwa, M.; van der Auweraer, M.; de Borggraeve, W. M.; Beljonne, D.; van Averbeke, B.; Boens, N. *J. Phys. Chem. A* **2008**, *112*, 6104.
77. Diring, S.; Puntoriero, F.; Nastasi, F.; Campagna, S.; Ziessel, R. *J. Am. Chem. Soc.* **2009**, *131*, 6108.
78. Goze, C.; Ulrich, G.; Mallon, L. J.; Allen, B. D.; Harriman, A.; Ziessel, R. *J. Am. Chem. Soc.* **2006**, *128*, 10231.
79. Thivierge, C.; Bandichhore, R.; Burgess, K. *Org. Lett.* **2007**, *9*, 2135.
80. Umezawa, K.; Matsui, A.; Nakamura, Y.; Citterio, D.; Suzuki, K. *Chem. Eur. J.* **2009**, *15*, 1096.
81. Umezawa, K.; Nakamura, Y.; Makino, H.; Citterio, D.; Suzuki, K. *J. Am. Chem. Soc.* **2009**, *130*, 1550.
82. Rohand, T.; Qin, W.; Boens, N.; Dehaen, W. *Eur. J. Org. Chem.* **2006**, 4658.
83. Killoran, J.; Allen, L.; Gallagher, J. F.; Gallagher, W. M.; O'Shea, D. F. *Chem. Commun.* **2002**, 1862.
84. Buyukcakir, O.; Bozdemir, O. A.; Kolemen, S.; Erbas, S.; Akkaya, E. U. *Org. Lett.* **2009**, *11*, 4644.
85. Ertan-Ela, S.; Yilmaz, M. D.; Icli, B.; Dede, Y.; Icli, S.; Akkaya, E. U. *Org. Lett.* **2008**, *10*, 3299.
86. Bura, T.; Retailleau, P.; Ulrich, G.; Ziessel, R. *J. Org. Chem.* **2011**, *76*, 1109.

# APPENDIX A

## NMR SPECTRA

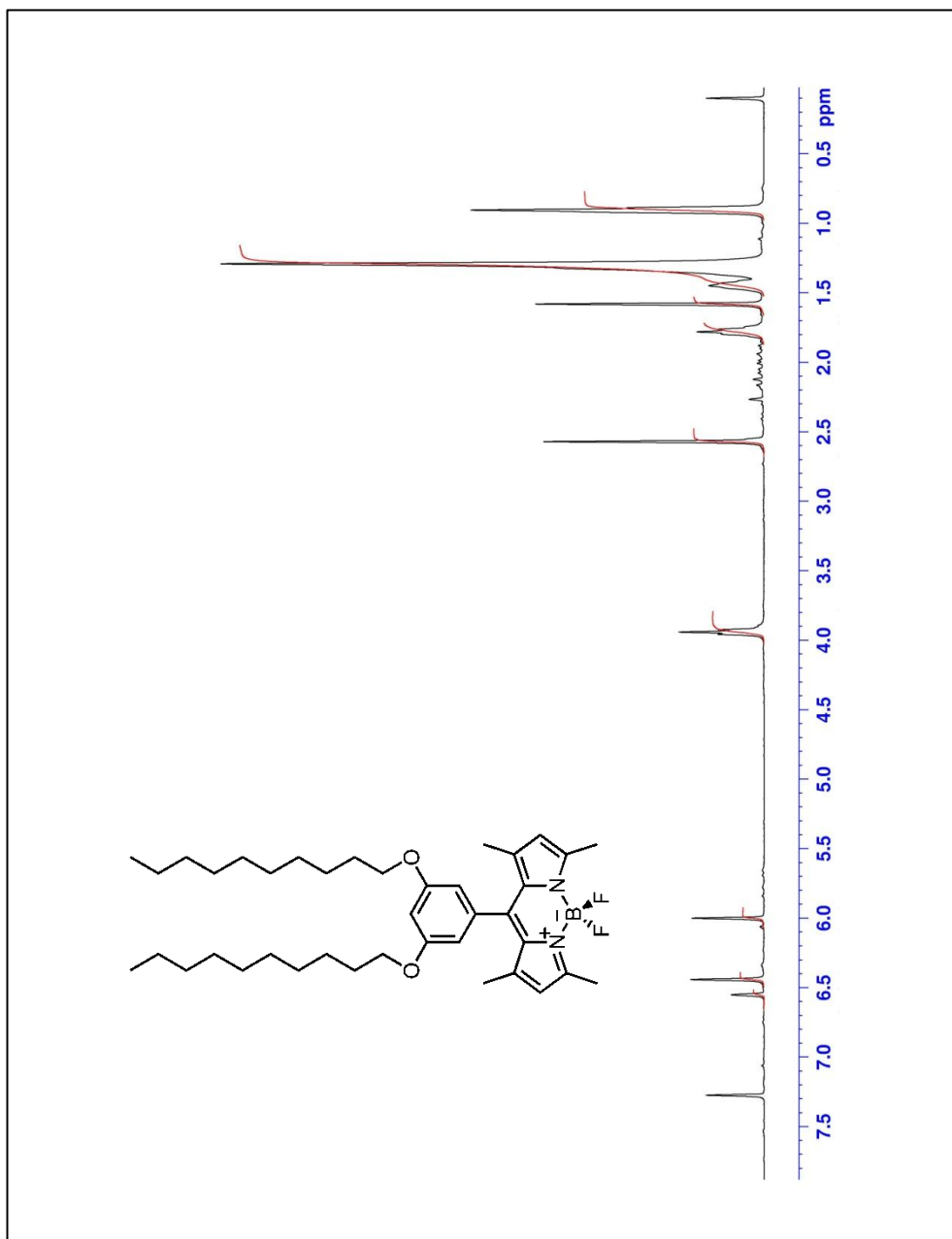


**Figure 46.** <sup>1</sup>H NMR spectrum of compound **29**

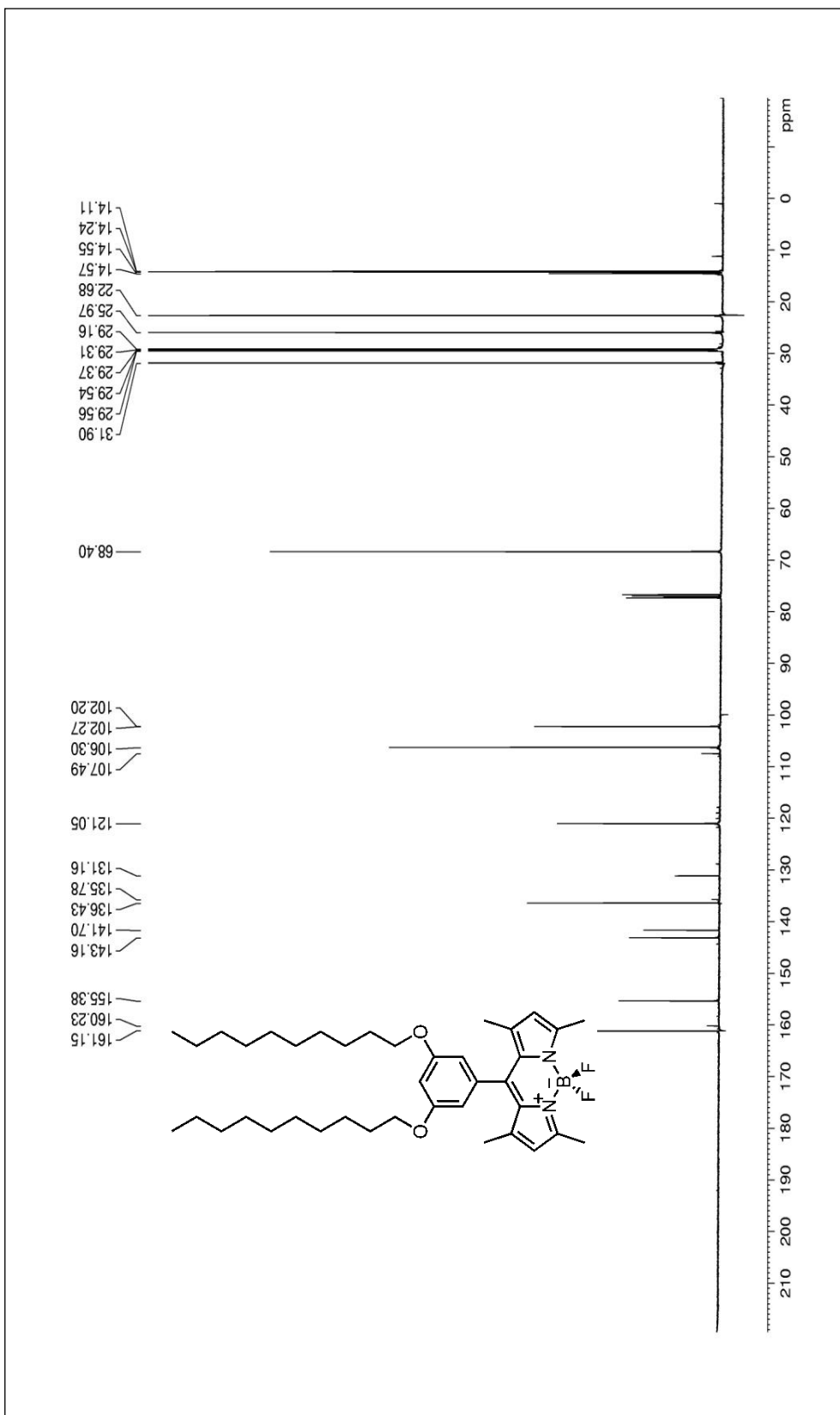


**Figure 47.**  $^{13}\text{C}$  NMR spectrum of compound **29**

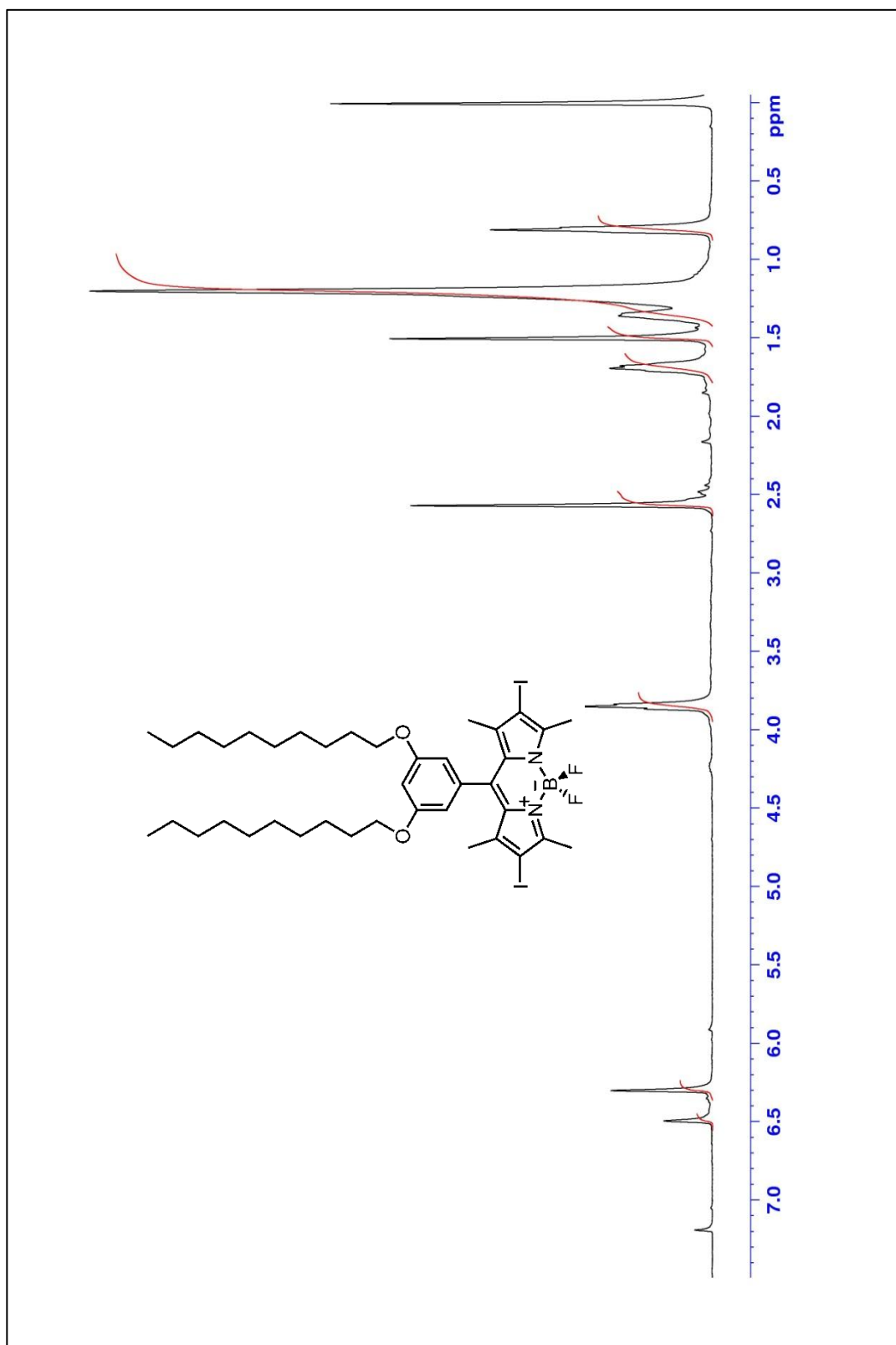


**Figure 48.**  $^1\text{H}$  NMR spectrum of compound 30



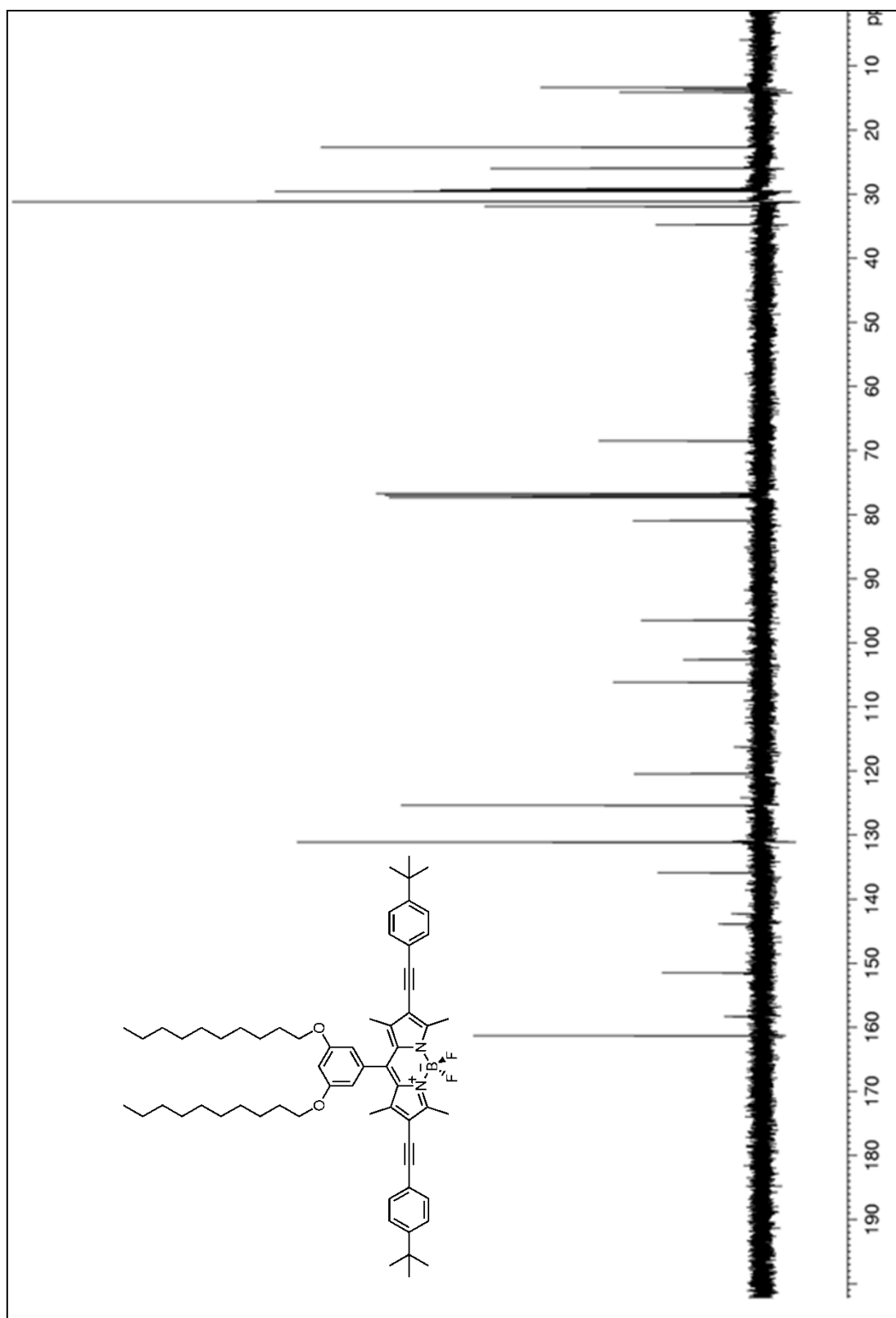


**Figure 50.**  $^{13}\text{C}$  NMR spectrum of compound 32

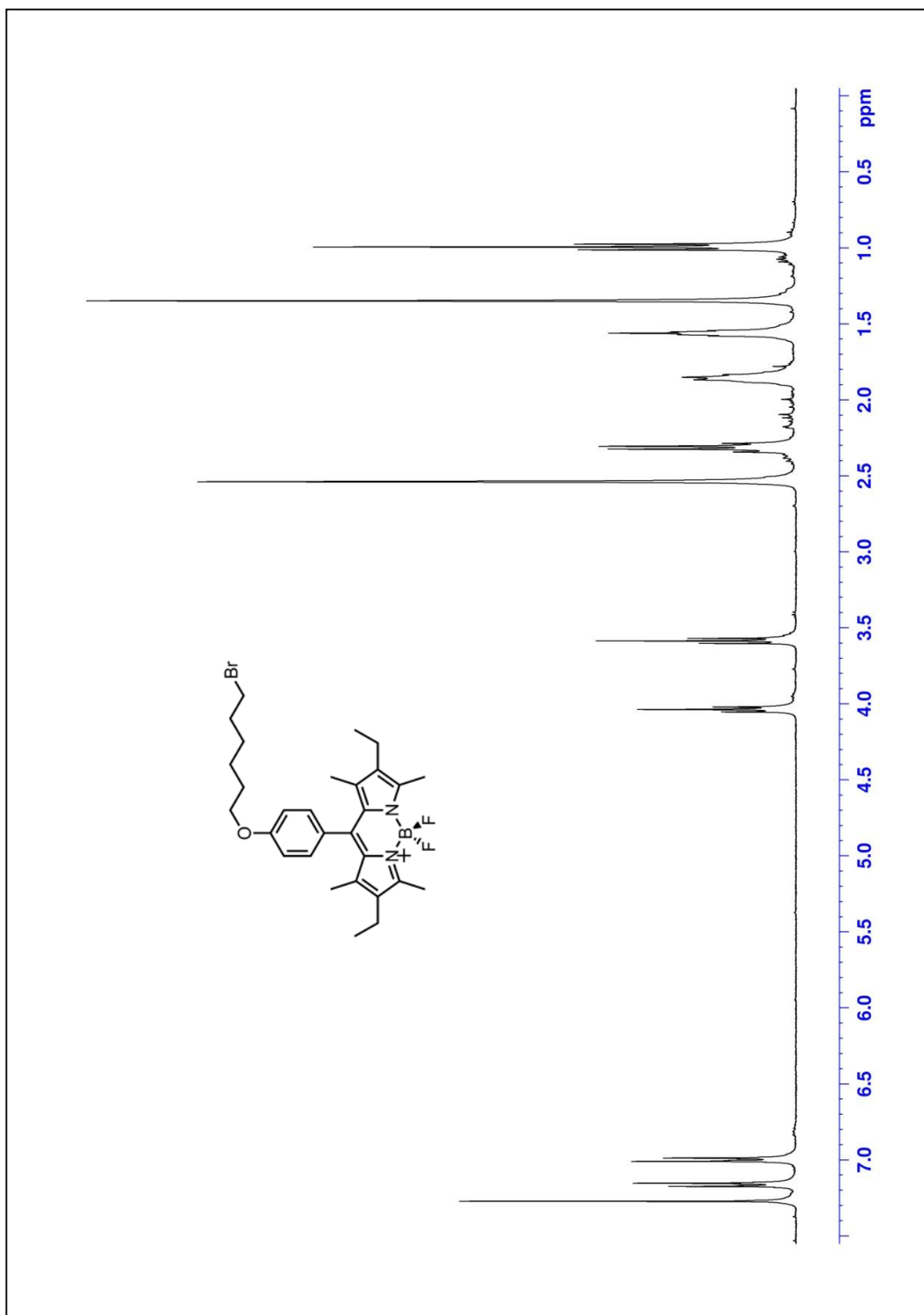


**Figure 51.** <sup>1</sup>H NMR spectrum of compound 35

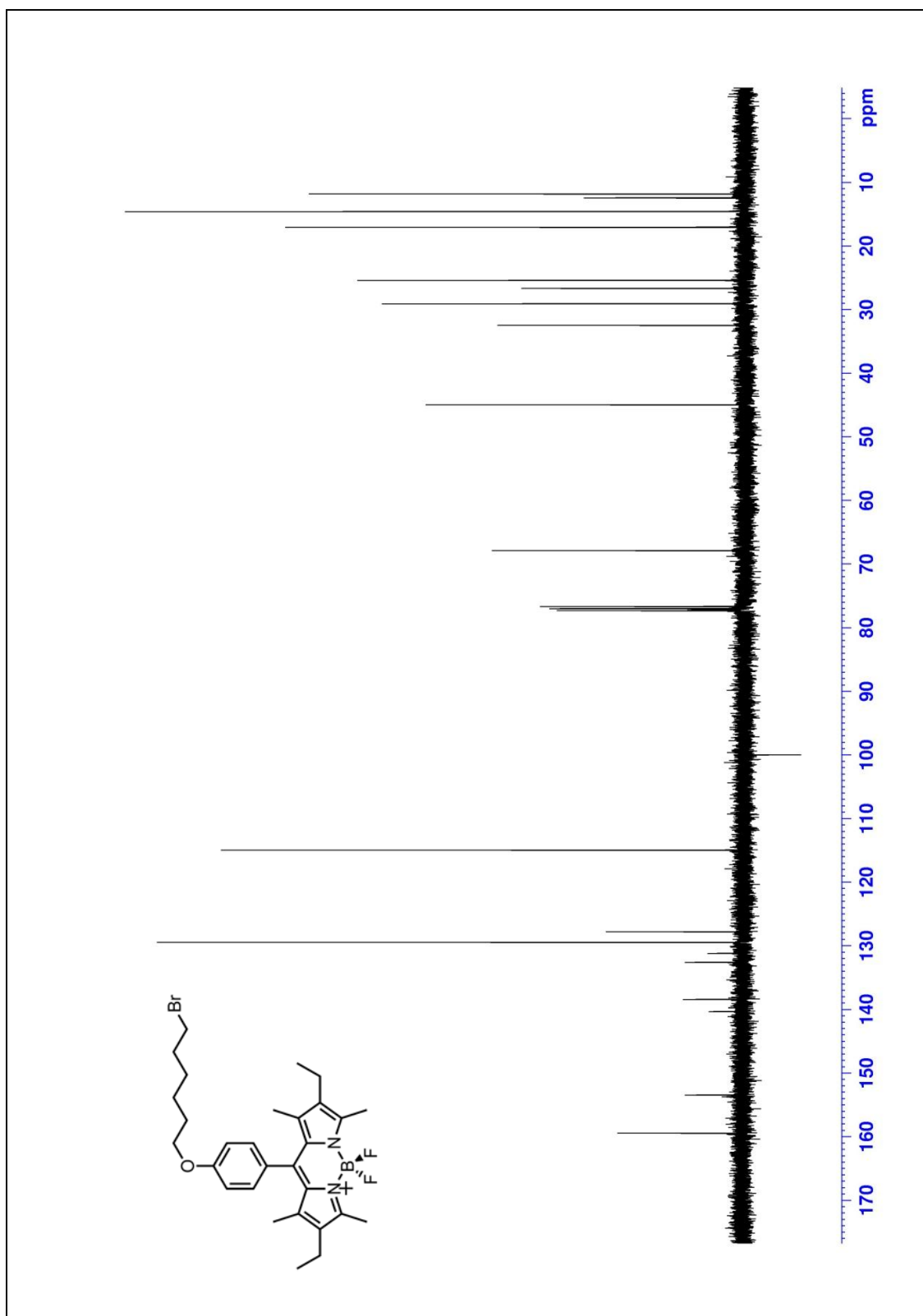


**Figure 52.**  $^{13}\text{C}$  NMR spectrum of compound 35

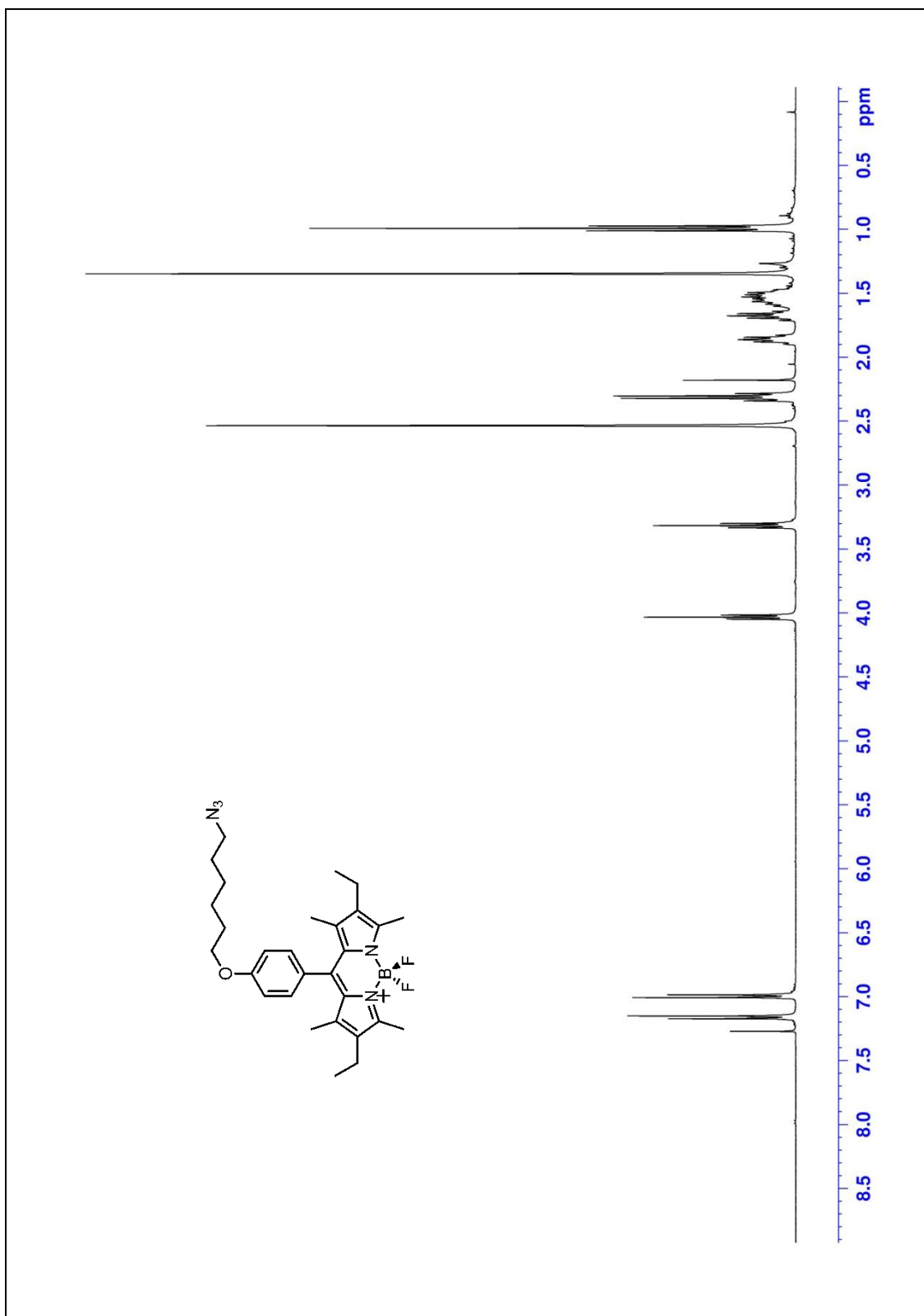


**Figure 53.** <sup>1</sup>H NMR spectrum of compound 36

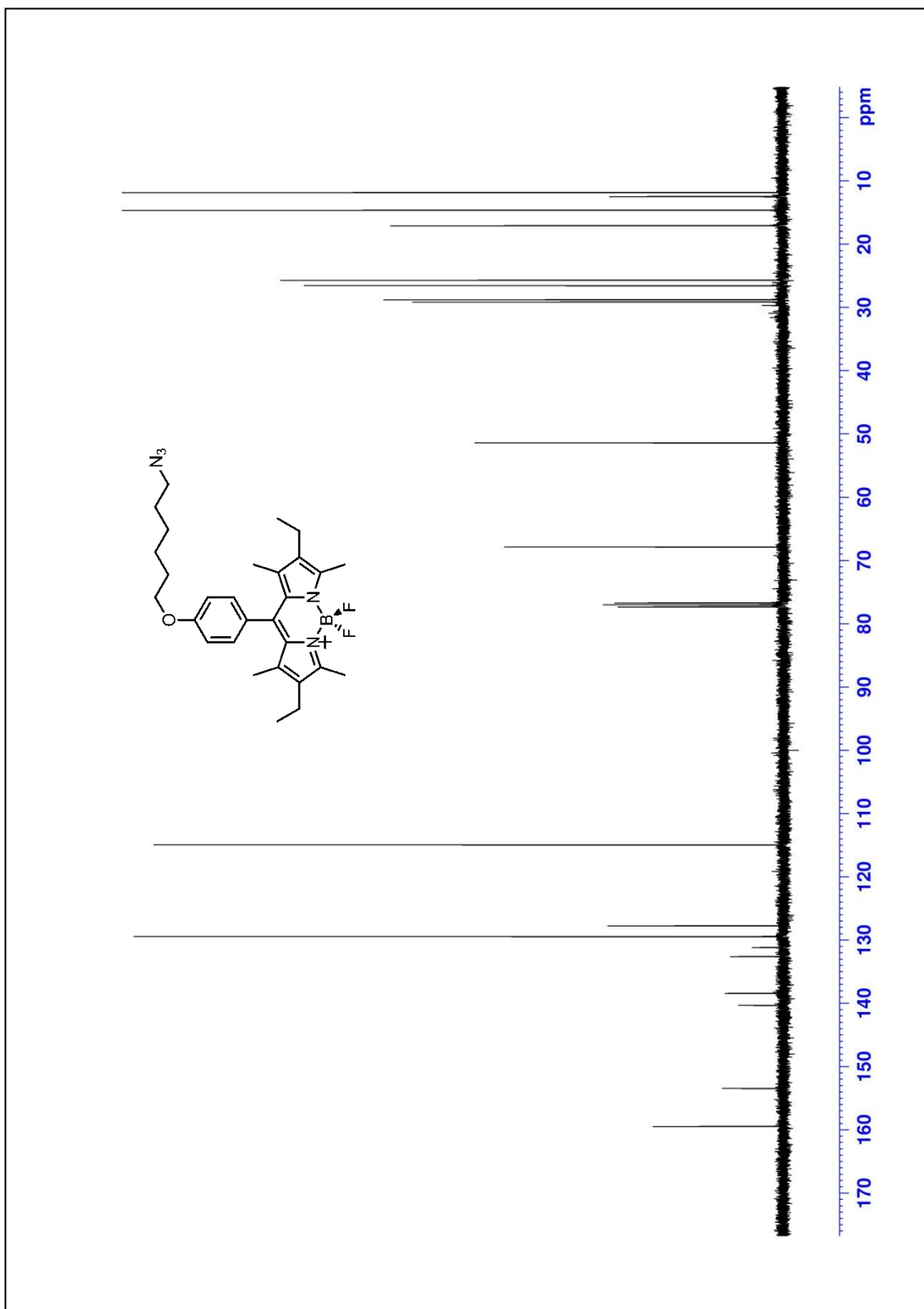


**Figure 54.**  $^{13}\text{C}$  NMR spectrum of compound 36

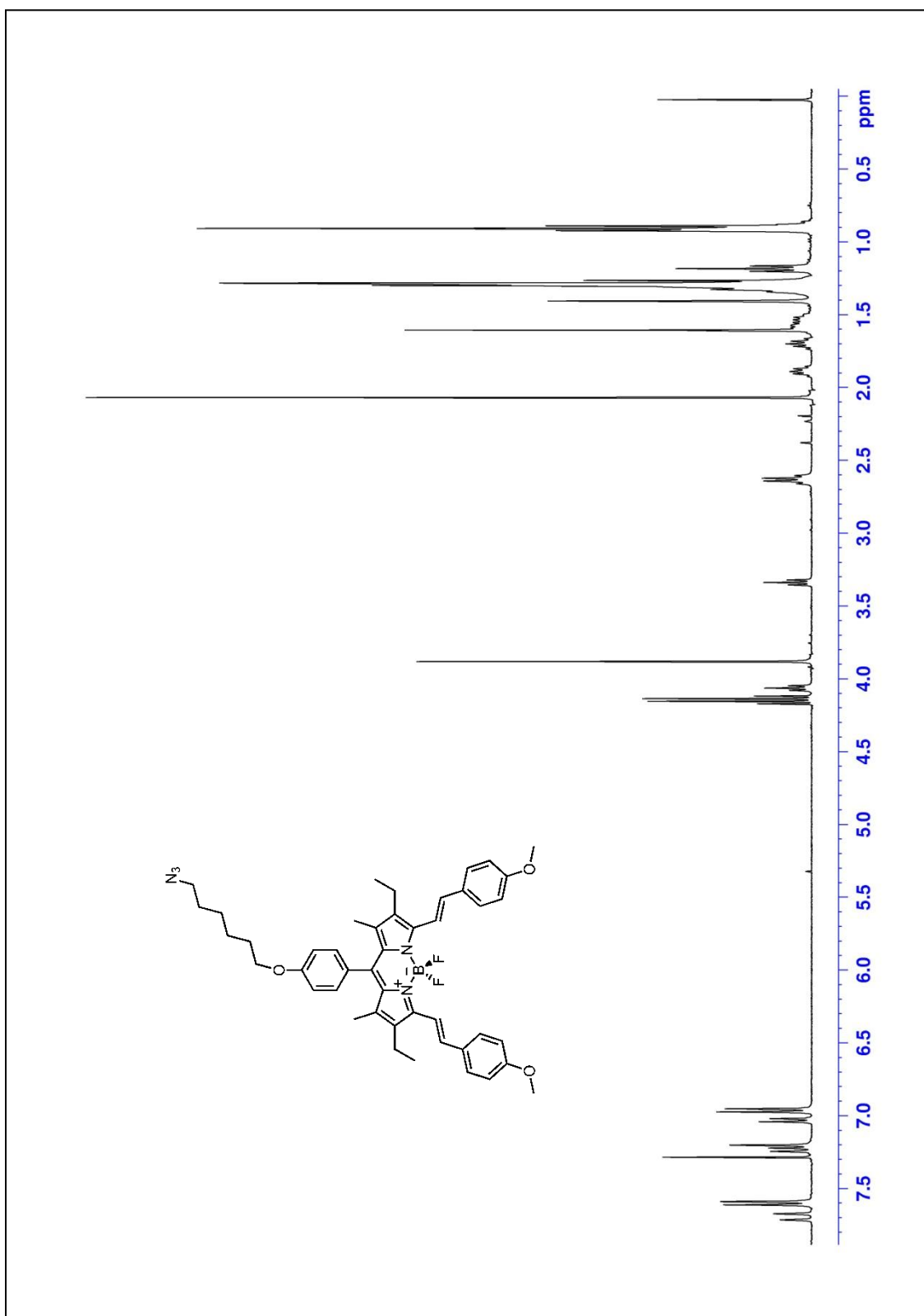


**Figure 55.** <sup>1</sup>H NMR spectrum of compound 37

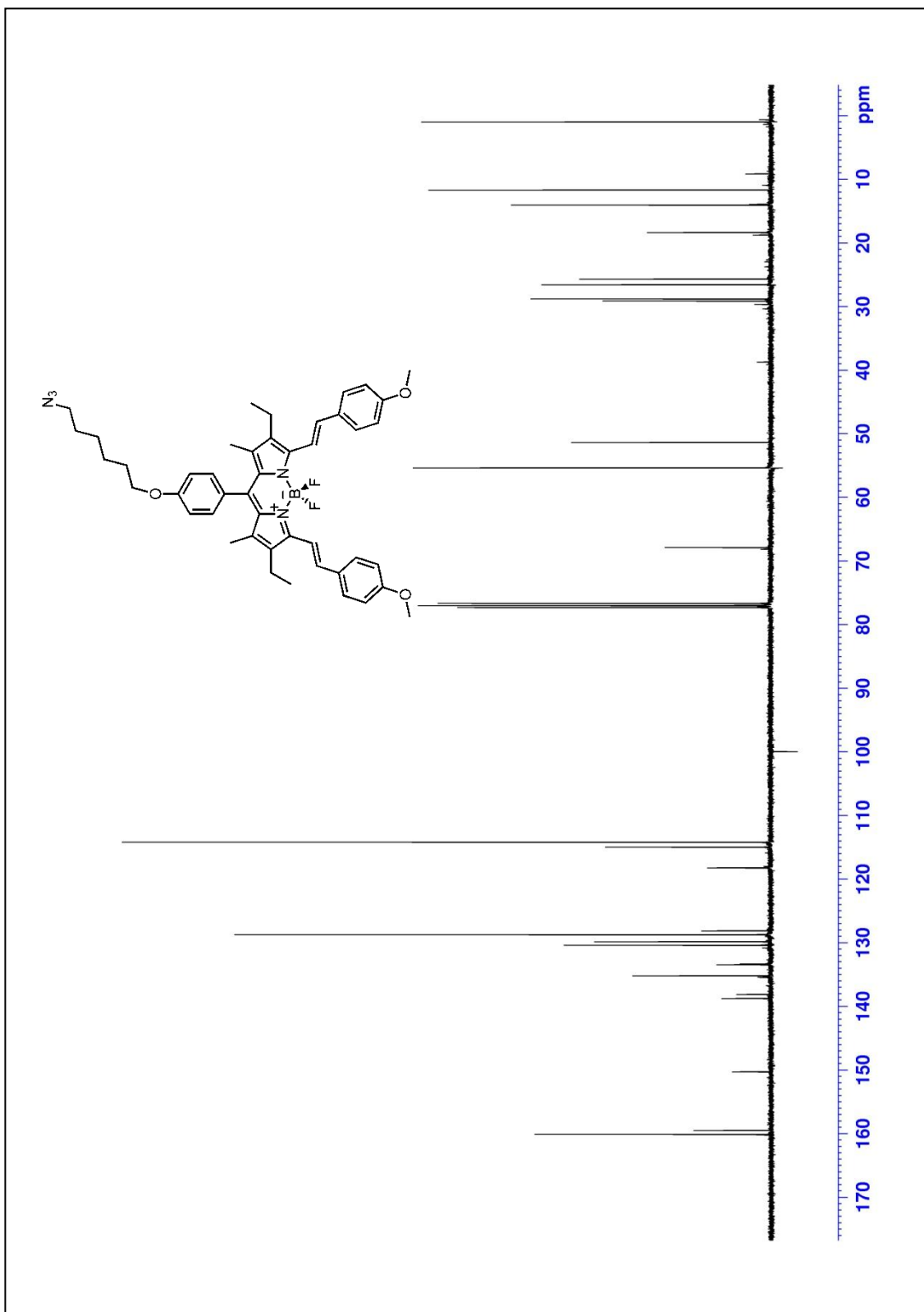


**Figure 56.**  $^{13}\text{C}$  NMR spectrum of compound 37

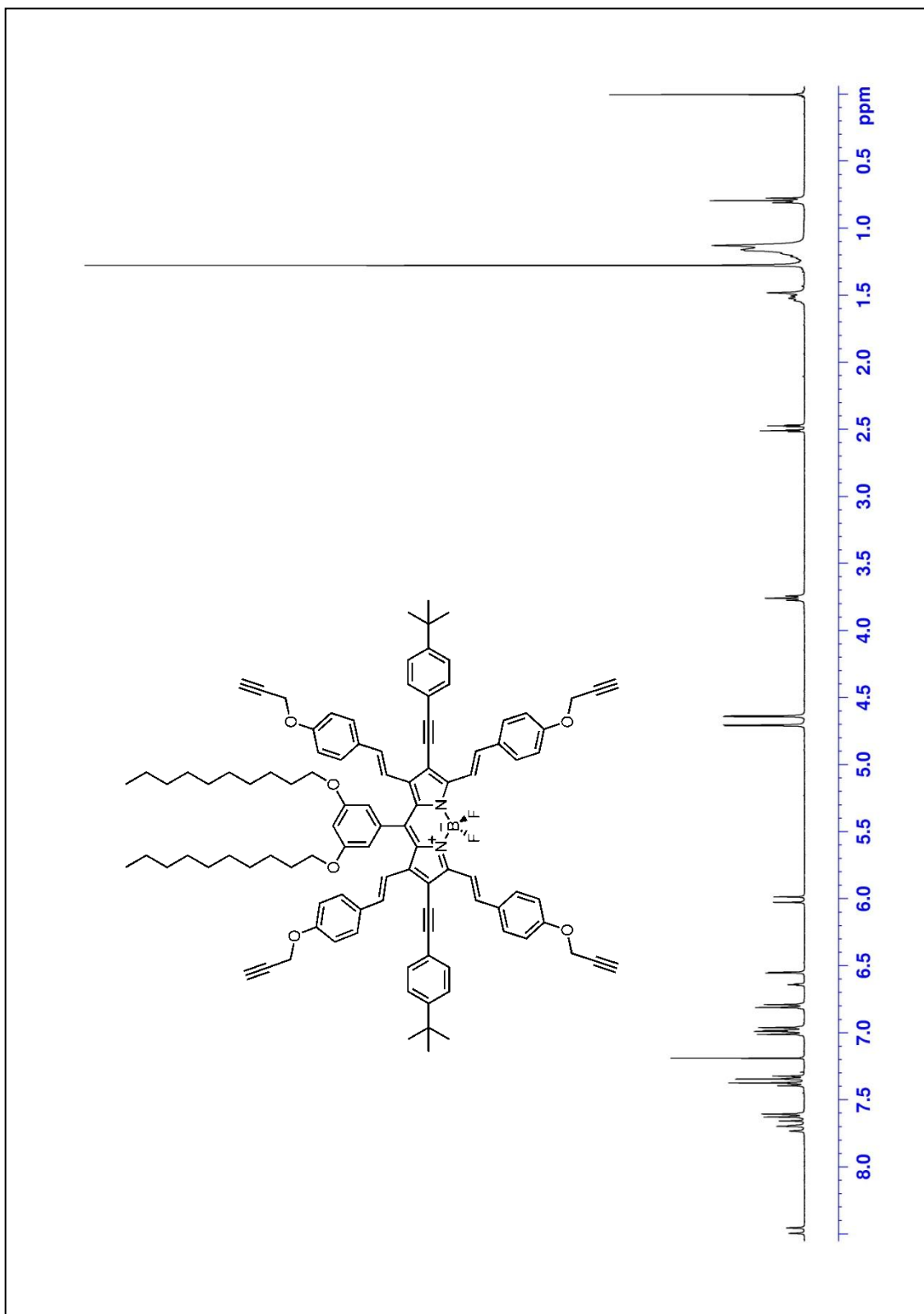


**Figure 57.** <sup>1</sup>H NMR spectrum of compound 39

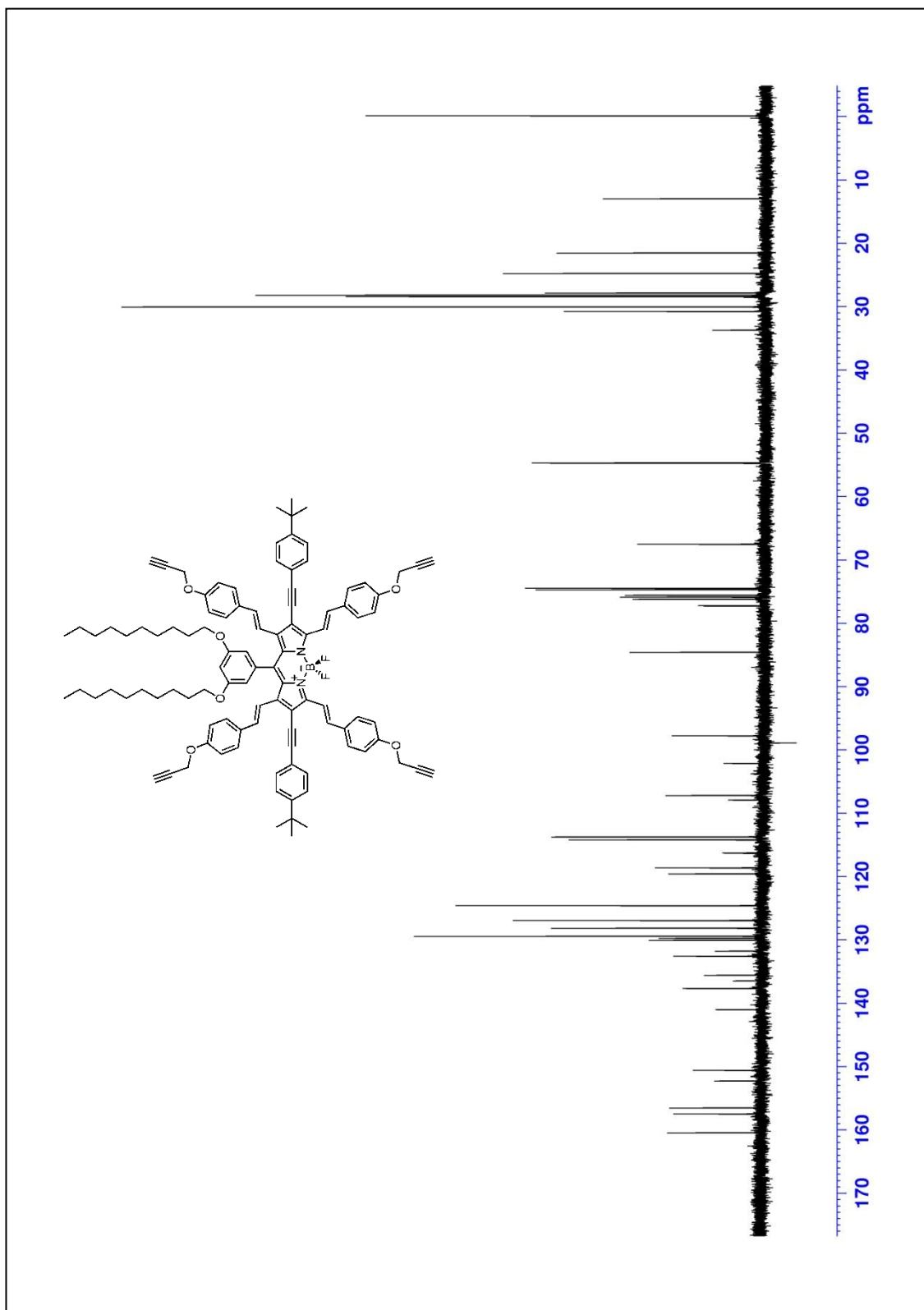


**Figure 58.**  $^{13}\text{C}$  NMR spectrum of compound 39

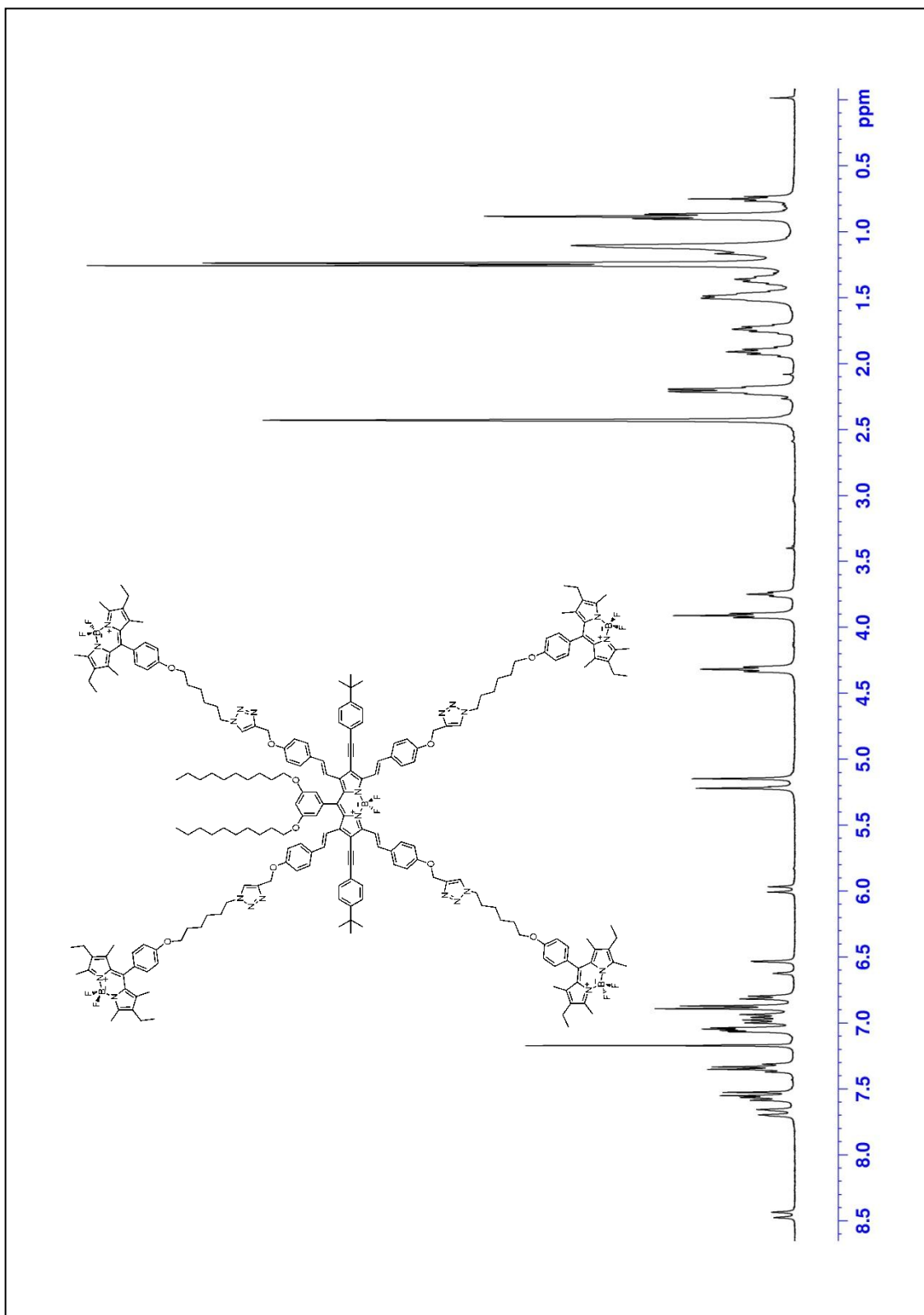


**Figure 59.** <sup>1</sup>H NMR spectrum of compound 40

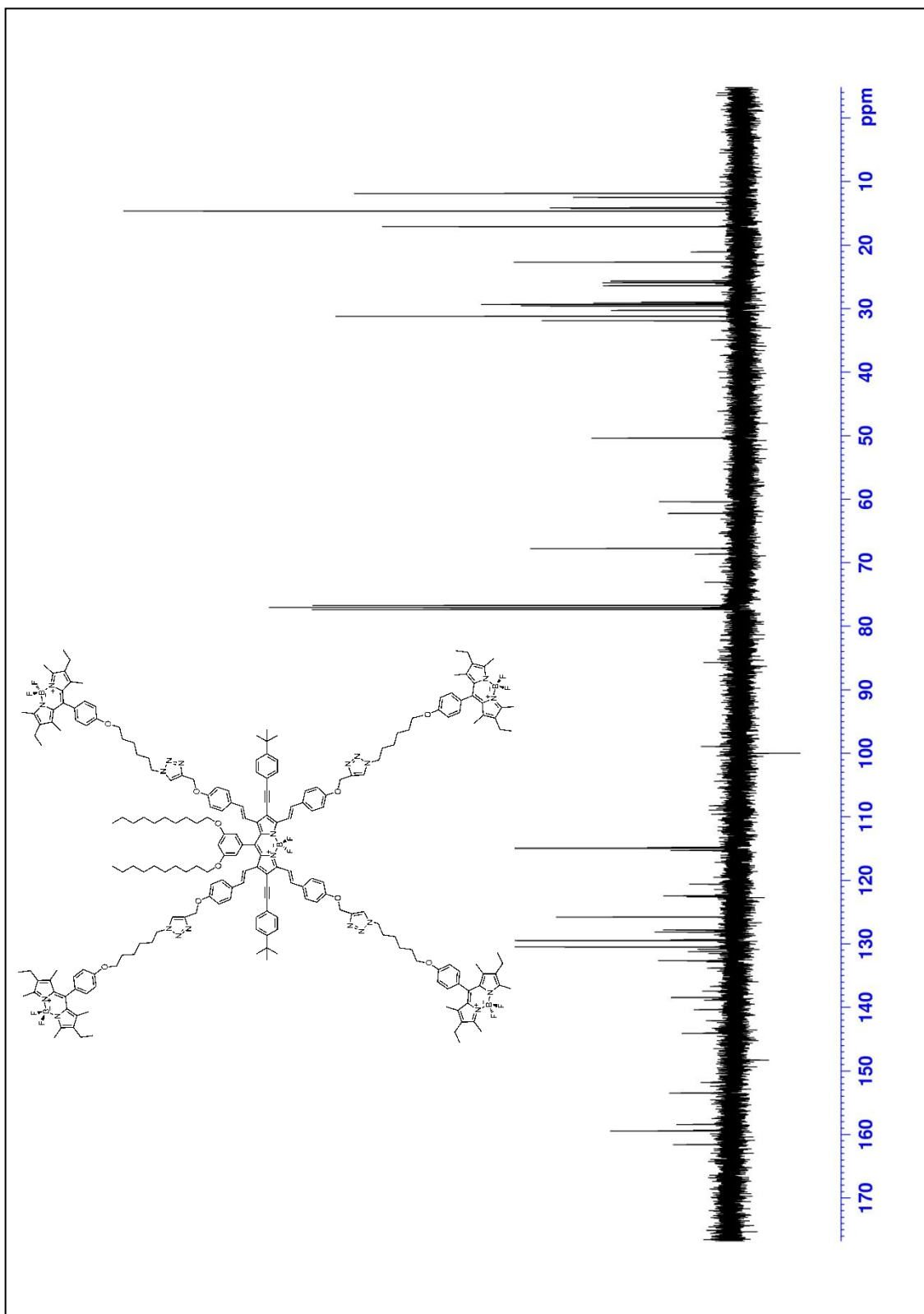


**Figure 60.**  $^{13}\text{C}$  NMR spectrum of compound 40

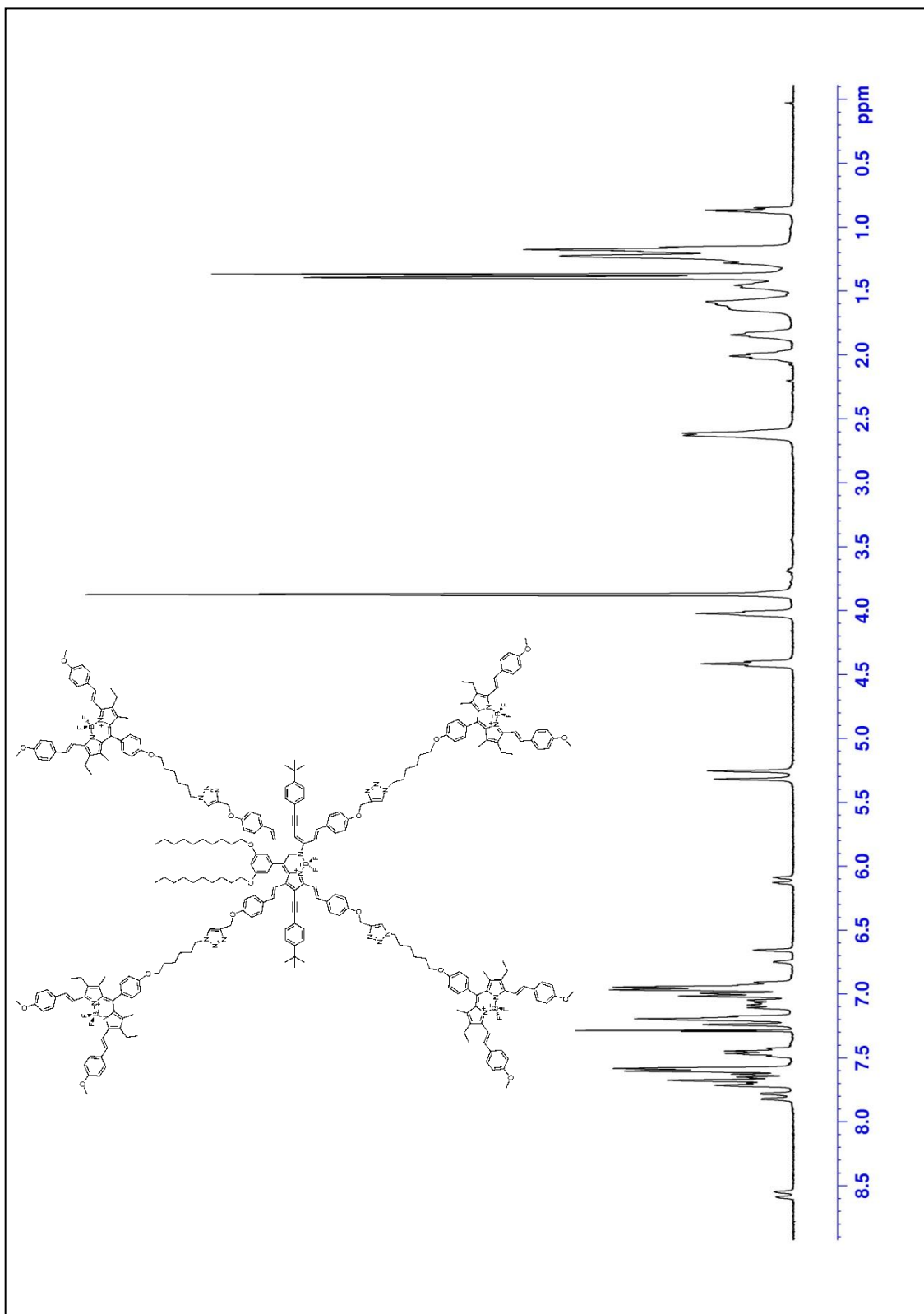


**Figure 61.**  $^1\text{H}$  NMR spectrum of compound 41

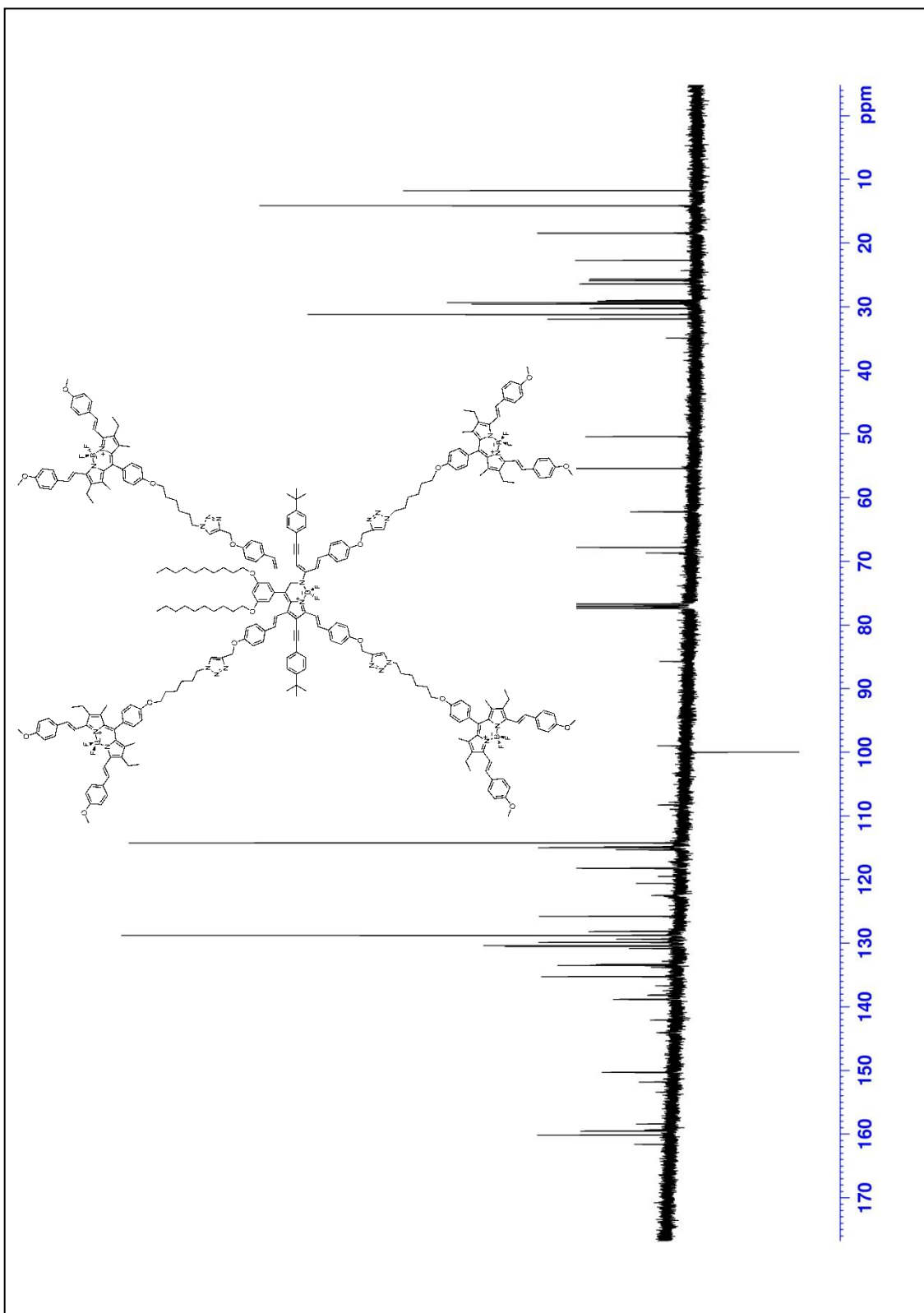


**Figure 62.**  $^{13}\text{C}$  NMR spectrum of compound 41

# APPENDIX B

## MASS SPECTRA

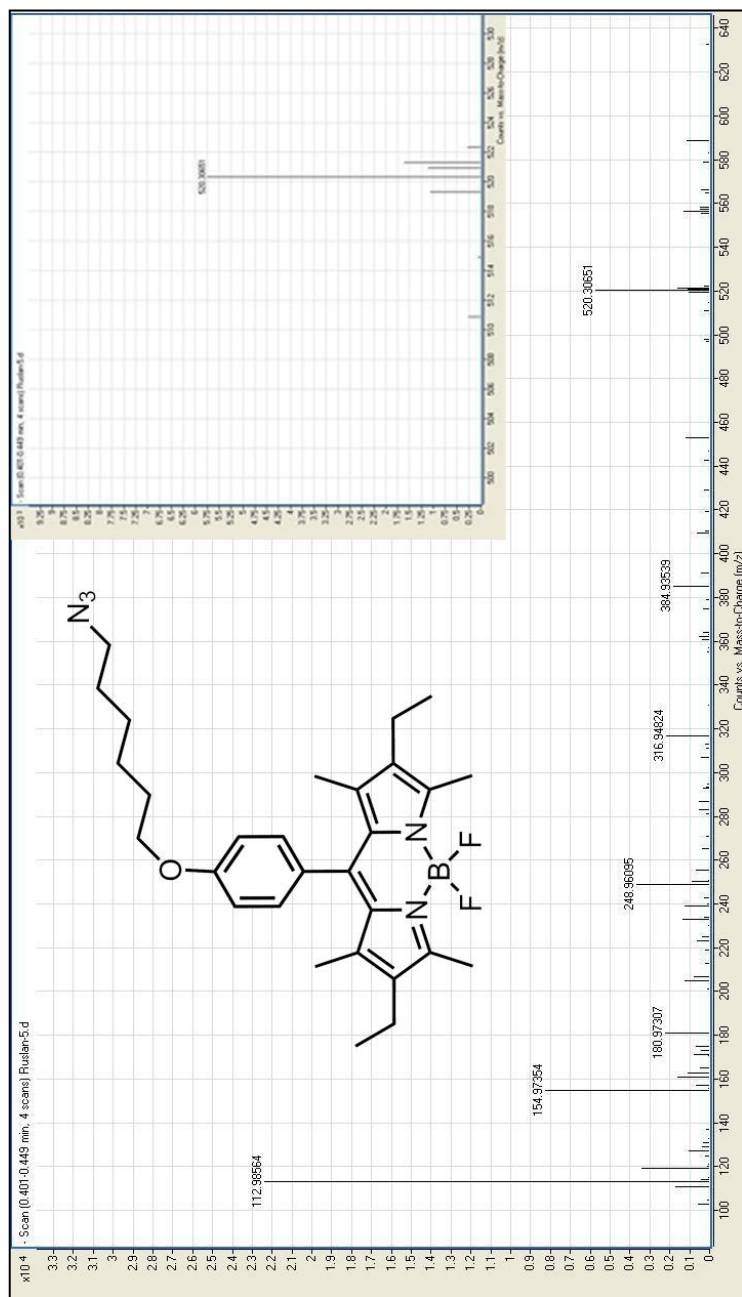


**Figure 63.** ESI-HRMS of compound 36

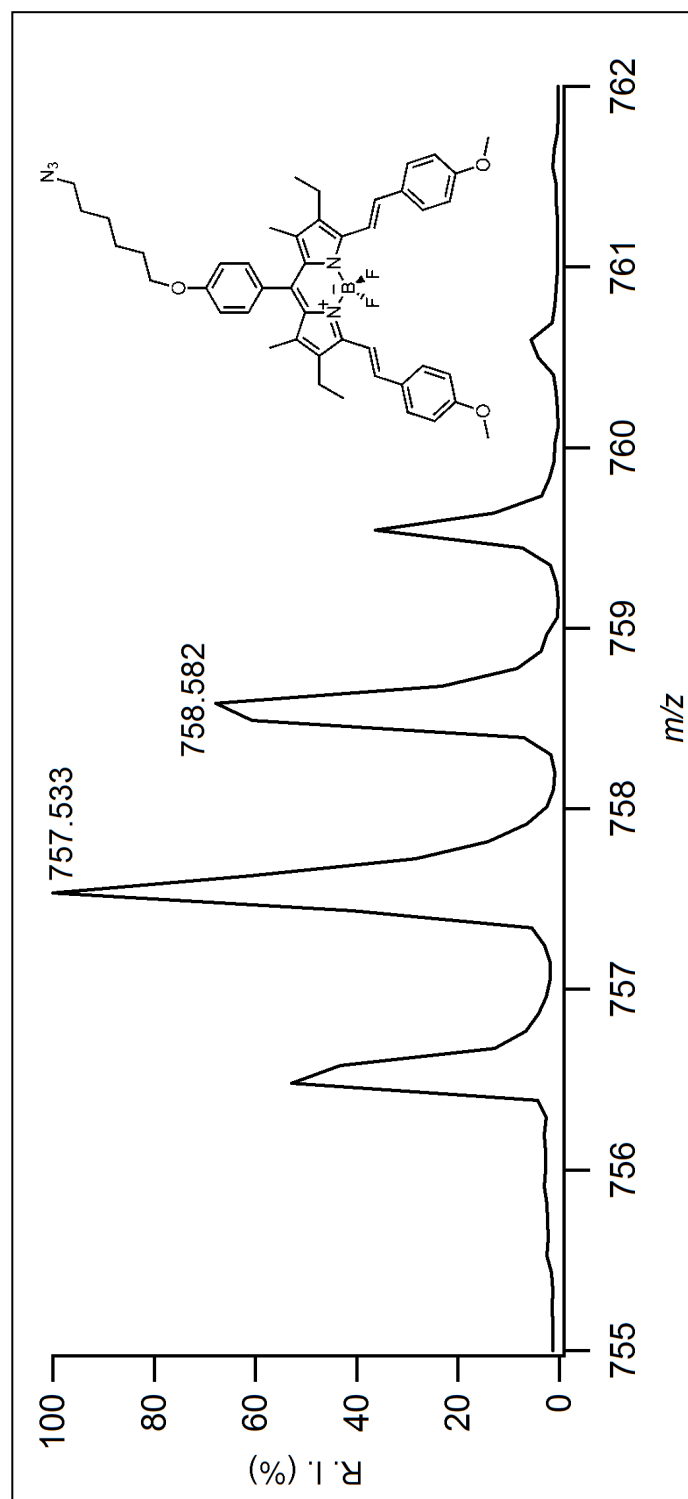


**Figure 64.** ESI-HRMS of compound 37

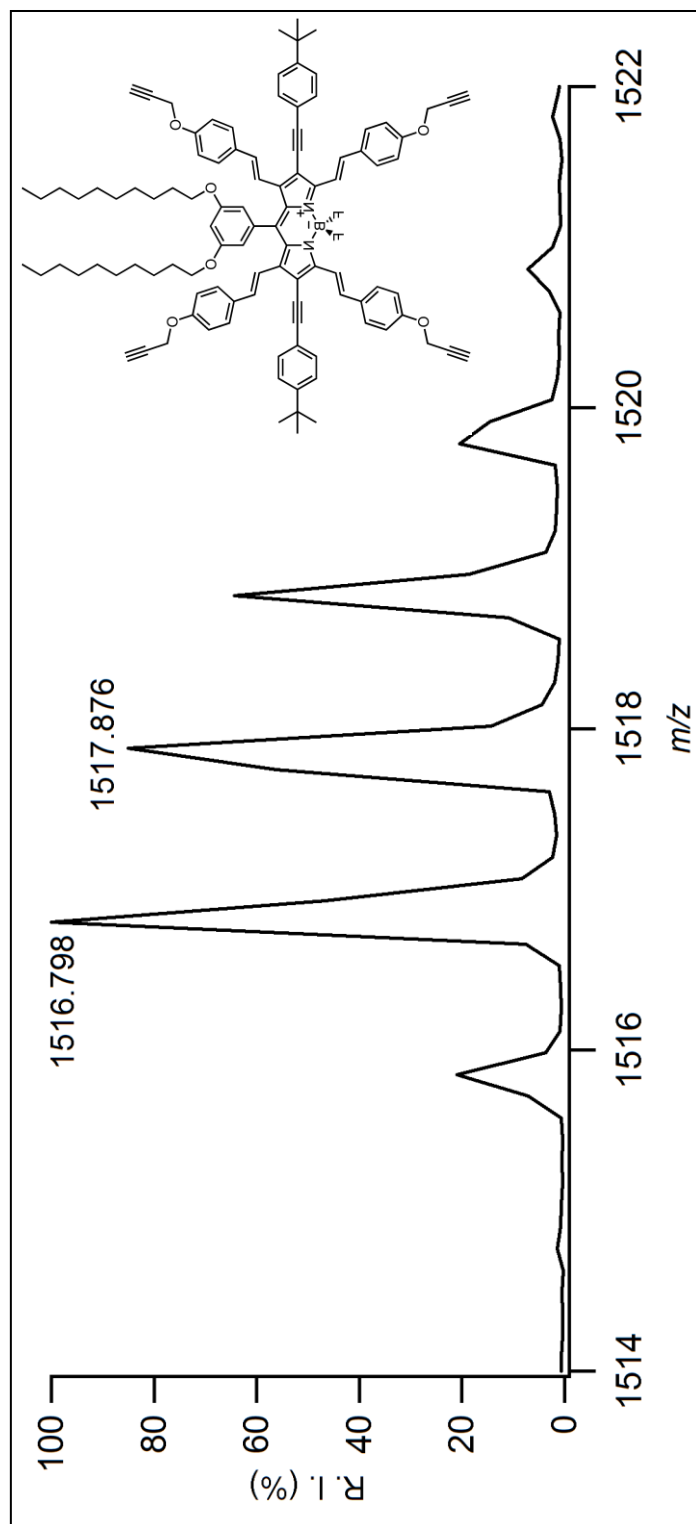


**Figure 65.** ESI-HRMS of compound **39**

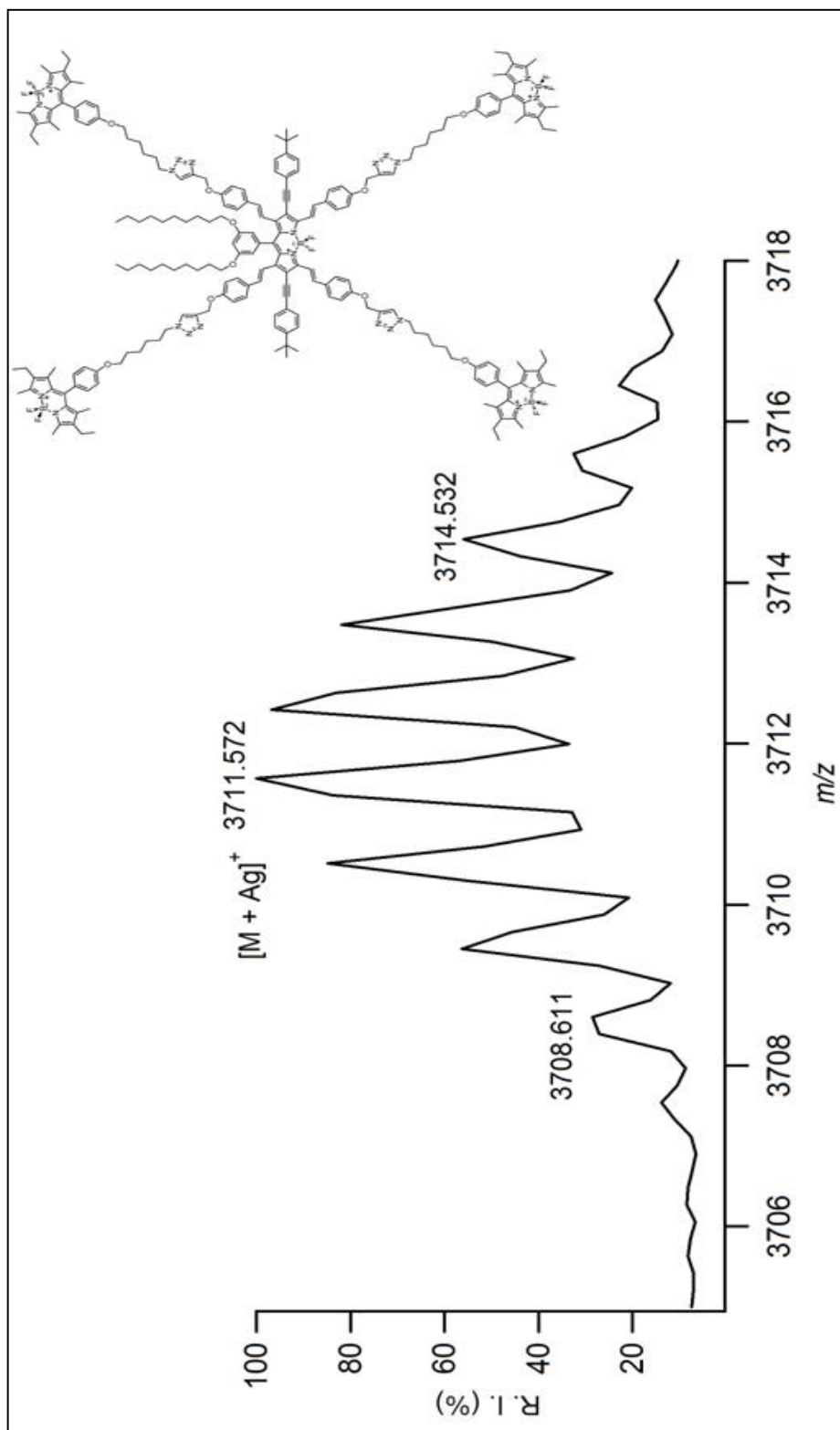


**Figure 66.** MALDI-MS of compound 40

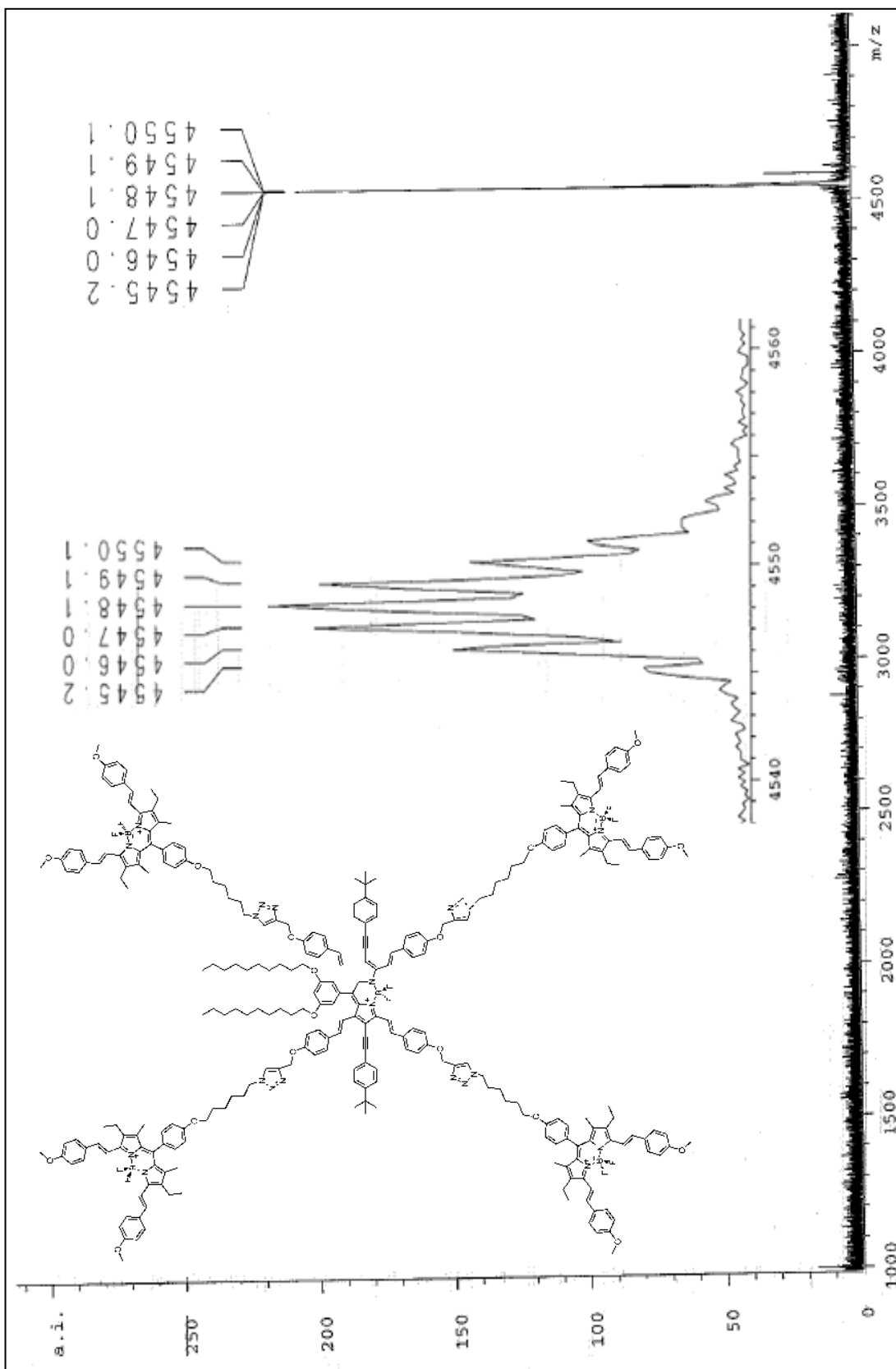


Figure 67. MALDI-MS of compound 41